SENSITIVITY OF OFDM SYSTEMS TO SYNCHRONIZATION ERRORS

AND SPATIAL DIVERSITY

A Dissertation

by

YI ZHOU

Submitted to the Office of Graduate Studies of
Texas A&M University
in partial fulfillment of the requirements for the degree of

DOCTOR OF PHILOSOPHY

December 2010

Major Subject: Electrical Engineering

SENSITIVITY OF OFDM SYSTEMS TO SYNCHRONIZATION ERRORS

AND SPATIAL DIVERSITY

A Dissertation

by

YI ZHOU

Approved by:

Co-Chairs of Committee,   Erchin Serpedin
                          Khalid Qaraqe
Committee Members,   Costas N. Georghiades
                          Aydin Karsilayan
                          Nancy M. Amato
Head of Department,   Costas N. Georghiades

December 2010

Major Subject: Electrical Engineering

ABSTRACT

Sensitivity of OFDM Systems to Synchronization Errors

and Spatial Diversity. (October 2010)

Yi Zhou, B.S., Southeast University;

M.S., Southeast University

Co–Chairs of Advisory Committee: Erchin Serpedin
Khalid Qaraqe

In this dissertation, the problem of synchronization for OFDM-based wireless communication systems is studied. In the first part of this dissertation, the sensitivity of both single input single output (SISO) OFDM and multiple input multiple output (MIMO) OFDM receivers to carrier and timing synchronization errors are analyzed. Analytical expressions and numerical results for the power of inter-carrier interference (ICI) are presented. It is shown that the OFDM-based receivers are quite sensitive to residual synchronization errors. In wide-sense stationary uncorrelated scattering (WSSUS) frequency-selective fading channels, the sampling clock timing offset results in rotation of the subcarrier constellation, while carrier frequency offsets and phase jitter cause inter-carrier interference. The overall system performance in terms of symbol error rate is limited by the inter-carrier interference. For a reliable information reception, compensatory measures must be taken.

The second part of this dissertation deals with the impact of spatial diversity (usage of multiple transmit/receive antennas) on synchronization. It is found that

with multiple transmit and receive antennas, MIMO-OFDM systems can take advantage of the spatial diversity to combat carrier and timing synchronization imperfections. Diversity can favorably improve the synchronization performance. Data-aided and non-data-aided maximum likelihood symbol timing estimators for MIMO-OFDM systems are introduced. Computer simulations show that, by exploiting the spatial diversity, synchronization performance of MIMO-OFDM systems in terms of mean squared error (MSE) of residual timing offset becomes significantly more reliable when compared to conventional SISO OFDM systems. Therefore, spatial diversity is a useful technique to be exploited in the deployment of MIMO-OFDM communication systems.

In MIMO systems with synchronization sequences, timing synchronization is treated as a multiple hypotheses testing problem. Generalized likelihood ratio test (GLRT) statistics are developed for MIMO systems in frequency flat channels and MIMO-OFDM systems in frequency selective fading environments. The asymptotic performance of the GLRT without nuisance parameters is carried out. It is shown that the asymptotic performance of the GLRT can serve as an upper bound for the detection probability in the presence of a limited number of observations as well as a benchmark for comparing the performances of different timing synchronizers.

To my beloved wife and parents.

ACKNOWLEDGMENTS

First, I would like to express my appreciation to my advisor, Dr. Erchin Serpedin, for his precious advice on my research work. His patience and continuous support helped me overcome many crisis situations and finish this dissertation. I would also like to thank Dr. Khalid Qaraqe, Dr. Costas N. Georghiades, Dr. Aydin Karsilayan, and Dr. Nancy M. Amato, for their advice and time serving on my academic committee.

Next, I would like to thank the students from the wireless communications group for their warm-hearted help. In particular, Kai Shi, Yik-Chung Wu, and Wenyan He, should receive special credit for the stimulating discussions and their generosity in sharing knowledge. Special thanks go also to Qasim M. Chaudhari, Kyoung-Lae Noh, Lingjia Liu, and many other friends.

Last but not least, I am grateful to my parents for their love and support throughout my many-year education. I would also like to thank my wife, Wenjie Yu. She has always been patient and provided me endless understanding, love and support.

NOMENCLATURE

AWGN	Additive White Gaussian Noise
BOF	Beginning Of a Frame
CLT	Central Limit Theorem
CFAR	Constant False Alarm Rate
CP	Cyclic Prefix
CCRB	Conditional Cramer-Rao Bound
CFO	Carrier Frequency Offset
CRLB	Cramer-Rao Lower Bound
DA	Data-Aided
DFT	Discrete Fourier Transform
EGC	Equal Gain Combining
FFT	Fast Fourier Transform
GLRT	Generalized Likelihood Ratio Test
ICI	Inter-Carrier Interference
IDFT	Inverse Discrete Fourier Transform
i.i.d.	Independent, Identically Distributed
ISI	Inter-Symbol Interference
MB	Multi-Band
MCRB	Modified Cramer-Rao Bound
MIMO	Multiple Input and Multiple Output
MISO	Multiple Input Single Output
MLE	Maximum Likelihood Estimator
MRC	Maximum Ratio Combining
MSE	Mean Squared Error

NCFO	Normalized Carrier Frequency Offset
NDA	Non-Data-Aided
OFDM	Orthogonal Frequency Division Multiplexing
pdf	Probability Density Function
PSD	Power Spectral Density
QAM	Quadrature Amplitude Modulation
QPSK	Quadrature Phase Shift Keying
RF	Radio Frequency
ROC	Receiver Operating Characteristic
SIMO	Single Input Multiple Output
SINR	Signal-to-Interference-and-Noise Ratio
SISO	Single Input Single Output
SNR	Signal-to-Noise Ratio
STBC	Space-Time Block Codes
STTC	Space-Time Trellis Codes
SVD	Singular Value Decomposition
UWB	Ultra Wideband
WSSUS	Wide Sense Stationary Uncorrelated Scattering
ZP	Zero Padding

TABLE OF CONTENTS

LIST OF FIGURES

FIGURE   Page

CHAPTER I

INTRODUCTION

A.   Motivation

The concept of Orthogonal Frequency Division Multiplexing (OFDM) was introduced
in the '60s (see e.g., [1,2]). OFDM is an efficient technique for transmitting data over
frequency selective channels and exhibits numerous advantages over the conventional
serial transmission schemes. It is a block modulation scheme where a block of in-
formation symbols is transmitted in parallel on subcarriers [3]. A simplified block
diagram of an OFDM system is shown in Fig. 1. The time duration of an OFDM
symbol is in general much larger than that of a single-carrier system.
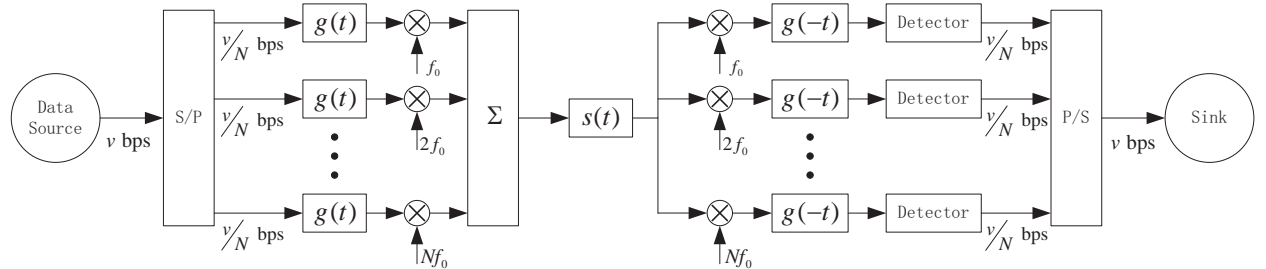
Fig. 1. A simplified block diagram of OFDM.

An OFDM modulator can be implemented as an inverse discrete Fourier trans-
form (IDFT) on a block of information symbols followed by an analog-to-digital con-
verter (ADC). To mitigate the effects of intersymbol interference (ISI) caused by
channel time spread, each block of IDFT coefficients is typically preceded by a cyclic
prefix (CP) or a guard interval consisting of samples, such that the length of the CP

is at least equal to the multipath channel delay spread. Under this condition, the linear convolution between the transmitted sequence and the channel is converted into a circular convolution. As a result, the effects of the ISI are easily and completely eliminated. In frequency domain, OFDM converts a frequency-selective channel into a parallel collection of frequency flat subchannels.

The subcarriers exhibit the minimum frequency separation required to maintain orthogonality of their corresponding time domain waveforms, yet the signal spectra corresponding to the different subcarriers overlap in the frequency domain. Hence, the available bandwidth is used very efficiently. If knowledge of the channel is available at the transmitter, then the OFDM transmitter can adapt its signaling strategy to match the channel. Due to the fact that OFDM uses a large collection of narrowly spaced subchannels, these adaptive strategies can approach the ideal water pouring capacity of a frequency-selective channel.

The high spectral efficiency advantage of OFDM systems is due to the orthogonality among subcarriers. However, in an OFDM link, the subcarriers are orthogonal only if the receiver is perfectly synchronized to the transmitter. Before an OFDM receiver can demodulate the subcarriers, it has to perform at least two synchronization tasks. First, it has to find out the location of the symbol boundary and the optimal symbol timing to minimize the effects of inter-carrier interference and inter-symbol interference. Second, it has to estimate and correct the carrier frequency offset of the received signal since any frequency offset introduces inter-carrier interference. This is not surprising since imperfect synchronization causes system performance degradation even in a noiseless environment. However, obtaining near perfect synchronization is not simple. In the presence of channel fading, synchronization becomes a very challenging task. Therefore, it is of much significance to find measures to improve the existing synchronization methods.

Multiple antennas can be employed both at the transmitter and receiver to form an arrangement called a multiple-input multiple-output (MIMO) system. MIMO communications provides a number of potential performance benefits compared to traditional single antenna links [4, 5]. One of the benefits of MIMO systems is the availability of spatial diversity. Diversity is a powerful technique for mitigating the effects of fading due to the multipath propagation of wireless signals. The main idea behind diversity is to provide different replicas of the transmitted signal to the receiver. If these different replicas fade independently, it is less probable to have all copies of the transmitted signal in deep fades simultaneously. Therefore, the receiver can reliably recover the transmitted signal using these received signals. Hence, diversity as a common signal processing technique can also be expected to help the synchronization task of communication systems.

In principle, timing synchronization is a continuous parameter estimation problem. However, in practical implementations, most digital communication receivers sample the output of the demodulator periodically at the symbol rate or a multiple of the symbol rate. Therefore, the potential timing offsets are in a discrete set. Given this discrete set, synchronization is a multiple statistical hypothesis test [6]. Without the knowledge of channel transfer function and noise statistical property, timing synchronization becomes a composite hypothesis testing problem. In composite hypotheses tests, generalized likelihood ratio test (GLRT) is believed to be asymptotically optimal in the situation where no uniformly most powerful test exists [7]. Therefore, GLRT can be expected to provide satisfactory results for timing synchronization, especially in the presence of spatial diversity.

The objective of this study is to develop compensatory measures to improve the synchronization in OFDM-based communication systems.

B. Literature Survey

The demand for multimedia wireless communications is growing at a rapid pace and this trend is expected to continue in the future. The common feature of many current wireless standards for high-rate multimedia transmission is the adoption of a multi-carrier air interface based on orthogonal frequency division multiplexing (OFDM). The idea behind OFDM is to convert a frequency-selective channel into a collection of frequency-flat subchannels with partially overlapping spectra. This goal is achieved by splitting the input high-rate data stream into a number of substreams that are transmitted in parallel over orthogonal subcarriers [8,9]. Compared to conventional single-carrier systems, OFDM offers increased robustness against multipath distortions as channel equalization can easily be performed in the frequency domain through a bank of one-tap multipliers [10]. Furthermore, it provides larger flexibility by allowing independent selection of the modulation parameters (like the constellation size and coding scheme) over each subcarrier [11]. Due to its favorable features, OFDM has been adopted in some commercial systems such as digital audio broadcasting (DAB) [12], terrestrial digital video broadcasting (DVB-T) [13], and the IEEE 802.11a wireless local area network (WLAN) [14].

Despite its appealing features, the design of an OFDM system poses several technical challenges. One basic issue is related to the stringent requirement on frequency and timing synchronization [15, 16]. OFDM is extremely sensitive to timing errors and carrier frequency offsets between the incoming waveform and the local references used for signal demodulation. Inaccurate compensation of the frequency offset destroys orthogonality among subcarriers and produces inter-carrier interference (ICI). Timing errors result in inter-symbol interference (ISI) and must be counteracted to avoid severe error rate degradations. Using a sufficiently long guard interval between

adjacent OFDM symbols (in the form of a cyclic prefix) provides intrinsic protection against timing errors at the expense of some reduction in data throughput as a consequence of the extra overhead. However, timing accuracy becomes a stringent requirement in those applications where the cyclic prefix (CP) is made as short as possible to minimize the overhead. The impact of these synchronization errors on the performance of CP-OFDM systems has been analyzed in literature quite thoroughly (see e.g., [17–20] and the references cited therein).

Recently a zero-padding (ZP) scheme has been proposed as an alternative to the CP in OFDM transmissions [21]. The advantage of using a ZP is that the transmitter requires less power back-off at the analog amplifier. Since the correlation caused by the cyclic prefix creates discrete spectral lines (ripples) into the average power spectral density of the transmitted signal and the radio emission power levels are limited by the FCC, the presence of any ripples in the power spectral density (PSD) requires additional power back-off at the transmitter. In fact, the amount of power back-off that is required is equal to the peak-to-average ratio of the PSD. For a CP-OFDM system, this power back-off could be as large as 1.5 dB, which would result in a lower overall range for the system [22]. When a ZP is used instead of CP, the ripples in the PSD can be reduced to zero with enough averaging. Therefore, ZP-OFDM is currently adopted in multiband (MB) OFDM based ultra-wideband (UWB) systems [23]. However, the problem of assessing the effects of residual synchronization errors in MB-ZP-OFDM based UWB systems has not yet been addressed. These residual synchronization errors always exist no matter what kind of synchronization technique is employed. Due to the high sensitivity of OFDM systems to the synchronization errors, it is worthwhile to investigate the effects of residual carrier frequency error, phase jitter and timing offset on the performance of a MB-ZP-OFDM system, as these are the actual errors that the receiver has to tolerate.

The MIMO technique is mainly based on the theoretical work accomplished by Telatar [5] and Foschini [24]. It provides diversity in a fading environment and increases the capacity of the wireless channel linearly by proper coding techniques [25, 26]. Combining OFDM with MIMO technique is a promising approach to provide higher rate transmissions [3]. Similarly to conventional single-input single output (SISO) OFDM, MIMO-OFDM is also sensitive to synchronization errors.

Since the synchronization problem is of paramount importance to OFDM based systems, many synchronization methods have been proposed (see e.g. [27–32]). In particular, synchronization methods associated with OFDM systems are divided into two classes, i.e., data-aided and blind methods. Data-aided frequency acquisition and tracking were proposed in [29], where periodically inserted known symbols were explicitly used. In [27], Schmidl and Cox proposed a training symbol based timing/frequency synchronization using an OFDM symbol with identical halves. The drawback of data-aided synchronization methods is the overhead associated with the pilots or training in the OFDM symbols. Blind estimators are bandwidth efficient and have attracted increasing interests in this area, since they do not require extra overhead. Method in [30] extracts carrier frequency offset (CFO) information by correlating the last samples of OFDM symbols with the CP. However, the estimation error is usually higher than 1% of the subcarrier spacing at moderate signal-to-noise ratio (SNR) since the CP is affected by the frequency selective fading. Liu and Tureli [31] applied super-resolution MUSIC-like methods to the CFO estimation. Since subspace methods need the search of the unknown frequency offset, the computational complexity is high.

Due to its high spectral efficiency, the MIMO-OFDM transmission concept is being considered as a potential candidate for future communication systems to provide high data rate and operate at low SNR. For OFDM, several subcarriers are employed

within a limited bandwidth carrying orthogonal subcarrier signals. The multiple antenna technique, known by the term MIMO, allows the simultaneous transmission of independent spatially multiplexed data streams. Additional to this feature, a MIMO system offers spatial diversity, which results from the fact that multiple independently faded copies of each transmitted signal are present at a multi-antenna receiver. The multiple versions of the signals created by diversity need to be combined together to improve the performance of the receiver. There are four main combining methods that are in general utilized at the receiver [33]: maximum ratio combining (MRC), where the received signals are weighted with respect to their signal-to-noise ratio (SNR) and then summed up; selection combining, where the signal with the highest SNR is used; equal gain combining (EGC), where all the received signals are summed coherently with equal weights; and switched combining, where the receiver switches to another signal when the current signal drops below a predefined threshold. The spatial diversity available in MIMO systems expands another dimension that can be exploited to improve the synchronization procedure [34–36]. In [34], only receive diversity is exploited to improve timing/frequency synchronization, moreover, the performance analysis was omitted. In [35,36], unmodulated (virtual) subcarriers and receive diversity are utilized to improve the blind CFO estimator. Highly accurate blind frequency offset estimation can be achieved by exploiting the orthogonality between the signal subspace expanded by modulated subcarriers and the noise subspace expanded by unmodulated subcarriers. However, when there is no virtual subcarriers, these methods will fail.

Timing synchronization has been investigated in various contexts. For SISO systems, synchronization is often achieved by finding the peak in the correlation between received date and a known reference [37]. This concept can be extended to MIMO systems [32, 38]. If the OFDM system uses a preamble, then reference-

correlation approaches can be exploited [39]. As an alternative, it is common to exploit the delayed-correlation properties of cyclic prefixes used by OFDM systems for synchronization [27, 30]. Cyclic-prefix-based test statistics can also be extended to MIMO systems [32, 40].

In essence, timing synchronization is a continuous parameter estimation problem. However, in practical implementations, most digital communication receivers require timing synchronization no better than a fraction of a sample period. Therefore, the potential timing offsets are in a discrete set. Given this discrete set, in principle, timing synchronization is a multiple statistical hypothesis test [6, 41]. This type of multiple hypothesis test can be treated as a sequence of binary statistical hypothesis tests [42]. At each potential timing offset, the null hypothesis is that the signal is mis-aligned or does not exist. And the alternative hypothesis is that the signal of interest is properly aligned in time. At each testing point in time, a test statistic is evaluated given the observed data. Synchronization is declared if the test statistic threshold is exceeded. In composite hypotheses tests where the conditional probability densities contain unknown nuisance parameters, the optimal test statistic is not clear. However, it is believed that the generalized likelihood ratio test (GLRT) is asymptotically optimal in the situation where no uniformly most powerful (UMP) test exists [7]. Given its superiority in the presence of nuisance parameters, a GLRT-based timing synchronization method can be developed [6].

C. Outline and Contributions of this Dissertation

The content of this dissertation is separated into two parts. In the first part of this dissertation, the sensitivity of OFDM systems to the residual synchronization errors is studied in Chapter II. The second part of this dissertation focuses on the impact

of spatial diversity on synchronization performance. It is found that spatial diversity can be used as an effective compensatory measure to combat the synchronization errors. Finally Chapter V concludes this dissertation.

In Chapter II, a theoretical analysis is conducted to quantitatively study the effects of residual synchronization errors on OFDM-based communication systems. In particular, for zero-padding (ZP) OFDM systems, a tight upper bound of the inter-carrier interference (ICI) power is obtained. It is shown that the system performance is limited by the ICI due to imperfect synchronization. In MIMO-OFDM systems, the ICI power due to residual synchronization errors is accumulated from multiple receive antennas, therefore degrades the system performance even more. All these results suggest that for a reliable information reception, compensatory measures must be taken to relieve the performance degradation. Most of the material in Chapter II has been partially presented in [43–47].

The second part of dissertation proposes some compensatory measures to enhance the synchronization reliability for OFDM receivers. In Chapter III, the spatial diversity in MIMO communications is introduced as a measure to compensate the synchronization errors. A conventional preamble-based synchronization scheme originally proposed for SISO OFDM systems was extended to MIMO-OFDM systems. This scheme exploits the spatial diversity inherent to MIMO systems at both transmitter side and receiver side. The performance of the synchronization method in terms of detection probability of acquisition, mean-square errors of the frame boundary of frame and carrier frequency offset is assessed through both theoretical analysis and computer simulations. It is shown that spatial diversity can favorably improve the synchronization performance. Data-aided and non-data-aided maximum likelihood symbol timing estimators for MIMO-OFDM systems are introduced. It is shown by computer simulations that by exploiting the spatial diversity, synchronization per-

formance of MIMO-OFDM systems in terms of mean-square error of residual timing offsets becomes significantly more reliable when compared to conventional SISO OFDM systems, and thus it can improve the overall signal reception. The material in Chapter III has been published in [44].

In Chapter IV, GLRT-based timing synchronization methods are proposed for MIMO and MIMO-OFDM systems in frequency flat and frequency selective fading environments, respectively. Test statistics are developed. The performance of the proposed methods in terms of asymptotic detection probability is analyzed. It is shown that the asymptotic performance can serve as an upper bound even in the presence of a limited number of observations. Computer simulations show that the asymptotic bound is tight with more than 64 observations. Therefore, a good benchmark for comparing the performance of different timing synchronizers is obtained. The selection of several system design parameters is also discussed. The material in Chapter IV has been partly published in [48].

D.   Related Publications

The research work conducted by the candidate Yi Zhou for his Ph.D. dissertation leads to the following publications:

1. **Yi Zhou**, Yik-Chung Wu, Erchin Serpedin, and Khalid Qaraqe, "The Effects of Spatial Diversity on the Synchronization of MIMO-OFDM Systems," invited book chapter in OFDM and OFDMA with Linear Diversity for Future Wireless Communications, Bentham Science Publishers, 2010.

2. **Yi Zhou**, and Erchin Serpedin, "Generalized Likelihood Ratio Test for Data-Aided Timing Synchronization in MIMO Systems," submitted to IEEE Transaction on Communications.

3. Kai Shi, **Yi Zhou**, Burak Kelleci, Timothy W. Fischer, Erchin Serpedin and Aydin I. Karsilayan, "Impacts of Narrowband Interference on OFDM-UWB Receivers: Analysis and Mitigation," IEEE Transaction on Signal Processing, Vol. 55, No. 3, pp. 1118-1128, Mar. 2007.

4. **Yi Zhou**, Aydin I. Karsilayan and Erchin Serpedin, "Sensitivity of Multi-Band ZP-OFDM Ultra Wideband Receivers to Synchronization Errors," IEEE Transaction on Signal Processing, Vol. 55, No. 2, pp. 729-734, Feb. 2007.

5. Burak Kelleci, Timothy W. Fischer, Kai Shi, **Yi Zhou**, Aydin I. Karsilayan, and Erchin Serpedin, "Narrowband Interference Suppression in Multi-Band OFDM Ultra Wideband Communication Systems: A Mixed-Mode Approach," in Proceedings of the 12th Digital Signal Processing Workshop and the 4th Signal Processing Education Workshop, 2006, pp. 55-59.

6. Kai Shi, **Yi Zhou**, Burak Kelleci, Timothy W. Fischer, Erchin Serpedin and Aydin I. Karsilayan, "Impact of Narrowband Interference on Multi-Band OFDM Ultra Wideband Communication Systems," in Proceedings of the 12th Digital Signal Processing Workshop and the 4th Signal Processing Education Workshop, 2006, pp. 50-54.

7. Kai Shi, Burak Kelleci, Timothy W. Fischer, **Yi Zhou**, Erchin Serpedin and Aydin I. Karsilayan, "On the Design of Robust Multiband OFDM Ultra-Wideband Receivers," 2005 Texas Wireless Symposium, Oct. 2005.

E.   Commonly Used Notations

The following are the notations commonly used in this dissertation. The symbols $\mathbf{x}^*$, $\mathbf{x}^T$, $\mathbf{x}^\dagger$ and $\|\mathbf{x}\|$ denote the complex conjugate, transpose, Hermitian transpose and

the Euclidean norm of vector $\mathbf{x}$, respectively. $|\mathbf{H}|$ and $\|\mathbf{H}\|_F$ stand for the determinant and the Frobenius norm of matrix $\mathbf{H}$, respectively. Notation $\otimes$ denotes the Kronecker product and $\text{vec}(\mathbf{H})$ stands for the column vector formed by stacking the columns of $\mathbf{H}$ one on top of each other. Matrix $\mathbf{I}_N$ denotes the identity matrix of order N. Notations $\Re\{x\}$, $\Im\{x\}$ and $\mathbf{E}\{x\}$ denote the real part, imaginary part and expectation of x, respectively. The symbol $\delta(\cdot)$ stands for the Kronecker delta function. Notation j is defined as $\sqrt{-1}$.

CHAPTER II

SENSITIVITY OF OFDM RECEIVERS TO SYNCHRONIZATION ERRORS

In this chapter, we will analyze the sensitivity of both single input single output (SISO) OFDM and multiple input multiple output (MIMO) OFDM systems to the residual synchronization errors. In particular, in the SISO setup, we will investigate the zero-padding (ZP) OFDM technique which was proposed for multi-band ultra-wideband communication systems [23] due to its relatively lower variation in spectrum. In the MIMO case, the conventional cyclic prefix (CP) OFDM is studied. The sensitivity is measured in terms of the inter-carrier-interference power and symbol error rate of the overall link.

A. Sensitivity of Multi-Band ZP-OFDM Ultra Wideband Receivers to Synchronization Errors

1.   Introduction

In 2002, the Federal Communications Commission (FCC) allocated 7.5 GHz of spectrum for unlicensed use to commercial ultra wideband (UWB) communication devices [49]. For highly dispersive channels, an orthogonal frequency-division multiplexing receiver is more efficient for capturing the multipath energy than an equivalent single-carrier system using the same total bandwidth. OFDM systems possess additional desirable properties, such as high spectral efficiency, inherent resilience to narrow-band RF interference, and spectral flexibility, which are attractive features to UWB devices. A multi-band (MB) zero-padding (ZP) OFDM based approach to design UWB transceivers has been recently proposed in [22, 23]. In the MB-ZP-OFDM based UWB system the transmitted symbols are time-interleaved across different

frequency subbands as depicted in Fig. 2, where the first ZP-OFDM symbol is transmitted on sub-band 1, the second ZP-OFDM symbol is transmitted on sub-band 3, the third ZP-OFDM symbol is transmitted on sub-band 2, the fourth ZP-OFDM symbol is transmitted on sub-band 1, and so on and so forth.
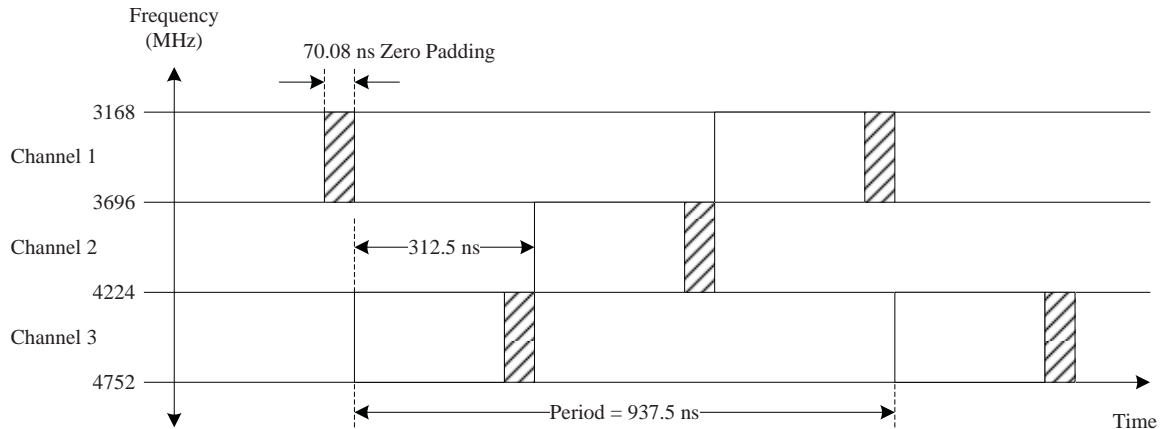
Fig. 2. Signaling diagram of the MB-OFDM system.

Conventionally, the cyclic prefix (CP) is used to eliminate the inter-symbol interference (ISI) caused by multi-path. With cyclic extension, the linear convolution channel is transformed into a circular convolution channel, and the inter-symbol interference can be easily resolved [2]. However, usage of cyclic prefix is not the only solution to combat the multipath. Zero-padding (ZP) has been recently proposed as an alternative to the CP in OFDM transmissions [21]. The advantage of using a ZP is that the transmitter requires less power back-off at the analog amplifier. Since the correlation caused by the cyclic prefix creates discrete spectral lines (ripples) into the average power spectral density of the transmitted signal and the radio emission power levels are limited by the FCC, the presence of any ripples in the power spectral density (PSD) requires additional power back-off at the transmitter. In fact, the amount of power back-off that is required is equal to the peak-to-average ratio of the PSD. For

a CP-OFDM system, this power back-off could be as large as 1.5 dB, which would result in a lower overall range for the system [22]. When a ZP is used instead of CP, the ripples in the PSD can be reduced to zero with enough averaging. Therefore, ZP-OFDM is currently adopted in MB-OFDM based UWB systems [23].

The high spectral efficiency advantage of OFDM systems is due to the orthogonality among sub-carriers. Similar to the standard CP-OFDM systems, ZP-OFDM systems are sensitive to carrier and timing synchronization errors. The presence of carrier frequency offset causes a reduction of desired signal amplitude at the detector output and introduces inter-carrier interference (ICI) due to the loss of orthogonality among sub-carriers. Timing offset results in the rotation of the OFDM sub-carrier constellation. As a result, an OFDM system cannot recover the transmitted signal without a near perfect synchronization, especially when high order QAM constellations are used.

The synchronization errors studied herein are carrier offset errors and sampling time errors. The carrier offset is the difference between the local-oscillator (LO) in the receiver and the carrier of the transmitted signal, and includes carrier frequency error as well as carrier phase error. The synchronization error due to the difference between the optimum sampling time in the receiver and the actual sampling time is called sampling timing error. The ZP-OFDM synchronization process can be divided into an initial coarse frequency and timing acquisition step followed by a fine frequency and timing tracking step. The coarse acquisition can be achieved by correlating the received and the transmitted preamble in time domain [23]. After the initial acquisition step, the carrier frequency and timing offsets are usually quite small, e.g., the carrier frequency offset could be less than one half of the carrier spacing and the timing offset might be within a single sample interval. The impact of these synchronization errors on the performance of CP-OFDM systems has been analyzed

in literature quite thoroughly (see e.g., [17–20]). However, the problem of assessing the effects of residual synchronization errors in multiband ZP-OFDM based UWB systems has not yet been addressed. These residual synchronization errors always exist no matter what kind of synchronization technique is employed. Due to the high sensitivity of OFDM systems to the synchronization errors, it is worthwhile to investigate the effects of residual carrier frequency error, phase jitter and timing offset on the performance of a MB-ZP-OFDM system, as these are the actual errors that the receiver has to tolerate.

2. System Model

Since the transmissions in different subbands of a MB-ZP-OFDM transceiver are independent one with respect to another, and only one common frequency synthesizer is recommended to be used for all subbands in the receiver due to implementation complexity and cost reason (see [23]), the overall performance loss of a MB-ZP-OFDM receiver due to imperfect synchronization is the same as the loss induced by synchronization errors in a ZP-OFDM receiver operating in a single frequency subband. Therefore, it is sufficient to analyze the performance of a ZP-OFDM receiver that assumes only a single frequency subband.

The single-band ZP-OFDM system to be considered is depicted in Fig. 3. To combat the interference introduced by the dispersive channel, each ZP-OFDM symbol (with N subcarriers) is appended with V zero samples. Thus, a number of $P = N + V$ samples are to be transmitted. At the receiver end, an overlap and add method is used to transform the linear convolution channel into a circular convolution channel. Upon truncation of the trailing zero part and its addition to the start of the symbol, each block is transformed via the fast Fourier transform (FFT) - an operation that converts the frequency-selective channel into a set of parallel flat-fading independent

subchannels.
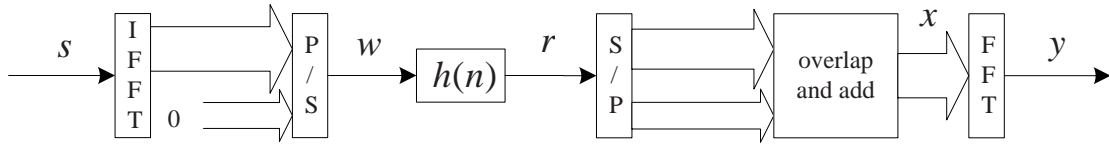
Fig. 3. Transmission scheme of ZP-OFDM systems.

The ZP-OFDM symbol assumes the following expression after sampling:

$$w_k = \begin{cases} \sum_{n=0}^{N-1} s_n e^{j\frac{2\pi kn}{N}}, & k = 0, \cdots, N-1 \\ 0, & k = N, \cdots, N+V-1 \end{cases}, \tag{2.1}$$

where w_k and s_n stand for the transmitted samples and information bits, respectively. Without loss of generality, the transmitted symbol stream is assumed uncorrelated and normalized to unit power:

$$\mathbf{E}\left\{s_{n_1} s_{n_2}^*\right\} = \delta(n_1 - n_2) . \tag{2.2}$$

Upon passing through a frequency selective FIR channel, the received sequence is expressed as

$$r_m = e^{j\phi_m} \sum_{k=0}^{P-1} w_k h_{m-k} + v_m, \quad m = 0, \cdots, P-1 , \tag{2.3}$$

where ϕ_m represents the residual carrier phase jitter which varies in a random manner and is modeled as a zero-mean stationary random process with variance σ_ϕ^2. Here, note that no specific distribution is assumed for ϕ_m. The L complex coefficients of the FIR channel h_p, $p = 0, \cdots, L-1$, are assumed independent circularly and normally distributed random variables with correlation:

$$\mathbf{E}\left\{h_{p_1} h_{p_2}^*\right\} = \sigma_{h,p_1}^2 \delta(p_1 - p_2) , \tag{2.4}$$

and the channel power normalized to unity:

$$\sum_{p=0}^{L-1} \mathbf{E}\left\{|h_p|^2\right\} = \sum_{p=0}^{L-1} \sigma_{h,p}^2 = 1 \ . \tag{2.5}$$

For $p \notin \{0, 1, \cdots, L-1\}$, $h_p = 0$. To avoid inter-symbol interference (ISI), the length of channel is assumed to satisfy the condition $L \leq V$. The additive noise term v_m is modeled as an independent circularly and normally distributed random variable with zero-mean and variance σ^2. Since the noise is uncorrelated with the transmitted symbol stream, and the goal is to assess only the effects of the synchronization errors on the performance of ZP-OFDM receiver, the additive noise term is for the moment dropped from derivations. The effect of additive noise will be considered later.

Upon the overlap and add operation, the received signal is expressed as

$$x_l = \begin{cases} r_l, & l = V, \cdots, N-1 \\ r_l + r_{l+N}, & l = 0, \cdots, V-1 \end{cases}, \tag{2.6}$$

and the output of FFT is given by:

$$y_q = \frac{1}{N} \sum_{l=0}^{N-1} x_l e^{-j\frac{2\pi(l+\Delta l)(q+\Delta q)}{N}}, \quad q = 0, \cdots, N-1 \ , \tag{2.7}$$

where Δq and Δl stand for the normalized carrier frequency offset (NCFO) and timing offset, respectively. Assuming the timing offset varies slowly compared to the ZP-OFDM symbol duration, Δl can be treated as a constant within the observation time.

3.   Effects of Imperfect Synchronization

In this section, we analyze the effects of imperfect synchronization. Using a first-order Taylor series expansion and omitting the second and higher order terms, the following

approximation holds for small values of ϕ_l:

$$e^{j\phi_l} \approx 1 + j\phi_l \ . \tag{2.8}$$

Plugging (2.8) into (2.7) and ignoring the second-order imperfections, Eq. (2.7) takes the form:

$$y_q = Z_q + J_{1q} + J_{2q} \ , \tag{2.9}$$

where

$$
Z_q = \frac{e^{-j\frac{2\pi q\Delta l}{N}}}{N} \left[\sum_{l=0}^{N-1}\sum_{k=0}^{N-1}\sum_{n=0}^{N-1} s_n e^{j\frac{2\pi kn}{N}} h_{l-k} e^{-j\frac{2\pi(q+\Delta q)}{N}} \right.
$$
$$
\left. + \sum_{l=0}^{V-1}\sum_{k=0}^{N-1}\sum_{n=0}^{N-1} s_n e^{j\frac{2\pi kn}{N}} h_{l+N-k} e^{-j\frac{2\pi(q+\Delta q)}{N}} \right] \tag{2.10}
$$

$$
J_{1q} = \frac{je^{-j\frac{2\pi q\Delta l}{N}}}{N} \sum_{l=0}^{N-1}\sum_{k=0}^{N-1}\sum_{n=0}^{N-1} s_n e^{j\frac{2\pi kn}{N}} h_{l-k}\phi_l e^{-j\frac{2\pi(q+\Delta q)}{N}} \tag{2.11}
$$

$$
J_{2q} = \frac{je^{-j\frac{2\pi q\Delta l}{N}}}{N} \sum_{l=0}^{V-1}\sum_{k=0}^{N-1}\sum_{n=0}^{N-1} s_n e^{j\frac{2\pi kn}{N}} h_{l+N-k}\phi_{l+N} e^{-j\frac{2\pi(q+\Delta q)}{N}} \ . \tag{2.12}
$$

The component Z_q contains not only the desired signal part but also the inter-carrier interference (ICI) caused by carrier frequency errors, while J_{1q} and J_{2q} denote the interference induced by carrier phase jitter. Furthermore, since symbol windowing is not necessary in ZP-OFDM systems, the constant timing offset during a symbol interval results in only the rotation of the sub-carrier constellation and it can be corrected by equalizer on symbol basis. Hence, it will not cause system performance degradation.

The ICI part of Z_q can be upper bounded by

$$ICI(\Delta q) \le \frac{1}{N} \sum_{m=0}^{N-1}\sum_{\substack{n=0 \\ n\neq m}}^{N-1} \left| \frac{\sin(\pi(n-m+\Delta q))}{N\sin(\pi(n-m+\Delta q)/N)} \right|^2 \ , \tag{2.13}$$

a result whose proof is deferred to the Appendix. Assuming that the residual car-

rier frequency offset and phase jitter are independent, the total ICI power can be approximated as:

$$
\begin{aligned}
ICI_{total} &= ICI(\Delta q) + \mathbf{E}\left\{|J_{1q}|^2\right\} + \mathbf{E}\left\{|J_{2q}|^2\right\} \\
&\approx \frac{1}{N}\sum_{m=0}^{N-1}\sum_{\substack{n=0 \\ n\neq m}}^{N-1}\left|\frac{\sin(\pi(n-m+\Delta q))}{N\sin(\pi(n-m+\Delta q)/N)}\right|^2 + \frac{\sigma_\phi^2}{N}\sum_{k=0}^{N-1}\sum_{l=k}^{k+V-1}\sigma_{h,l-k}^2 \\
&= \frac{1}{N}\sum_{m=0}^{N-1}\sum_{\substack{n=0 \\ n\neq m}}^{N-1}\left|\frac{\sin(\pi(n-m+\Delta q))}{N\sin(\pi(n-m+\Delta q)/N)}\right|^2 + \sigma_\phi^2\,,
\end{aligned}
\tag{2.14}
$$

where in deriving the terms of the second line in equation (2.14), expressions (A.12) and (A.13) from the Appendix were used.

Due to the random nature of the normalized residual carrier frequency offset, it makes more practical sense to take expectation of ICI with respect to Δq. However, as can be found in expression (2.14), it is very difficult to obtain a closed-form expression for ICI even for the simplest probability distribution of Δq. Therefore, numerical evaluation is required.

The signal power can be estimated as:

$$
S_1 = \left|\frac{\sin(\Delta q\pi)}{N\sin((\Delta q\pi)/N)}\right|^2 \approx \left|\frac{\sin(\Delta q\pi)}{\Delta q\pi}\right|^2\,.
\tag{2.15}
$$

The overlap and add operation slightly increases the noise power at the receiver end, and it is straightforward to show that the noise power in one subcarrier is given by:

$$
N_w = \frac{N+V}{N}\sigma^2\,.
\tag{2.16}
$$

As the transmitted signal and the channel impulse response are both normalized to unit power, the signal power at the output of the FFT block is still equal to unity. Thus, the signal-to-interference and noise ratio (SINR) degradation due to imperfect

synchronization is given by

$$D = 10\log\frac{S_1 N_w}{N_w + ICI_{total}} \ .$$

(2.17)

4.   Simulation Results

In this section, the performance of the ZP-OFDM system under imperfect synchronization will be evaluated by conducting computer simulations. Since the large bandwidth of UWB waveforms significantly increases the ability of the receiver to resolve the different paths in the channel, a special statistical model should be used to take into account this unique characteristic of UWB channels. The IEEE 802.15.3a standard group selected the Saleh-Valenzuela (S-V) model to capture this behavior [50]. This model relies on a statistical process to model the discrete arrivals of the multipath components in clusters, as well as the rays within a cluster. The channel model used here is Channel Model 1 (CM1) [51] (the best 90 out of 100 channel realizations). The ZP-OFDM system assumes a 128-point FFT operation and a 37-sample long zero-padding. The information sequence is QPSK modulated.

In the presence of only carrier frequency offset, the inter-carrier interference power is plotted versus the normalized carrier frequency offset in Fig. 4. The curve marked with circles represents the actual ICI power from computer simulations while the curve with stars denotes the upper bound derived in (A.11). Fig. 4 illustrates that the derived upper bound predicts very accurately the ICI power. This shows that the upper bound can be used to estimate the ICI power in (2.14). And it is also easily found that the ICI power assumes a monotonic increasing behavior with respect to the normalized carrier frequency error.

Fig. 5 plots the ICI power versus the normalized carrier frequency offset assuming various levels of carrier phase jitter. These simulation results point out that the ZP-
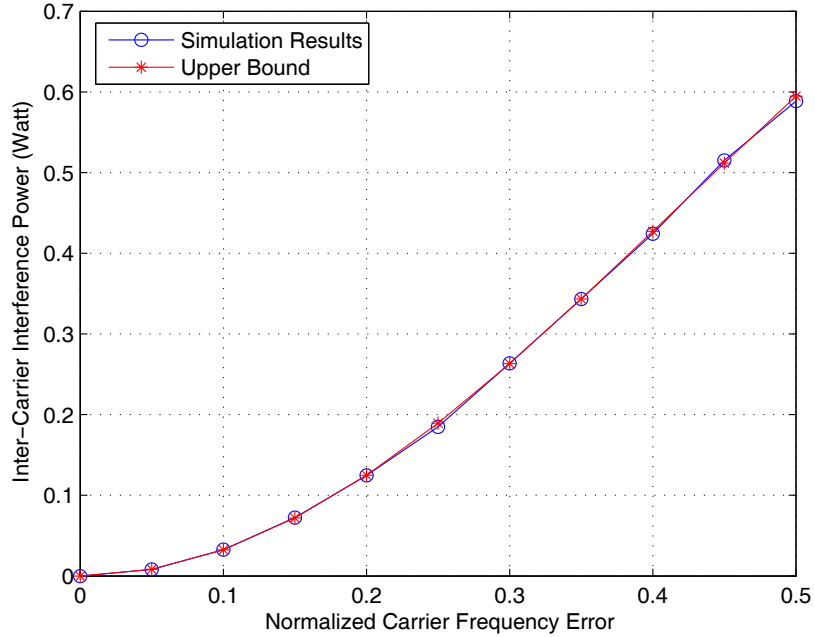
Fig. 4. ICI caused by carrier frequency offset.

OFDM receiver is not very sensitive to carrier phase jitters under the assumption that different channel coefficients are uncorrelated. However, the ICI power raises rapidly when the carrier frequency offset increases.

Assuming the normalized residual carrier frequency offset Δq follows a Gaussian distribution with zero mean and σ_q^2 variance, the total ICI power is plotted in Fig. 6 versus the standard deviation over the range of $[1/12 \quad 1/4]$ for various levels of the carrier phase jitter. It is shown that the ICI power increases with the NCFO almost linearly in this range. With σ_q being sufficiently large, the Gaussian distribution can be considered a good approximation of a uniform distribution. In this case, one can obtain $ICI_{total} = 0.226W$ in the case of no carrier phase jitter.

The SINR loss due to the synchronization imperfection is shown in Fig. 7. It is found that as the transmitted SNR increases, the SINR degradation caused by
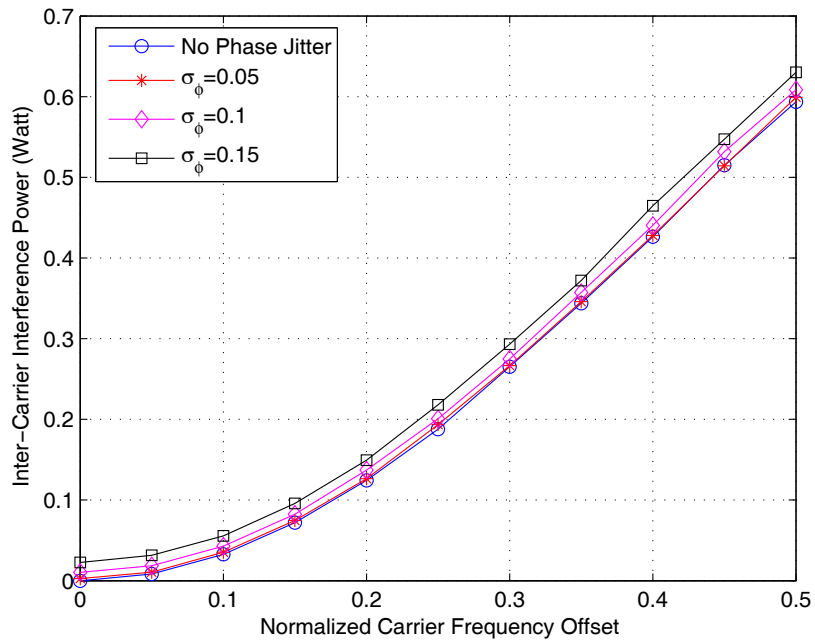
Fig. 5. ICI caused by carrier synchronization imperfection.
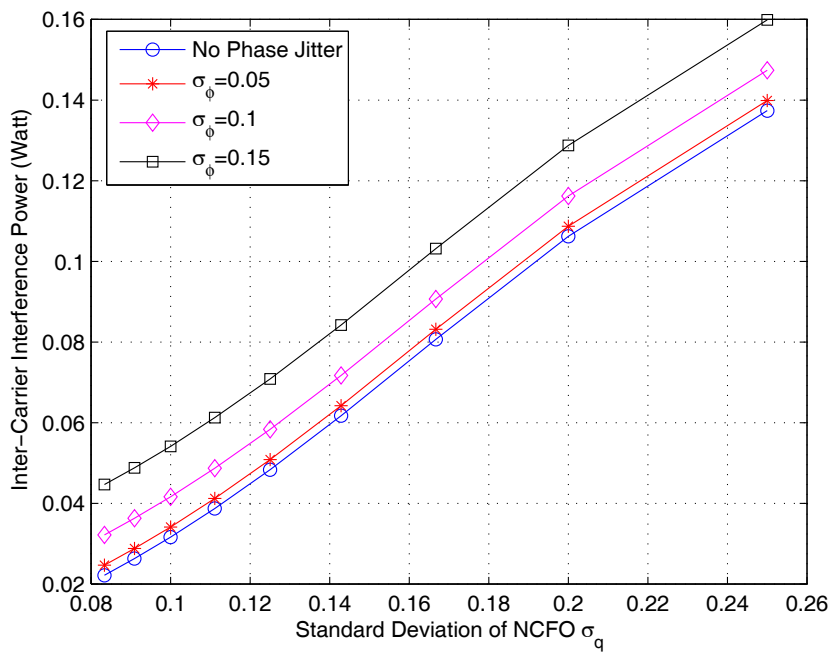
Fig. 6. ICI caused by carrier synchronization errors.
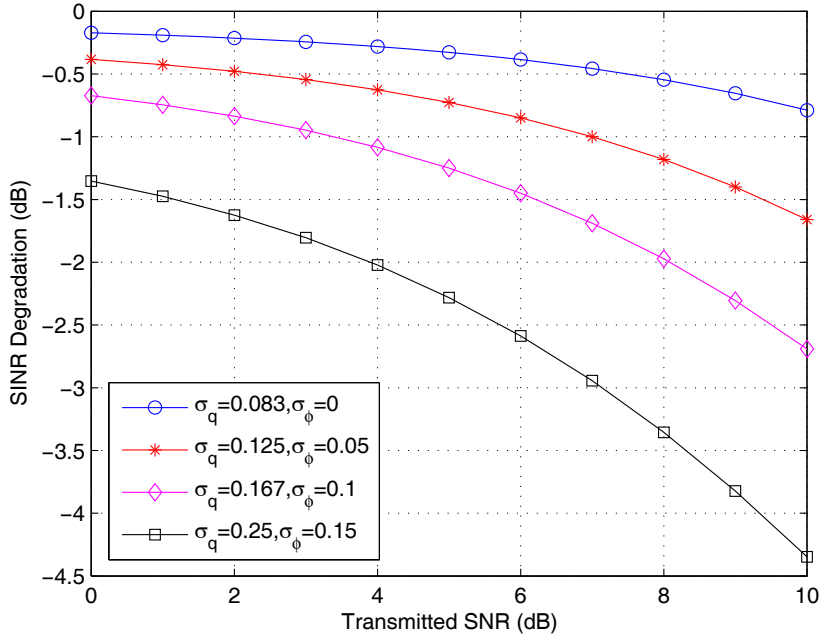
Fig. 7. SINR degradation.

imperfect synchronization becomes more severe.

Fig. 8 illustrates the overall impacts of imperfect synchronization on the ZP-OFDM system. Three groups of curves are presented corresponding to SNR = 10 dB, 6 dB and 0 dB respectively, each of which consisting of two setups, with and without carrier phase jitter, respectively. Compared to carrier frequency offset, ZP-OFDM systems are robust to carrier phase jitter, a fact which matches the conclusion inferred from Fig. 5. It is also observed in Fig. 8 that the gap between the curves in each group increases as the SNR goes up. This is because the ICI due to imperfect synchronization becomes dominant in the high SNR regime compared to thermal noise.
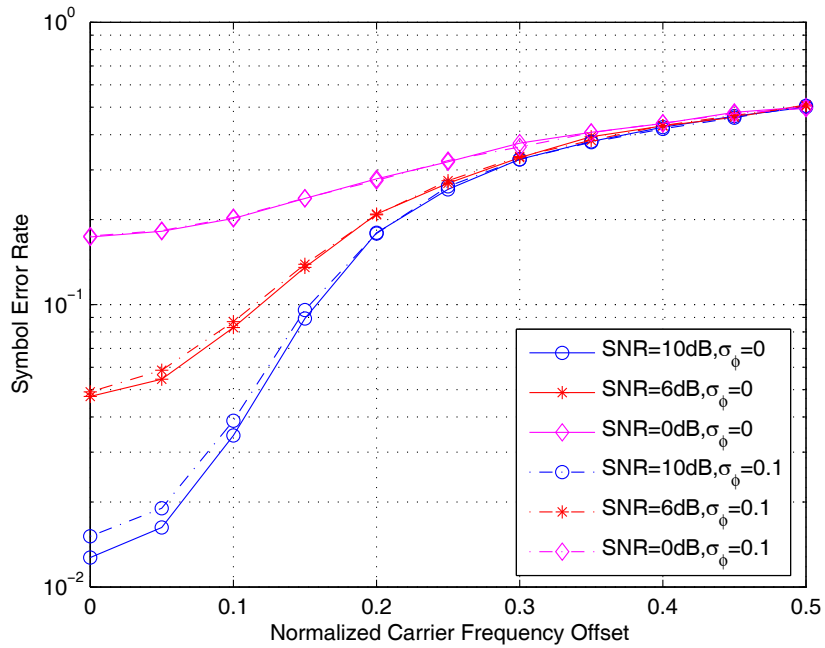
Fig. 8. Symbol error rates with imperfect synchronization.

B. Sensitivity of MIMO-OFDM Receivers to Synchronization Errors

Multiple input multiple output (MIMO) systems exploit spatial diversity by using several transmit and receive antennas. MIMO-OFDM combines together OFDM and MIMO techniques, thereby, achieving spectral efficiency and spatial diversity or increased throughput. A MIMO-OFDM system transmits independent OFDM modulated data from multiple antennas simultaneously. In this section, the sensitivity of MIMO-OFDM receivers to both carrier frequency offset and symbol timing offset is analyzed.

Consider a MIMO-OFDM system with N transmit and M receive antennas. The signal transmitted by the nth transmit antenna at the pth OFDM symbol and at subcarrier k is denoted in terms of the variable $d_n^k(p)$ and assumes the mean transmit

power:

$$\sigma_d^2 = E\{|d_n^k(p)|^2\}.$$

The OFDM complex baseband signal for the nth transmit antenna is expressed as follows:

$$s_n(t) = \frac{1}{\sqrt{T_u}} \sum_{p=-\infty}^{+\infty} \sum_{k=-K/2}^{K/2-1} d_n^k(p) e^{j\frac{2\pi k}{T_u}(t-T_g-pT_s)} u(t-pT_s) \qquad (2.18)$$

where

$$u(t) = \begin{cases} 1 & 0 \le t < T_s \ , \\ 0 & \text{elsewhere} \ . \end{cases}$$

The notation $T_s = T_u + T_g$ stands for the total symbol duration, and consists of the original information-bearing part of length T_u which is preceded by a guard interval of length T_g. Only K out of L possible subcarriers are used for data transmission, the rest of subcarriers being padded with zeros.

The signal is transmitted over the frequency selective fading channel

$$h_{mn}(\tau, t) = \sum_{i=1}^{L_{mn}} h_{mn}^i(t) \delta(\tau - \tau_{mn}^i), \qquad (2.19)$$

which assumes not only the actual channel impulse response but also the transmission filter, and it is received simultaneously by the M antennas of the receiver. The channel consists of L_{mn} discrete paths with time-variant complex path weights $h_{mn}^i(t)$ and corresponding path delays τ_{mn}^i. For the subject under consideration herein, the wide sense stationary uncorrelated scattering (WSSUS) channel model is assumed, i.e., the weights $h_{mn}^i(t)$ are modeled as wide sense stationary processes and are assumed to be uncorrelated with respect to each other. The channel is further assumed to be quasi-static within one OFDM symbol duration with the dispersion limited in time, specifically, $\tau_{mn}^i < T_g$.

The received signal $r_m(t)$ at the mth antenna is then expressed as

$$r_m(t) = \sum_{n=1}^{N} \sum_{i=1}^{L_{mn}} h_{mn}^i(t) s_n(t - \tau_{mn}^i) + \eta_m(t), \tag{2.20}$$

where $\eta_m(t)$ represents complex additive white Gaussian noise (AWGN) with power σ_N^2. Sampling the signal at time instants $t_l = lT$ and removing the guard interval, the pth received OFDM symbol at antenna m is described by the pre-FFT vector:

$$\mathbf{r}_m^p = [r_{m,0}^p \; r_{m,1}^p \; \cdots \; r_{m,L-1}^p]^T,$$

where $r_{m,l}^p = r_m((l + L_g + pL_s)T)$, $T_u = LT$, $T_g = L_gT$ and $T_s = L_sT$. Following the principle of OFDM, the subcarriers are demodulated applying an FFT of length L on the vector $\mathbf{r}_m^p$. The demodulated subcarrier symbols at the mth receive antenna are then given by

$$z_{m,k}^p = \sum_{l=0}^{L-1} e^{-j\frac{2\pi k}{T_u}lT} r_{m,l}^p = \sum_{n=1}^{N} d_n^k(p) H_{mn}^k(p) + \eta_{m,k}^p, \tag{2.21}$$

where $\eta_{m,k}^p$ denotes the complex additive white Gaussian noise with variance σ_N^2 and

$$H_{mn}^k(p) = \sum_{i=1}^{L_{mn}} h_{mn}^i(pT_s) e^{-j\frac{2\pi k}{T_u}\tau_{mn}^i}$$

represents the channel transfer function at the subcarrier frequency $f_k = k/T_u$ between the nth transmit antenna and the mth receive antenna.

Eq. (2.21) holds only under the assumption of perfect synchronization between transmitters and the receiver. In order to analyze the impact of synchronization imperfections at the receiver, the following disturbances are considered [52]:

- The sampling period of the transmitter T' can be different from T at the receiver. This leads to the relative sampling frequency error of $\zeta = (T' - T)/T'$ and a transmit symbol duration of $T_u' = LT'$.

- The carrier frequencies used for modulating and demodulating the signal are often not necessarily the same. Assuming a small frequency offset relative to the transmission bandwidth, the frequency difference between the transmitter and the receiver oscillators can be modeled as a time-variant phase offset $\theta(t)$ at the receiver. In the following, we will consider a constant phase offset $\theta(t) = \Delta f \cdot t$, where Δf is the carrier frequency offset between transmitter and receiver.

- Due to the burst transmission and the fact that the time scale T' at transmitter is unknown to the receiver, the OFDM symbol window at the receiver which controls the guard interval removal, will usually exhibit an offset from its ideal position by a time denoted by ϵT, where $\epsilon \in [0, L_s)$ and ϵ is restricted without loss of generality to integers to simplify the exposition.

The resulting transmission model is depicted in Fig. 9. The received signal at the mth antenna is then represented as

$$r_m^\epsilon(lT) = \sum_{n=1}^{N} \sum_{i=1}^{L_{mn}} h_{mn}^{\epsilon,i}(lT)e^{j2\pi\Delta flT}s_n(lT - \tau_{mn}^{\epsilon,i}) + \eta_m(lT), \qquad (2.22)$$

where the timing offset is incorporated into the channel model, resulting in the effective channel model that is relevant to the receiver time scale [52]

$$h_{mn}^\epsilon(\tau, t) = h_{mn}(\tau, t) * \delta(\tau - \epsilon T). \qquad (2.23)$$

Therefore, $h_{mn}^{\epsilon,i}(t) = h_{mn}^i(t)$ and $\tau_{mn}^{\epsilon,i} = \tau_{mn}^i - \epsilon T$.

The demodulation of the signals received at the mth receive antenna yields

$$z_{m,k}^p = \sum_{l=0}^{L-1} e^{-j\frac{2\pi k}{T_u}lT} r_m^\epsilon((l + L_g + pL_s)T). \qquad (2.24)$$

Due to the different sampling periods, the optimal symbol timing in the receiver changes with respect to the transmitters. This effect is modeled by an additional
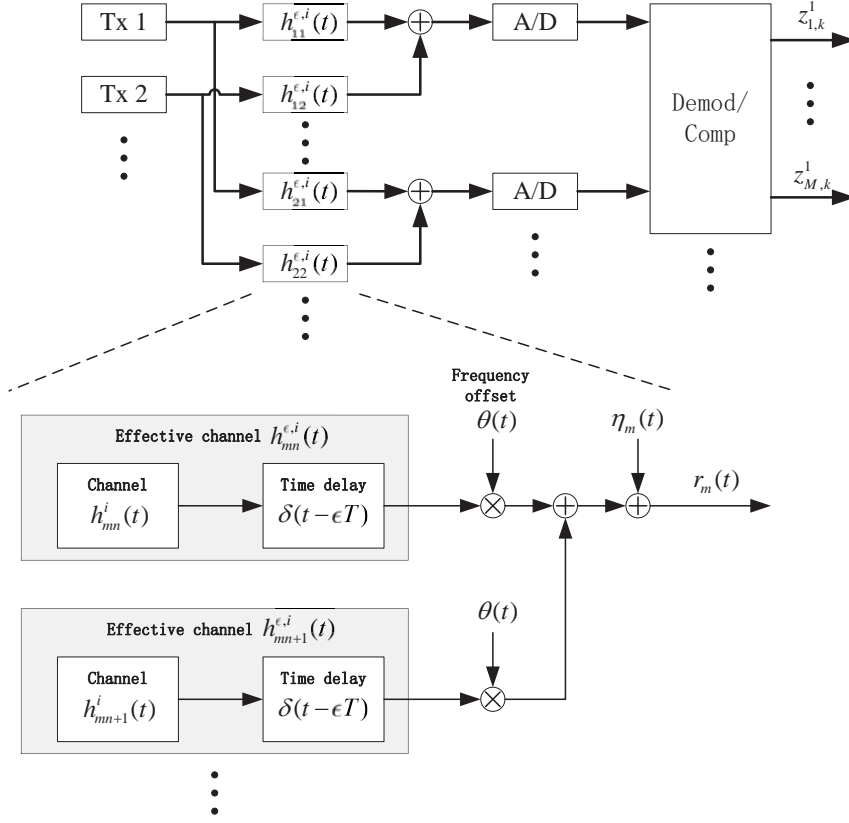
Fig. 9. Baseband model of MIMO transmission including synchronization imperfections.

time variant delay $l_D(p) = (L_g + pL_s)\zeta$. Under these assumptions, in an AWGN channel, the demodulated signal takes the expression:

$$
\begin{aligned}
z_{m,k}^p = & \sum_{n=1}^{N} \sum_{l=0}^{L-\epsilon-1} e^{-j\frac{2\pi k}{T_u}lT} e^{j2\pi\Delta f(l+L_g+pL_s)T} \frac{1}{L} \sum_{i=-K/2}^{K/2-1} d_n^k(p) e^{j\frac{2\pi i}{T_u'}(l+l_D(p)+\epsilon)T} \\
& + \sum_{n=1}^{N} \sum_{l=L-\epsilon}^{L-1} e^{-j\frac{2\pi k}{T_u}lT} e^{j2\pi\Delta f(l+L_g+pL_s)T} \frac{1}{L} \sum_{i=-K/2}^{K/2-1} d_n^k(p+1) e^{j\frac{2\pi i}{T_u'}(l-(L-l_D(p)-\epsilon))T} \\
& + \eta_{m,k}^p \\
= & \, \breve{z}_{m,k}^p + \ddot{n}_{m,k}^p + \eta_{m,k}^p.
\end{aligned}
\tag{2.25}
$$

The demodulated signal (2.25) now consists of a useful portion $\breve{z}_{l,k}^p$, the disturbance caused by the inter-symbol interference (ISI) and inter-channel interference (ICI) $\ddot{n}_{l,k}^p$,

and AWGN $\eta_{m,k}^p$, respectively,

$$\breve{z}_{m,k}^p = \frac{1}{L} \sum_{n=1}^{N} \sum_{l=0}^{L-\epsilon-1} e^{-j\frac{2\pi k}{T_u}lT} e^{j2\pi\Delta f(l+L_g+pL_s)T} d_n^k(p) e^{j\frac{2\pi k}{T_u'}(l+l_D(p)+\epsilon)T}$$

$$\ddot{n}_{m,k}^p = \frac{1}{L} \sum_{n=1}^{N} \left(\sum_{l=0}^{L-\epsilon-1} e^{-j\frac{2\pi k}{T_u}lT} e^{j2\pi\Delta f(l+L_g+pL_s)T} \sum_{i=-K/2, i\neq k}^{K/2-1} d_n^i(p) e^{j\frac{2\pi i}{T_u'}(l+l_D(p)+\epsilon)T} \right.$$

$$\left. + \sum_{l=L-\epsilon}^{L-1} e^{-j\frac{2\pi k}{T_u}lT} e^{j2\pi\Delta f(l+L_g+pL_s)T} \sum_{i=-K/2}^{K/2-1} d_n^i(p+1) e^{j\frac{2\pi i}{T_u'}(l-(L-l_D(p)-\epsilon))T} \right).$$

Define $\Phi_k = \Delta f T_u + k\zeta$ as the local frequency offset [52]. For small residual errors with $\zeta \ll 1$, $\Delta f T_u \ll 1$ and $|\epsilon| \ll L$, $\breve{z}_{m,k}^p$ can be further simplified to [53]

$$\breve{z}_{m,k}^p \approx \sum_{n=1}^{N} e^{j2\pi(\Phi_{0,k}+\Phi_k pL_s)}(1 - \epsilon/L)\mathrm{si}(\pi\Phi_k)d_n^k(p), \qquad (2.26)$$

where $\mathrm{si}(x) = \sin(x)/x$. Here all the phase terms that are constant in time are attributed to $\Phi_{0,k}$.

The interference component $\ddot{n}_{m,k}^p$ is caused by data from other subcarriers and symbols due to the loss of orthogonality. Therefore, $\ddot{n}_{m,k}^p$ is always uncorrelated to $\breve{z}_{m,k}^p$. Ignoring the AWGN,

$$E\{|z_{m,k}^p|^2\} = E\{|\breve{z}_{m,k}^p + \ddot{n}_{m,k}^p|^2\} = E\{|\breve{z}_{m,k}^p|^2\} + E\{|\ddot{n}_{m,k}^p|^2\}. \qquad (2.27)$$

The variance of $\ddot{n}_{m,k}^p$ can be determined as follows:

$$\begin{aligned} \sigma_s^2 &= E\{|\ddot{n}_{m,k}^p|^2\} = E\{|z_{m,k}^p|^2\} - E\{|\breve{z}_{m,k}^p|^2\} \\ &\approx \sigma_d^2 \sum_{n=1}^{N} 1 - \mathrm{si}^2(\pi\Phi_k)[1 - 2|\epsilon/L| + (\epsilon/L)^2], \end{aligned} \qquad (2.28)$$

since $E\{|d_n^k(p)d_m^k(p)|^2\} = 0$ for all $n \neq m$ and because of the channel gain which is assumed to be normalized to unity for each receiving antenna.

Figs. 10 and 11 plot the impact of symbol timing and carrier frequency offset on

the variances of the induced interference normalized to the transmitted symbol power, respectively. The timing and carrier frequency offsets are assumed to be identical across all N transmit antennas. The power of the interference increases linearly with the number of transmit antennas. This means that the power of resulting interference in the case of a MIMO transmission essentially consists of the sum of the interference powers caused by the different single transmit antennas.
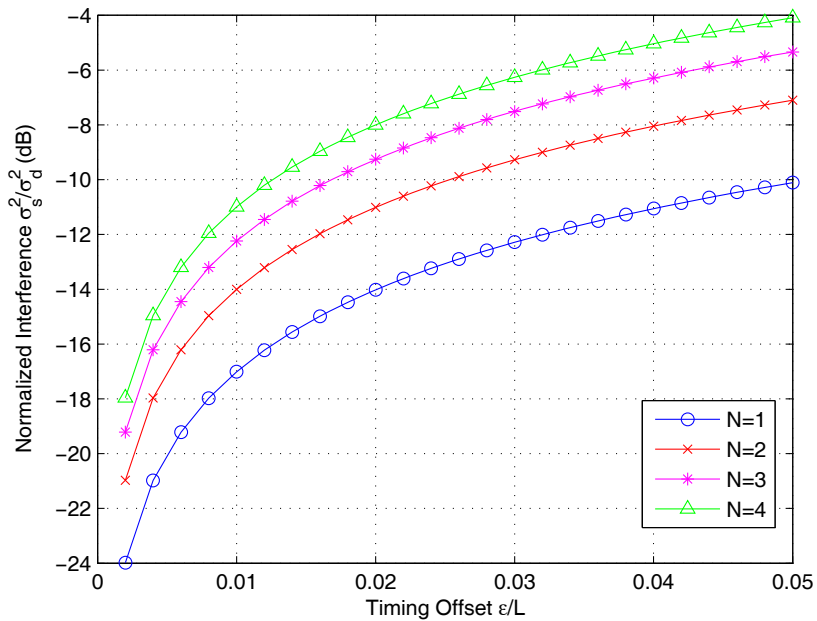
Fig. 10. Power of interference due to timing offset.

As expected, as the residual synchronization errors increase, the induced interference is getting larger resulting in unreliable signal reception. Therefore, effective synchronization methods are greatly needed.
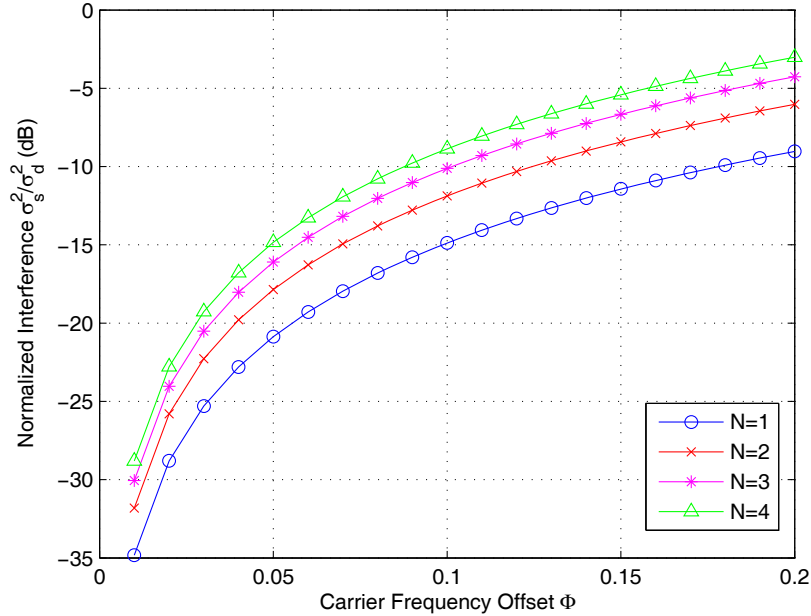
Fig. 11. Power of interference due to carrier frequency offset.

C. Conclusions

This chapter has investigated the effects of synchronization imperfections in SISO multi-band ZP-OFDM based UWB receivers. The types of synchronization errors considered includes residual carrier frequency offset, carrier phase jitter and sampling clock timing offset. In wide-sense stationary uncorrelated scattering (WSSUS) frequency-selective fading channels, the sampling clock timing offset results in rotation of the subcarrier constellation, while carrier frequency offsets and phase jitter cause inter-carrier interference. A tight upper bound of the ICI distortion has been obtained. In addition, a closed-form expression for the SINR degradation due to imperfect synchronization is reported. Simulation results show that the multi-band ZP-OFDM system is very sensitive to carrier frequency offsets. In fact, the system performance in terms of symbol error rate is limited by the inter-carrier interfer-

ence caused by synchronization errors. MIMO-OFDM systems are also sensitive to synchronization errors. Inter-carrier interferences from all the receive antennas are getting accumulated at the receiver, therefore degrade the system performance even more. We conclude this chapter by stating that both SISO and MIMO OFDM systems are sensitive to the residual synchronization errors. For a reliable information reception, compensatory measures must be taken.

CHAPTER III

THE EFFECTS OF SPATIAL DIVERSITY ON THE SYNCHRONIZATION OF
MIMO-OFDM SYSTEMS

This chapter studies the influence of spatial diversity on the synchronization of MIMO-OFDM systems. The effects of spatial diversity on symbol timing and carrier frequency synchronization are investigated. We expect that by exploiting the spatial diversity in MIMO systems, the synchronization performance can be significantly improved. Therefore, spatial diversity can be used as a compensatory measure in wireless fading channels to combat the loss in performance induced by the synchronization errors.

A. Introduction

Multiple antennas can be used both at the transmitter and receiver, an arrangement called a multiple-input multiple-output (MIMO) system. As a special case, a system with only one transmit antenna and multiple receive antennas is called a single-input multiple-output (SIMO) system. Similarly, a system with multiple transmit antennas and one receive antenna is referred to as a multiple-output single-input (MISO) system. A MIMO system takes advantage of the spatial diversity that is achieved by spatially separated antennas in a dense multipath scattering environment. MIMO systems may be implemented in a number of different ways to obtain either a diversity gain to combat signal fading or to achieve a capacity gain. Generally, there are three categories of MIMO signaling mechanisms. The first signaling mechanism aims to improve the power efficiency by maximizing the spatial diversity. Such techniques include delay diversity, space-time block codes (STBC) [54], [25] and space-time trellis codes (STTC) [26]. The second class of MIMO signaling techniques uses a layered

approach to increase capacity. One popular example of such a system is V-BLAST suggested by Foschini et al. [24] where full spatial diversity is usually not achieved. Finally, the third class of signaling methods exploits the knowledge of channel at the transmitter. These methods decompose the channel coefficient matrix using the singular value decomposition (SVD) and exploit the resulting unitary matrices from the SVD as pre- and post-filters at the transmitter and receiver to achieve transmission rates near the channel capacity [55].

Recent developments in MIMO physical layer techniques promise a significant boost in the performance of OFDM systems. Broadband MIMO-OFDM systems with bandwidth efficiencies on the order of 10 b/s/Hz are feasible for LAN/MAN environments [3].

All digital communication systems require some type of synchronization. In passband systems, the carrier frequency is generated in the transmitter from a local timing reference such as a crystal oscillator. In the case of coherent demodulation, the receiver is required to generate reference signals whose phases are identical (except perhaps to a constant offset due to the propagation delay) to those of the signaling alphabet at the transmitter. These reference signals are compared with the incoming signals in the process of making maximum-likelihood symbol decisions. In digital communication systems, the receiver must also be able to sample the output of the demodulator periodically at the symbol rate or a multiple of the symbol rate, in order to recover the transmitted information. Since the propagation delay from the transmitter to the receiver is generally unknown at the receiver, symbol timing must be derived from the received signal.

The high spectral efficiency advantage of OFDM systems is due to the orthogonality among subcarriers. OFDM systems are sensitive to carrier and timing synchronization errors [56–58]. Carrier frequency offset causes a reduction of the desired

signal amplitude at the detector output and introduces intercarrier interference (ICI) due to the loss of orthogonality among subcarriers [59]. Timing offset results in the rotation of the OFDM subcarrier constellation. As a result, an OFDM system cannot recover the transmitted signal without a near perfect synchronization, especially when high-order QAM constellations are used. In particular, for an OFDM system, the problem of carrier frequency offset synchronization reduces to the measurement and correction of the carrier frequency between the receiver and transmitter. Typically the carrier frequency offset is estimated using an autocorrelation operation. In the case of MIMO systems, the results of the autocorrelations applied to each antenna stream can be combined together to provide a more accurate estimate of the frequency offset. The idea of combining the antenna streams for frequency offset detection is justified if the same oscillator is used at all the mixers of the receive antennas. The function of timing synchronization is to determine the proper OFDM symbol alignment, in other words, the determination of the starting time of the FFT window. With known preambles transmitted, timing synchronization can be implemented as a filtering operation through a matched filter.

Diversity is a powerful technique for mitigating the effects of fading due to multipath propagation of wireless signals. The main idea behind diversity is to provide different replicas of the transmitted signal to the receiver. If these different replicas fade independently, it is less probable to have all copies of the transmitted signal in deep fade simultaneously. Therefore, the receiver can reliably recover the transmitted signal using these received signals. There are two important issues related to the concept of diversity. The first aspect is how to provide the replicas of the transmitted signal at the receiver with the lowest possible consumption of the power, bandwidth, processing complexity and other resources. The second issue is how to use these replicas of the transmitted signal at the receiver in order to have the highest reduction in

the probability of error.

The replicas of the transmitted signal can be sent through different means. They can be transmitted in different time slots, via different frequency bands with different polarizations, or through different antennas corresponding to time, frequency, polarization or spatial diversity, respectively. Thus, the general goal is to send two or more copies of the signal through independent fades. The multiple versions of the signals created by different diversity schemes need to be combined together to improve the performance of the receiver. There are four main combining methods that are in general utilized at the receiver [33]: maximum ratio combining (MRC), where the received signals are weighted with respect to their signal-to-noise ratio (SNR) and then summed up; selection combining, where the signal with the highest SNR is used; equal gain combining (EGC), where all the received signals are summed coherently with equal weights; and switched combining, where the receiver switches to another signal when the current signal drops below a predefined threshold.

Diversity as a common signal processing technique is also expected to help the synchronization task of communication systems [60]. This chapter presents an overview on the effects of spatial diversity on the synchronization of MIMO-OFDM systems. The rest of the chapter is organized as follows. Section B investigates the effect of spatial diversity on a preamble-based synchronization scheme for MIMO-OFDM systems. In Section C, a maximum likelihood approach for both data-aided and non-data-aided symbol timing estimation for MIMO-OFDM systems is proposed. The effects of the spatial diversity on the estimators performance are illustrated through computer simulations. Finally, Section D concludes the chapter with general remarks about the effects of diversity on synchronization of MIMO-OFDM systems.

B. Spatial Diversity for the Synchronization of MIMO-OFDM Systems

In this section, we study the influence of spatial diversity on the synchronization of MIMO-OFDM systems. Herein, we analyze the performance of the preamble-based synchronization scheme [61] in terms of detection probability and study the influence of spatial diversity on the symbol timing and carrier frequency offset estimation algorithms. The conventional preamble-based synchronization scheme originally proposed for conventional single-input single output (SISO) OFDM systems was recently extended to MIMO-OFDM systems in [61]. This scheme exploits the spatial diversity inherent to MIMO systems. It is shown to exhibit significantly improved performance when compared to the performance of synchronization algorithms proposed for SISO systems.

The frequency difference between the oscillators at transmitter and receiver is denoted as the carrier frequency offset (CFO) [62]. At the receiver, the CFO leads to a shift of the baseband information signal in the frequency domain. As shown in the previous chapter, in a MIMO-OFDM system, a frequency shift has a devastating effect, as the mutual orthogonality of the subcarrier signals is destroyed and severe interference for the single subcarrier signals arises. To enable a reliable detection of the subcarrier signals, compensation of the CFO is mandatory. In addition, in a burst transmission, where data may be transmitted at random time instants in several consecutive blocks, called frames, the timing information must be available. As the exact beginning of a frame (BOF) cannot be predicted at the receiver, it has to be reliably detected.

These two tasks, detection and compensation of CFO, and detection of the BOF, are addressed jointly within a single synchronization procedure. Often to ease the receiver's synchronization, predefined training symbols are inserted into every trans-

mission frame. Also, at the receiver, the specific structure of these training symbols is exploited to obtain estimates of the CFO and BOF. When a burst transmission is started, the receiver usually operates in the acquisition mode [63]. At that time, usually no prior information about the quantities to be estimated is available, therefore the estimation process has to be very robust and reliable. For acquisition purposes, each transmission frame is preceded by a synchronization sequence, called a preamble. For OFDM systems, the preamble usually consists of a repetition of predefined OFDM symbols. Next, we will show the synchronization scheme in detail.

1. Timing and Carrier Frequency Synchronization Algorithms

a. Basic Algorithm

Many synchronization algorithms for OFDM systems in the acquisition mode are based on the scheme developed by Schmidl and Cox [27]. Synchronization is performed in the time domain. At the BOF, at time instant $d = 0$, two identical OFDM symbols of length L are transmitted by the transmitter (see Fig. 12). At the receiver, an autocorrelation is performed by correlating the received signal $r(d)$ with its complex conjugated and shifted by L samples replica:

$$P(d) = \sum_{m=0}^{L-1} r(d+m)r^*(d+m+L),$$

(3.1)

where d denotes the discrete time index, and the size of the correlation window is equal to L. If the two succeeding identical synchronization symbols are correlated, the amplitude of the correlation function $P(d)$ generates a peak value. Detection of this peak value provides the information regarding the BOF, denoted here by the estimated time instant $\hat{d}$. Assuming a frequency-flat channel, the BOF will lie at $\hat{d} = 0$.
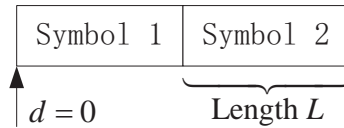
Fig. 12. Synchronization sequence at the beginning of frame.

As the CFO causes a shift of the information signal in the frequency domain, in the time domain the samples of the information signal are phase-rotated with a time-continuous phase. It then follows that all the terms in the sum of Eq. (3.1) present a constant phase ϕ, if the two identical symbols are correlated. Thus, we can estimate ϕ by determining the actual phase of function P at time instant $\hat{d}$:

$$\hat{\phi} = \arg\left(P(\hat{d})\right). \tag{3.2}$$

As the estimation range of the phase ϕ is limited to $[-\pi, \pi]$, the frequency range for the CFO estimation is limited as well. With this estimation method, a CFO up to half the subcarrier spacing present within one OFDM synchronization symbol can be estimated properly. To increase the estimation range of the method, a larger subcarrier spacing can be chosen by using only every n-th subcarrier present within the synchronization symbols. This leads to shorter synchronization symbols, since L is decreased by a factor of n. To maintain robustness against the system noise, the number of repetitive synchronization symbols is increased by the same factor, and the size of the correlation window in Eq. (3.1) is adapted to $(2n-1)L$ [61].

b.   Exploiting Spatial Diversity for Synchronization

The spatial diversity of the MIMO system can be exploited to improve the synchronization performance.

Consider a MIMO system with N transmit antennas and M receive antennas.

First transmit diversity is considered. Multiple transmit antennas create additional propagation paths between transmitter and receiver. As no prior knowledge of the channel is available during the initial synchronization phase, the power is distributed equally over all transmit antennas. If the synchronization signals which run over the different propagation paths are added constructively at the receiver, an averaging operation over all these different paths is enabled. Through the averaging process, the influence of propagation paths with poor transmission quality is diminished. Thus, it leads to an improvement in the quality of the synchronization signal at the receiver. Hence, an improvement of the synchronization is expected if transmit diversity is constructively exploited. Now assume that N different synchronization symbols $\mathbf{s}_n$, $n = 1, \cdots, N$, are represented as vectors, each containing L elements according to the length of the synchronization symbol. For achieving synchronization, transmit antenna n transmits $\mathbf{s}_n$ twice. Then the received signal at receive antenna m is expressed as

$$
\begin{aligned}
\mathbf{r}_{m,1} &= \sum_{n=1}^{N} h_{mn}\mathbf{s}_n + \mathbf{n}_{m,1} \\
\mathbf{r}_{m,2} &= e^{j\phi}\sum_{n=1}^{N} h_{mn}\mathbf{s}_n + \mathbf{n}_{m,2},
\end{aligned}
\tag{3.3}
$$

where $\mathbf{r}_{m,1} = [r_m(0)\ r_m(1)\ \cdots\ r_m(L-1)]^T$ and $\mathbf{r}_{m,2} = [r_m(L)\ r_m(L+1)\ \cdots\ r_m(2L-1)]^T$ are the received symbols corresponding to the first and second repetitive synchronization symbol at the mth receive antenna, respectively. The random variable h_{mn} stands for the complex channel gain between the nth transmit antenna and the mth receive antenna. It is further assumed that h_{mn}'s are independent, identically distributed (i.i.d.) zero mean, unit variance circularly symmetric complex Gaussian random variables, and that $\mathbf{n}_{m,1}$ and $\mathbf{n}_{m,2}$ are zero-mean complex Gaussian noise vectors with covariance matrix $\sigma_n^2\mathbf{I}_L$.

As the two consecutively transmitted symbols are identical, the signal parts of the two received vectors at the mth receive antenna differ only by a constant phase term stemming from the CFO. If orthogonal sequences are selected as synchronization symbols $\mathbf{s}_n$, $n = 1, \cdots, N$, the correlation of the two received symbols at the mth receive antenna according to Eq. (3.3) can be expressed as the inner product of the two vectors $\mathbf{r}_{m,1}$ and $\mathbf{r}_{m,2}$:

$$
\begin{aligned}
P_m(d)|_{d=0} &= \mathbf{r}_{m,1}^\dagger \mathbf{r}_{m,2} = e^{j\phi}(\sum_{n=1}^{N} h_{mn}\mathbf{s}_n + \mathbf{n}_{m,1})^\dagger (\sum_{n=1}^{N} h_{mn}\mathbf{s}_n + \mathbf{n}_{m,2}) \\
&= e^{j\phi}(L\sum_{n=1}^{N} |h_{mn}|^2 + \sum_{n=1}^{N} h_{mn}\mathbf{n}_{m,1}^\dagger \mathbf{s}_n + \sum_{n=1}^{N} h_{mn}^* \mathbf{s}_n^\dagger \mathbf{n}_{m,2} + \mathbf{n}_{m,1}^\dagger \mathbf{n}_{m,2}) \\
&= e^{j\phi}(L\sum_{n=1}^{N} |h_{mn}|^2 + U_m),
\end{aligned}
\tag{3.4}
$$

where $U_m = \sum_{n=1}^{N} h_{mn}\mathbf{n}_{m,1}^\dagger \mathbf{s}_n + \sum_{n=1}^{N} h_{mn}^* \mathbf{s}_n^\dagger \mathbf{n}_{m,2} + \mathbf{n}_{m,1}^\dagger \mathbf{n}_{m,2}$. This shows that by selecting orthogonal synchronization symbols, the correlation achieves an accumulation of the complete signal energy after channel transmission.

Turning next to receive diversity, a method to take advantage of the receive diversity in a SIMO system was proposed in [34]. Here, a similar approach is followed. At the mth receive antenna, a correlation similar to (3.4) is calculated based on the received signals $\mathbf{r}_{m,1}$ and $\mathbf{r}_{m,2}$ (see Fig. 13). The output signals of the single correlators all exhibit a peak at a nearly identical time instant $\hat{d} = 0$. At the individual peak positions, all correlation signals have an identical phase stemming from the CFO. In the samples lying closely around this peak, the phase is varying slowly and hence may be considered constant. Thus, if we consider the sum of the outputs of the single correlators on a sample-by-sample basis, all the signal components will be summed up coherently, forming an aggregated correlation function P_G with an improved signal-to-noise level, which then can be used for the proposed estimation task.
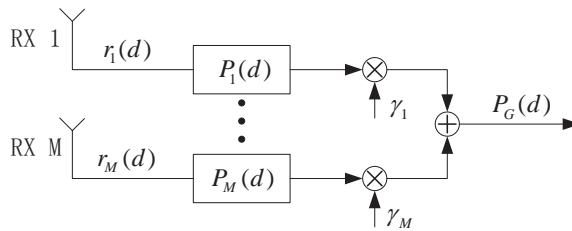
Fig. 13. Exploitation of receive diversity for synchronization.

To coherently combine the outputs of the correlators, we may apply the weights γ_m at the single output signals of the correlators as depicted in Fig. 13. It seems appropriate to choose these weights according to the amount of signal energy that is gathered at each receive antenna. Hence, a good choice would be the height of the peaks in the single autocorrelation functions P_m resulting in

$$\gamma_m = \max_d(|P_m(d)|) , \tag{3.5}$$

which is similar to the maximum ratio combining (MRC) approach. A simple addition of the signals without any prior weighting is referred to as equal gain combining (EGC), corresponding to $\gamma_m = 1$, $m = 1, \cdots, M$. This scheme has the benefit of being fairly easy to implement, for the price of a slight performance loss.

2.   Performance Analysis

At the ideal symbol timing position $\hat{d} = 0$, $P_m(0)$ can be decomposed into the in-phase (which assumes the phase $\hat{\phi}$) and quadrature components. This is just another way of looking at the problem with a new set of axes, with one axis in the direction of ϕ, and the other perpendicular to it. For practical SNR ranges, the quadrature part will be small compared to the in-phase component and thus can be neglected

$$|P_m(0)| \approx L \sum_{n=1}^{N} |h_{mn}|^2 + \Re\{U_m\}, \tag{3.6}$$

where $\Re\{\cdot\}$ stands for real part operation. By invoking the central limit theorem (CLT), $|P_m(0)|$ can be further approximated as a Gaussian random variable with mean

$$\mathbf{E}\{|P_m(0)|\} = LN,$$

and variance

$$\mathrm{Var}\{|P_m(0)|\} = L^2 N + LN\sigma_n^2 + \frac{1}{2}L\sigma_n^4.$$

Assuming equal gain combining (EGC) at the output of the M receive antennas,

$$P_G(0) = \sum_{m=1}^{M} P_m(0), \tag{3.7}$$

it can be readily shown that

$$P_G(0) \sim \mathcal{N}(\mu_p, \sigma_p^2),$$

where $\mu_p = LMN$ and $\sigma_p^2 = L^2 MN + LMN\sigma_n^2 + LM\sigma_n^4/2$.

When there is only noise present at the input of the M receive antennas, the aggregation of the correlation outputs denoted by P_a can be expressed as

$$P_a = \sum_{m=1}^{M} \mathbf{n}_{m,1}^{\dagger} \mathbf{n}_{m,2}. \tag{3.8}$$

It can be easily shown that

$$P_a \sim \mathcal{CN}(0, LM\sigma_n^4),$$

where $\mathcal{CN}(\mu, \sigma^2)$ stands for the complex Gaussian distribution with mean μ and variance σ^2. Therefore, $|P_a|$ follows the Rayleigh distribution,

$$f_{|P_a|}(x) = \frac{x}{\sigma_a^2} e^{-\frac{x^2}{2\sigma_a^2}}, \tag{3.9}$$

where $\sigma_a^2 = LM\sigma_n^4/2$.

The BOF detection problem can be treated as a hypothesis testing. After ob-

serving the output of the combiner, a decision statistic is formed and compared to a threshold. The synchronizer must choose between two possible situations

$$
\begin{aligned}
\mathcal{H}_0: \quad & \mathbf{r}_{m,1} = \mathbf{n}_{m,1} \\
& \mathbf{r}_{m,2} = \mathbf{n}_{m,2}, \ m = 1, \cdots, M, \\
\mathcal{H}_1: \quad & \mathbf{r}_{m,1} = \sum_{n=1}^{N} h_{mn} \mathbf{s}_n + \mathbf{n}_{m,1} \\
& \mathbf{r}_{m,2} = e^{j\phi} \sum_{n=1}^{N} h_{mn} \mathbf{s}_n + \mathbf{n}_{m,2}, \ m = 1, \cdots, M.
\end{aligned} \tag{3.10}
$$

Using the Neyman-Pearson criterion, the optimum test is

$$
\frac{f_{|P_G(0)|}(x)}{f_{|P_a|}(x)} \underset{\mathcal{H}_0}{\overset{\mathcal{H}_1}{\gtrless}} \tilde{T}. \tag{3.11}
$$

After some algebra manipulations, the detector reduces to

$$
g(x) = \frac{\sigma_p^2 - \sigma_a^2}{2\sigma_p^2 \sigma_a^2} x^2 + \frac{\mu_p}{\sigma_p^2} x - \ln x \underset{\mathcal{H}_0}{\overset{\mathcal{H}_1}{\gtrless}} \hat{T}. \tag{3.12}
$$

Letting $Y = g(X)$, the false alarm rate can be calculated as

$$
\alpha = \int_{T}^{\infty} f_{Y_0}(y) dy, \tag{3.13}
$$

where $f_{Y_0}(y)$ stands for the probability density function (pdf) of Y under the hypothesis $\mathcal{H}_0$. By solving $\hat{T}$ for specified α, one can infer the detection probability

$$
\beta = \int_{\hat{T}(\alpha)}^{\infty} f_{Y_1}(y) dy, \tag{3.14}
$$

where $f_{Y_1}(y)$ is the pdf of Y under the hypothesis $\mathcal{H}_1$. Since $g(x)$ is highly nonlinear, this can only be done numerically. Fig. 14 shows a numerical result of the BOF (also the optimal OFDM symbol timing) detection probabilities for various SNRs. The false alarm rate $\alpha = 0.01$ and $L = 16$ are adopted. It turns out that the spatial diversity improves the detection performance greatly. At detection probability of 95%, by
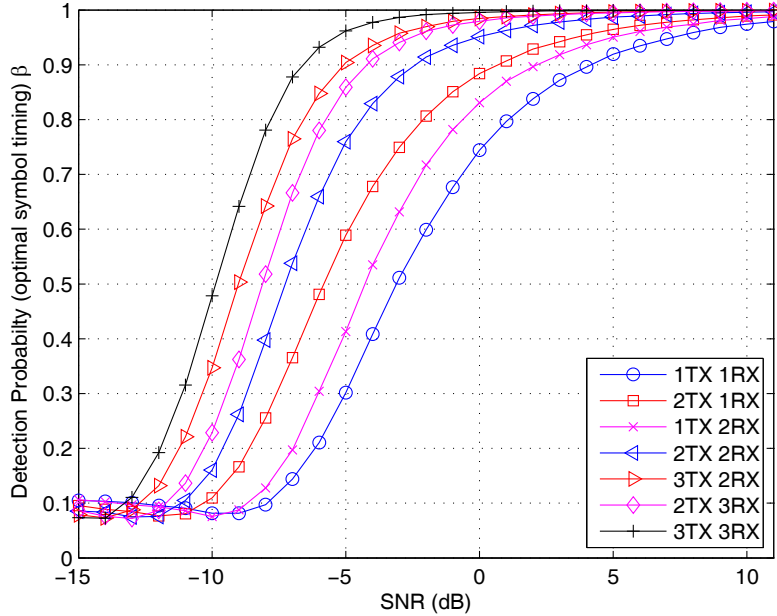
Fig. 14. BOF detection probabilities.

deploying 3 transmit antennas and 3 receive antennas more than 13 dB gain in SNR can be achieved compared to conventional SISO OFDM systems. Also, deploying additional transmit antennas is more efficient than deploying the same number of receive antennas, since more synchronization symbols are transmitted. Note that though the threshold $\hat{T}$ depends on the instantaneous SNR value, it varies little in the SNR region of interest. Hence, in a practical receiver, a default threshold can be applied upon acquiring the timing instant.

3.   Simulation Results

In this subsection, the standard deviations of the BOF and the CFO estimates are evaluated. Simulation is based on the Rayleigh fading MIMO channel model. The computer simulations are performed for different values of SNR at each receive antenna. Gold sequences of length $L = 16$ are chosen for the synchronization symbols in
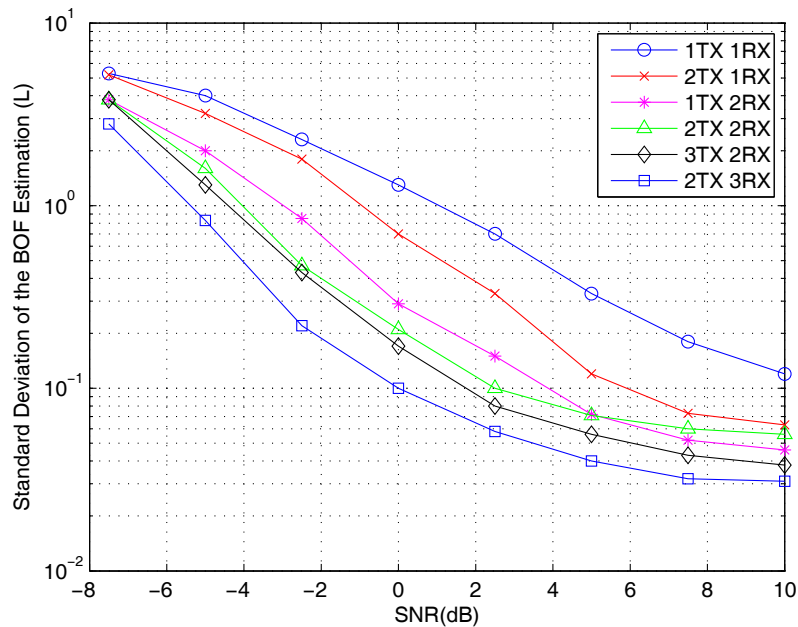
Fig. 15. Standard deviation of the BOF estimation.

the time domain. The entire synchronization preamble was constructed by repeating these symbols 10 times.

The standard deviations of the BOF and CFO estimates were determined for MIMO systems assuming various degrees of spatial diversity. In every simulation run, the synchronization procedure was performed for 10,000 independent channel realizations, the standard deviations of the estimated quantities being determined afterwards. Fig. 15 shows the simulation results for the BOF estimates. It is shown that the synchronization becomes significantly more robust if the spatial diversity is exploited. The comparison of the system performance with no spatial diversity (1×1 case) with that one which assumes a 2×2 diversity shows gains of 6 dB. If additional receive antennas are used, this gain can be further increased, since the utilization of additional receive antennas enables a better noise averaging.

Next we investigated the estimation of the CFO by applying the estimation
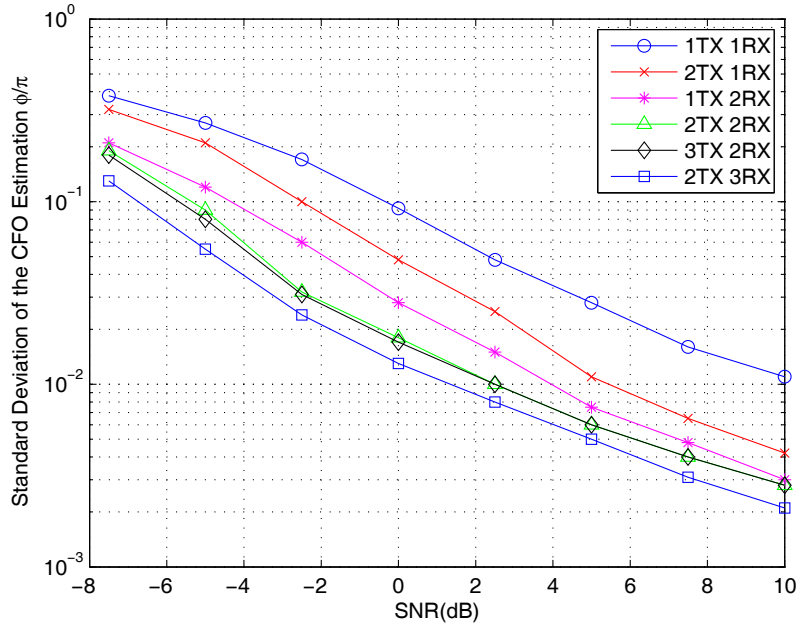
Fig. 16. Standard deviation of the CFO estimation.

algorithm described above. We choose a constant phase factor (resulting from a constant CFO) of $\phi = 0.3\pi$ for simulations. Fig. 16 shows the results. Similar conclusions can be drawn as stated before. A gain of 6 dB can be observed between the 1×1 and the 2×2 system performance at a standard deviation less than 10^{-2}.

In conclusion, a preamble-based synchronization scheme for acquisition was proposed and shown to exploit the available spatial diversity of a MIMO system to improve the overall quality of the synchronization. The scheme was evaluated through simulations, showing high performance gains compared with systems where the spatial diversity effect is totally or partially neglected for achieving the synchronization task. The benefits of the spatial diversity in the synchronization of MIMO-OFDM systems translate into more robust and reliable estimation and correction for the CFO especially for systems operating at low SNRs - a set-up which in particular holds for cellular applications.

C. Maximum Likelihood Symbol Timing Estimation for MIMO-OFDM Systems

In this section, data-aided (DA) and non-data-aided (NDA) maximum likelihood (ML) symbol timing estimators are proposed. This is a natural extension of the symbol timing estimator proposed in [64] to MIMO-OFDM systems. Their conditional Cramer-Rao bound (CCRB) in flat fading channels are derived and the effects of spatial diversity on the CCRB performance of ML estimators is analyzed by means of computer simulations. Our motivation of this choice is that it is mathematically prohibitive to derive the closed-form Cramer-Rao bound for frequency-selective fading channels and the bound for flat fading channels serves as a good approximation for frequency-selective fading channels.

1. Signal Model

Consider a MIMO-OFDM communication system with N transmit and M receive antennas. At each receiving antenna, a superposition of faded signals from all the transmit antennas plus noise is received. The channel is assumed to be frequency flat and quasi-static. The complex baseband representation of the received signal at the mth receive antenna can be expressed as:

$$r_m(t) = \sqrt{\frac{E_s}{NT_s}} \sum_{n=1}^{N} h_{mn} \sum_{k=-K/2}^{K/2-1} d_n^k(p) e^{\frac{j2\pi k}{T_u}(t-T_g-pT_s-\epsilon T)} + \eta_m(t), \ m = 1, 2, \cdots, M,$$

(3.15)

where E_s/N is the energy of each OFDM symbol, h_{mn} is the complex channel gain between the nth transmit antenna and the mth receive antenna. We consider an OFDM system using an inverse discrete Fourier transform of size L for modulation. Each OFDM symbol consists of $K < L$ data symbols $d_n^k(p)$, where n stands for the transmit antenna index, k denotes the subcarrier index and p represents the OFDM

symbol index. The data symbol $d_n^k(p)$ is further assumed to be complex valued with zero mean and $1/K$ variance. The number K is chosen to be small enough to provide guard bands at the edges of the transmission spectrum. Each data symbol is shaped by a rectangular pulse of length T_u and modulated onto a subcarrier with frequency $f_k = k/T_u$. The received signal is sampled with the sampling period $T = T_u/L$. In order to avoid inter-symbol interference (ISI), the OFDM symbol is preceded by a guard interval of length T_g. The resulting symbols are of length $T_s = T_u + T_g$, which is equivalent to $L_s = L + L_g$ samples. The variable ϵ stands for the unknown timing offset normalized to the sampling period and is assumed to be uniformly distributed in the range $[0, L_s)$. The term $\eta_m(t)$ denotes the symmetric complex circular Gaussian white noise at the mth receive antenna with constant power spectral density N_0. Note that the timing offsets between all pairs of transmit and receive antennas are assumed to be the same. This assumption holds for small size transmit and receive antenna arrays.

The received signal vector $\mathbf{r}_m$, which consists of L consecutive received samples from the mth receive antenna can be expressed as (without loss of generality, we assume $p = 0$ and drop the index p in $d_n^k(p)$ and denote it d_n^k in this section):

$$\mathbf{r}_m = \xi \mathbf{\Psi}_\epsilon \mathbf{Z} \mathbf{H}_{m,:}^T + \boldsymbol{\eta}_m, \tag{3.16}$$

where $\xi = \sqrt{\frac{E_s}{NT_s}}$

$$\mathbf{r}_m = [r_m(0)\, r_m(T)\, \cdots\, r_m((L_s-1)T)]^T,$$

$$\mathbf{\Psi}_\epsilon = \begin{bmatrix} e^{\frac{j2\pi(-K/2)(-T_g-\epsilon T)}{T_u}} & e^{\frac{j2\pi(-K/2+1)(-T_g-\epsilon T)}{T_u}} & \cdots & e^{\frac{j2\pi(K/2-1)(-T_g-\epsilon T)}{T_u}} \\ e^{\frac{j2\pi(-K/2)(T-T_g-\epsilon T)}{T_u}} & e^{\frac{j2\pi(-K/2+1)(T-T_g-\epsilon T)}{T_u}} & \cdots & e^{\frac{j2\pi(K/2-1)(T-T_g-\epsilon T)}{T_u}} \\ \vdots & \vdots & & \vdots \\ e^{\frac{j2\pi(-K/2)((L_s-1)T-T_g-\epsilon T)}{T_u}} & e^{\frac{j2\pi(-K/2+1)((L_s-1)T-T_g-\epsilon T)}{T_u}} & \cdots & e^{\frac{j2\pi(K/2-1)((L_s-1)T-T_g-\epsilon T)}{T_u}} \end{bmatrix}$$

$$\mathbf{Z} = [\mathbf{d}_1\, \mathbf{d}_2\, \cdots\, \mathbf{d}_N],$$

$$\mathbf{d}_n = [d_n^{-K/2}\, d_n^{-K/2+1}\, \cdots\, d_n^{K/2-1}]^T.$$

Notation $\mathbf{H}_{m,:}$ denotes the mth row of the matrix

$$\mathbf{H} = \begin{bmatrix} h_{11} & h_{12} & \cdots & h_{1N} \\ h_{21} & h_{22} & \cdots & h_{2N} \\ \vdots & \vdots & & \vdots \\ h_{M1} & h_{M2} & \cdots & h_{MN} \end{bmatrix},$$

and

$$\boldsymbol{\eta}_m = [\eta_m(0)\, \eta_m(T)\, \cdots\, \eta_m((L_s-1)T)]^T.$$

Stacking together the received vectors from all the M receive antennas yields

$$\mathbf{r} = \xi(\mathbf{I}_M \otimes \mathbf{\Psi}_\epsilon)\text{vec}(\mathbf{Z}\mathbf{H}^T) + \boldsymbol{\eta}, \tag{3.17}$$

where $\mathbf{r} = [\mathbf{r}_1^T\, \mathbf{r}_2^T\, \cdots\, \mathbf{r}_M^T]^T$ and $\boldsymbol{\eta} = [\boldsymbol{\eta}_1^T\, \boldsymbol{\eta}_2^T\, \cdots\, \boldsymbol{\eta}_M^T]^T$.

To include the correlation effects between channel coefficients, the channel matrix is expressed as follows:

$$\mathbf{H} = \sqrt{\mathbf{\Phi}_R}\mathbf{H}_{iid}\sqrt{\mathbf{\Phi}_T}^T,$$

where $\mathbf{\Phi}_T$ and $\mathbf{\Phi}_R$ are the power correlation matrices of transmit and receive an-

tenna arrays, respectively. Matrix $\mathbf{H}_{iid} \in \mathbb{C}^{M \times N}$ contains independent, identically distributed (i.i.d.) zero-mean, unit variance, circularly symmetric complex Gaussian entries. Therefore,

$$\mathbf{r} = \xi(\mathbf{I}_M \otimes \boldsymbol{\Psi}_\epsilon)\text{vec}(\mathbf{Z}\sqrt{\boldsymbol{\Phi}_T}\mathbf{H}_{iid}^T\sqrt{\boldsymbol{\Phi}_R}^T) + \boldsymbol{\eta}. \tag{3.18}$$

2. Symbol Timing Estimation with Known Training Data

a. ML Estimator

In this case, the matrix $\mathbf{Z}$ contains the known training data and the only unknown is the channel matrix $\mathbf{H}_{iid}$. Since $\text{vec}(\mathbf{sYB}) = (\mathbf{B}^T \otimes \mathbf{s})\text{vec}(\mathbf{Y})$, Eq. (3.18) can be re-expressed as

$$\begin{aligned}
\mathbf{r} &= \xi(\mathbf{I} \otimes \boldsymbol{\Psi}_\epsilon)(\sqrt{\boldsymbol{\Phi}_R} \otimes \mathbf{Z}\sqrt{\boldsymbol{\Phi}_T})\text{vec}(\mathbf{H}_{iid}^T) + \boldsymbol{\eta} \\
&= \xi(\sqrt{\boldsymbol{\Phi}_R} \otimes \boldsymbol{\Psi}_\epsilon\mathbf{Z}\sqrt{\boldsymbol{\Phi}_T})\text{vec}(\mathbf{H}_{iid}^T) + \boldsymbol{\eta} \\
&= \mathbf{s}_\epsilon\text{vec}(\mathbf{H}_{iid}^T) + \boldsymbol{\eta},
\end{aligned} \tag{3.19}$$

where $\mathbf{s}_\epsilon = \xi(\sqrt{\boldsymbol{\Phi}_R} \otimes \boldsymbol{\Psi}_\epsilon\mathbf{Z}\sqrt{\boldsymbol{\Phi}_T})$ and the second equality comes from the fact that $(\mathbf{s} \otimes \mathbf{B})(\mathbf{C} \otimes \mathbf{D}) = (\mathbf{sB}) \otimes (\mathbf{CD})$.

The joint ML estimate of ϵ and $\text{vec}(\mathbf{H}_{iid}^T)$ is thus obtained by minimizing

$$J_1(\mathbf{r}|\epsilon, \mathbf{h}) = (\mathbf{r} - \mathbf{s}_\epsilon\mathbf{h})^\dagger(\mathbf{r} - \mathbf{s}_\epsilon\mathbf{h}), \tag{3.20}$$

where $\mathbf{h}$ stands for the trial value of $\text{vec}(\mathbf{H}_{iid}^T)$.

Setting the derivative of J_1 with respect to $\mathbf{h}$ to zero, one can easily obtain the ML estimate for $\text{vec}(\mathbf{H}_{iid}^T)$

$$\hat{\mathbf{h}} = (\mathbf{s}_\epsilon^\dagger\mathbf{s}_\epsilon)^{-1}\mathbf{s}_\epsilon^\dagger\mathbf{r}. \tag{3.21}$$

Substituting Eq. (3.21) into Eq. (3.20), after some manipulations and dropping

irrelevant terms, the timing delay can be estimated by maximizing the following likelihood function:

$$\Lambda_{DA}(\epsilon) = \mathbf{r}^\dagger \mathbf{s}_\epsilon (\mathbf{s}_\epsilon^\dagger \mathbf{s}_\epsilon)^{-1} \mathbf{s}_\epsilon^\dagger \mathbf{r}. \tag{3.22}$$

Since $(\mathbf{s} \otimes \mathbf{B})^{-1} = \mathbf{s}^{-1} \otimes \mathbf{B}^{-1}$ and $(\mathbf{s} \otimes \mathbf{B})^\dagger = \mathbf{s}^\dagger \otimes \mathbf{B}^\dagger$, it follows that

$$
\begin{aligned}
\mathbf{s}_\epsilon (\mathbf{s}_\epsilon^\dagger \mathbf{s}_\epsilon)^{-1} \mathbf{s}_\epsilon^\dagger &= \left[\sqrt{\boldsymbol{\Phi}_R} (\sqrt{\boldsymbol{\Phi}_R}^\dagger \sqrt{\boldsymbol{\Phi}_R})^{-1} \sqrt{\boldsymbol{\Phi}_R}^\dagger \right] \\
&\otimes \left[\boldsymbol{\Psi}_\epsilon \mathbf{Z} \sqrt{\boldsymbol{\Phi}_T} (\sqrt{\boldsymbol{\Phi}_T}^\dagger \mathbf{Z}^\dagger \boldsymbol{\Psi}_\epsilon^\dagger \boldsymbol{\Psi}_\epsilon \mathbf{Z} \sqrt{\boldsymbol{\Phi}_T})^{-1} \sqrt{\boldsymbol{\Phi}_T}^\dagger \mathbf{Z}^\dagger \boldsymbol{\Psi}_\epsilon^\dagger \right] \\
&= \mathbf{I}_M \otimes \boldsymbol{\Psi}_\epsilon \mathbf{Z} (\mathbf{Z}^\dagger \boldsymbol{\Psi}_\epsilon^\dagger \boldsymbol{\Psi}_\epsilon \mathbf{Z})^{-1} \mathbf{Z}^\dagger \boldsymbol{\Psi}_\epsilon^\dagger,
\end{aligned}
\tag{3.23}
$$

where in the second equality, we exploited the fact that $\sqrt{\boldsymbol{\Phi}_R}$ and $\sqrt{\boldsymbol{\Phi}_T}$ are both non-singular square matrices.

Therefore, substituting this result back into Eq. (3.22), the DA likelihood function takes the expression

$$
\begin{aligned}
\Lambda_{DA}(\epsilon) &= \mathbf{r}^\dagger (\mathbf{I}_M \otimes \boldsymbol{\Psi}_\epsilon \mathbf{Z} (\mathbf{Z}^\dagger \boldsymbol{\Psi}_\epsilon^\dagger \boldsymbol{\Psi}_\epsilon \mathbf{Z})^{-1} \mathbf{Z}^\dagger \boldsymbol{\Psi}_\epsilon^\dagger) \mathbf{r} \\
&= \sum_{m=1}^M \mathbf{r}_m^\dagger \boldsymbol{\Psi}_\epsilon \mathbf{Z} (\mathbf{Z}^\dagger \boldsymbol{\Psi}_\epsilon^\dagger \boldsymbol{\Psi}_\epsilon \mathbf{Z})^{-1} \mathbf{Z}^\dagger \boldsymbol{\Psi}_\epsilon^\dagger \mathbf{r}_m.
\end{aligned}
\tag{3.24}
$$

The ML symbol timing estimator can thus be expressed as

$$\hat{\epsilon} = \arg\max_\epsilon \Lambda_{DA}(\epsilon). \tag{3.25}$$

b.   The CCRB

For the model used in Eq. (3.19), the CCRB for the timing delay ϵ is given by [64–66]

$$\text{CCRB}_{DA}(\epsilon) = \frac{\sigma^2}{2\text{tr}(\bar{\mathbf{D}}_\epsilon^\dagger \mathbf{P}_{\mathbf{s}}^\perp \bar{\mathbf{D}}_\epsilon \boldsymbol{\Gamma}_{\mathbf{h}})}, \tag{3.26}$$

where $\sigma^2 = N_0/T = N_0 L_s/T_s$ is the noise variance,

$$\bar{\mathbf{D}}_\epsilon = \frac{d\mathbf{s}_\epsilon}{d\epsilon} = \xi \sqrt{\boldsymbol{\Phi}_R} \otimes \mathbf{D}_\epsilon \mathbf{Z} \sqrt{\boldsymbol{\Phi}_T}, \tag{3.27}$$

with $\mathbf{D}_\epsilon = d\boldsymbol{\Psi}_\epsilon/d\epsilon$, and $\mathbf{P}_\mathbf{s}^\perp$ is the orthogonal projector onto the null space of $\mathbf{s}_\epsilon$ and it assumes the expression

$$
\begin{aligned}
\mathbf{P}_\mathbf{s}^\perp &= \mathbf{I}_{ML_s} - \mathbf{s}_\epsilon(\mathbf{s}_\epsilon^\dagger \mathbf{s}_\epsilon)^{-1}\mathbf{s}_\epsilon^\dagger \\
&= \mathbf{I}_M \otimes (\mathbf{I}_{L_s} - \boldsymbol{\Psi}_\epsilon \mathbf{Z}(\mathbf{Z}^\dagger \boldsymbol{\Psi}_\epsilon^\dagger \boldsymbol{\Psi}_\epsilon \mathbf{Z})^{-1}\mathbf{Z}^\dagger \boldsymbol{\Psi}_\epsilon^\dagger) \\
&= \mathbf{I}_M \otimes \mathbf{P}_{\boldsymbol{\Psi}\mathbf{Z}}^\perp,
\end{aligned}
\tag{3.28}
$$

where $\mathbf{P}_{\boldsymbol{\Psi}\mathbf{Z}}^\perp = \mathbf{I}_{L_s} - \boldsymbol{\Psi}_\epsilon \mathbf{Z}(\mathbf{Z}^\dagger \boldsymbol{\Psi}_\epsilon^\dagger \boldsymbol{\Psi}_\epsilon \mathbf{Z})^{-1}\mathbf{Z}^\dagger \boldsymbol{\Psi}_\epsilon^\dagger$, and

$$
\boldsymbol{\Gamma}_\mathbf{h} = \mathbf{E}\left[\text{vec}(\mathbf{H}_{iid}^T)\text{vec}(\mathbf{H}_{iid}^T)^\dagger\right] = \mathbf{I}_{MN} = \mathbf{I}_M \otimes \mathbf{I}_N.
\tag{3.29}
$$

Plugging Eq. (3.27), (3.28) and (3.29) into Eq. (3.26), one can further infer that

$$
\begin{aligned}
\text{CCRB}_{DA}(\epsilon) &= \frac{\sigma^2}{2\xi^2 \text{tr}\left((\sqrt{\boldsymbol{\Phi}_R} \otimes \mathbf{D}_\epsilon \mathbf{Z}\sqrt{\boldsymbol{\Phi}_T})^\dagger (\mathbf{I}_M \otimes \mathbf{P}_{\boldsymbol{\Psi}\mathbf{Z}}^\perp)(\sqrt{\boldsymbol{\Phi}_R} \otimes \mathbf{D}_\epsilon \mathbf{Z}\sqrt{\boldsymbol{\Phi}_T})(\mathbf{I}_M \otimes \mathbf{I}_N)\right)} \\
&= \frac{L_s N}{2\text{tr}(\sqrt{\boldsymbol{\Phi}_R}^\dagger \sqrt{\boldsymbol{\Phi}_R})\text{tr}(\sqrt{\boldsymbol{\Phi}_T}^\dagger \mathbf{Z}^\dagger \mathbf{D}_\epsilon^\dagger \mathbf{P}_{\boldsymbol{\Psi}\mathbf{Z}}^\perp \mathbf{D}_\epsilon \mathbf{Z}\sqrt{\boldsymbol{\Phi}_T})} \left(\frac{E_s}{N_0}\right)^{-1} \\
&= \frac{L_s}{2M\text{tr}(\tilde{\mathbf{Z}}^\dagger \mathbf{D}_\epsilon^\dagger \mathbf{P}_{\boldsymbol{\Psi}\mathbf{Z}}^\perp \mathbf{D}_\epsilon \tilde{\mathbf{Z}}\boldsymbol{\Phi}_T)} \left(\frac{E_s}{N_0}\right)^{-1},
\end{aligned}
\tag{3.30}
$$

where $\tilde{\mathbf{Z}} = \mathbf{Z}/\sqrt{N}$. In passing from the second line to the third line, we made use of the result that $\text{tr}(\mathbf{sB}) = \text{tr}(\mathbf{Bs})$ and that the diagonal entries of $\boldsymbol{\Phi}_R$ are all ones.

3. Non-Data Aided Symbol Timing Estimation

a. ML Estimator

In this case, no training sequence is available and $\mathbf{Z}$ contains unknown random user data. The matrices $\mathbf{Z}$ and $\mathbf{H}_{iid}$ in Eq. (3.18) are unknown and Eq. (3.18) can be expressed in the following form

$$
\mathbf{r} = \xi(\sqrt{\boldsymbol{\Phi}_R} \otimes \boldsymbol{\Psi}_\epsilon)\text{vec}(\mathbf{Z}\sqrt{\boldsymbol{\Phi}_T}\mathbf{H}_{iid}^T) + \boldsymbol{\eta}.
\tag{3.31}
$$

Note that $\boldsymbol{\Phi}_T$ is assumed to be known. However, it cannot be separated from $\mathbf{Z}$ and $\mathbf{H}_{iid}$ since the correlation present in transmit antennas can be merged into the correlation of unknown data or vice versa. Since the noise is white Gaussian, the ML estimator resumes to the minimization of

$$J_2(\mathbf{r}|\epsilon, \mathbf{x}) = (\mathbf{r} - \mathbf{B}_\epsilon \mathbf{x})^\dagger (\mathbf{r} - \mathbf{B}_\epsilon \mathbf{x}),$$

where $\mathbf{B}_\epsilon = \xi(\sqrt{\boldsymbol{\Phi}_R} \otimes \boldsymbol{\Psi}_\epsilon)$, and $\mathbf{x}$ stands for the trial value of $\text{vec}(\mathbf{Z}\sqrt{\boldsymbol{\Phi}_T}\mathbf{H}_{iid}^T)$.

The ML estimate for $\mathbf{x}$ is given by

$$\hat{\mathbf{x}} = (\mathbf{B}_\epsilon^\dagger \mathbf{B}_\epsilon)^{-1} \mathbf{B}_\epsilon^\dagger \mathbf{r}. \tag{3.32}$$

Substituting Eq. (3.32) into Eq. (3.31), after some straightforward calculations and dropping irrelevant terms, the ML symbol timing estimator reduces to the maximization of the following likelihood function

$$\Lambda_{NDA}(\epsilon) = \mathbf{r}^\dagger \mathbf{B}_\epsilon (\mathbf{B}_\epsilon^\dagger \mathbf{B}_\epsilon)^{-1} \mathbf{B}_\epsilon^\dagger \mathbf{r}. \tag{3.33}$$

It can be shown that

$$\mathbf{B}_\epsilon (\mathbf{B}_\epsilon^\dagger \mathbf{B}_\epsilon)^{-1} \mathbf{B}_\epsilon^\dagger = \mathbf{I}_M \otimes \boldsymbol{\Psi}_\epsilon (\boldsymbol{\Psi}_\epsilon^\dagger \boldsymbol{\Psi}_\epsilon)^{-1} \boldsymbol{\Psi}_\epsilon^\dagger,$$

which leads further to

$$\Lambda_{NDA}(\epsilon) = \sum_{m=1}^{M} \mathbf{r}_m^\dagger \boldsymbol{\Psi}_\epsilon (\boldsymbol{\Psi}_\epsilon^\dagger \boldsymbol{\Psi}_\epsilon)^{-1} \boldsymbol{\Psi}_\epsilon^\dagger \mathbf{r}_m. \tag{3.34}$$

The ML symbol timing estimation can thus be expressed as

$$\hat{\epsilon} = \arg \max_\epsilon \Lambda_{NDA}(\epsilon). \tag{3.35}$$

b.   The CCRB

For the model in Eq. (3.31), the CCRB for the timing delay ϵ is given by [64–66]

$$\text{CCRB}_{NDA}(\epsilon) = \frac{\sigma^2}{2\text{tr}(\check{\mathbf{D}}_\epsilon^\dagger \mathbf{P}_\mathbf{B}^\perp \check{\mathbf{D}}_\epsilon \mathbf{\Gamma}_\mathbf{x})}, \tag{3.36}$$

where

$$\check{\mathbf{D}}_\epsilon = \frac{d\mathbf{B}_\epsilon}{d\epsilon} = \xi\sqrt{\mathbf{\Phi}_R} \otimes \mathbf{D}_\epsilon, \tag{3.37}$$

$$\mathbf{P}_\mathbf{B}^\perp = \mathbf{I}_{ML_s} - \mathbf{B}_\epsilon(\mathbf{B}_\epsilon^\dagger \mathbf{B}_\epsilon)^{-1}\mathbf{B}_\epsilon^\dagger = \mathbf{I}_M \otimes \mathbf{P}_\mathbf{\Psi}^\perp, \tag{3.38}$$

with $\mathbf{P}_\mathbf{\Psi}^\perp = \mathbf{I}_{L_s} - \mathbf{\Psi}_\epsilon(\mathbf{\Psi}_\epsilon^\dagger \mathbf{\Psi}_\epsilon)^{-1}\mathbf{\Psi}_\epsilon^\dagger$, and $\mathbf{\Gamma}_\mathbf{x} = \mathbf{E}\left[\text{vec}(\mathbf{Z}\sqrt{\mathbf{\Phi}_T}\mathbf{H}_{iid}^T)\text{vec}(\mathbf{Z}\sqrt{\mathbf{\Phi}_T}\mathbf{H}_{iid}^T)^\dagger\right]$. It can be shown that

$$\mathbf{\Gamma}_\mathbf{x} = \mathbf{I}_M \otimes \mathbf{\Xi}, \tag{3.39}$$

where $\mathbf{\Xi}$ is a Hermitian Toeplitz matrix with elements $[\mathbf{\Xi}]_{mn} = \text{tr}(\mathbf{\Gamma}_\mathbf{z}(n-m)\mathbf{\Phi}_T)$ and $\mathbf{\Gamma}_\mathbf{z}(n-m) = \mathbf{E}\left[\mathbf{Z}_{n,:}^\dagger \mathbf{Z}_{m,:}\right]$ is the averaged cross-correlation matrix of the symbols transmitted with time index difference $n - m$.

Plugging Eqs. (3.37), (3.38) and (3.39) into Eq. (3.36), one can obtain

$$
\begin{aligned}
\text{CCRB}_{NDA}(\epsilon) &= \frac{\sigma^2}{2\xi^2\text{tr}\left((\sqrt{\mathbf{\Phi}_R} \otimes \mathbf{D}_\epsilon)^\dagger(\mathbf{I}_M \otimes \mathbf{P}_\mathbf{\Psi}^\perp)(\sqrt{\mathbf{\Phi}_R} \otimes \mathbf{D}_\epsilon)(\mathbf{I}_M \otimes \mathbf{\Xi})\right)} \\
&= \frac{L_s}{2M\text{tr}(\mathbf{D}_\epsilon^\dagger \mathbf{P}_\mathbf{\Psi}^\perp \mathbf{D}_\epsilon \mathbf{\Xi}/N)}\left(\frac{E_s}{N_0}\right)^{-1}. \tag{3.40}
\end{aligned}
$$

c.   Simulation Results

In this sub-section, the effects of the number of transmit and receive antennas on CCRBs are examined. First, let us assume, $\mathbf{\Phi}_T = \mathbf{I}_N$ and $\mathbf{\Phi}_R = \mathbf{I}_M$ for the moment. Furthermore, it is assumed there is no space-time coding in the NDA case. The effect of the number of transmit antennas N is shown in Figs. 17 and 18 for the DA and NDA cases, respectively, with $M = 4$. From these figures, it turns out that different
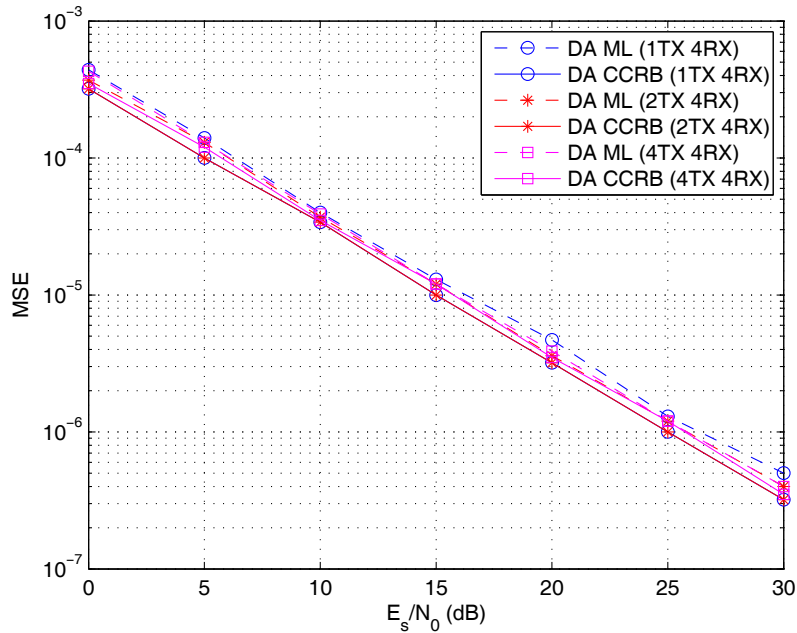
Fig. 17. The MSEs of the data-aided ML estimator and the CCRBs with different
number of transmit antennas.

numbers of transmit antennas result in similar estimation accuracies. Therefore, the
mean squared-errors (MSE) are approximately independent of N for both estimators.
Next, the effect of the number of receive antennas M is shown in Figs. 19 and 20 for
the DA and NDA case, respectively, with $N = 4$. It is clear that increasing M leads
to considerable MSE improvements. Since as expressed by Eqs. (3.30) and (3.40), the
CCRBs are inversely proportional to M and from Figs. 19 and 20, the performances
of both DA and NDA estimators are very close to their corresponding CCRBs, it
can be concluded that the MSEs of both DA and NDA estimators are approximately
inversely proportional to M.

Fig. 18. The MSEs of the non-data-aided ML estimator and the CCRBs with different number of transmit antennas.
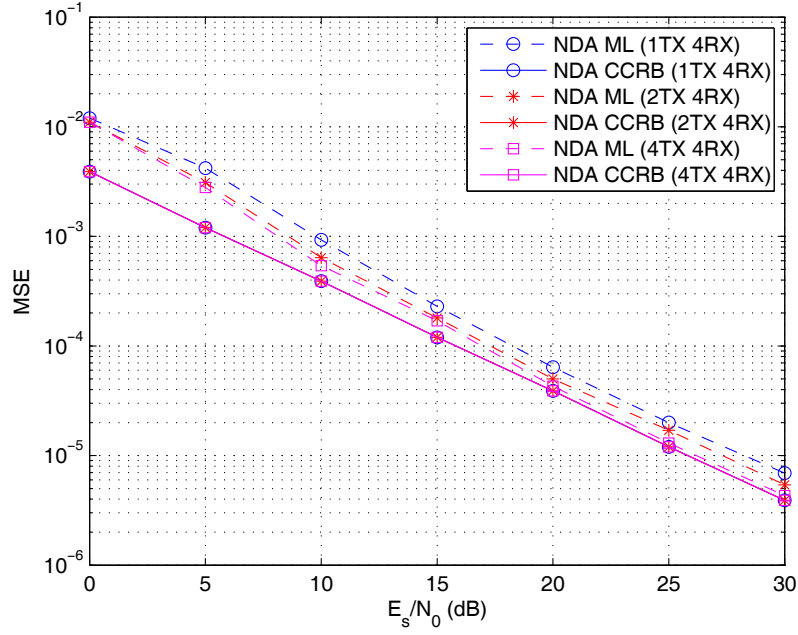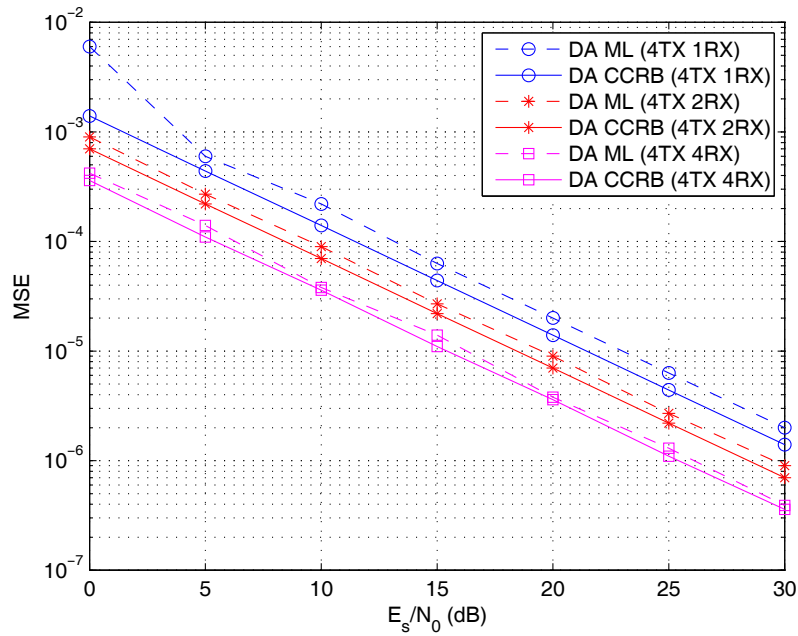

Fig. 19. The MSEs of the data-aided ML estimator and the CCRBs with different number of receive antennas.
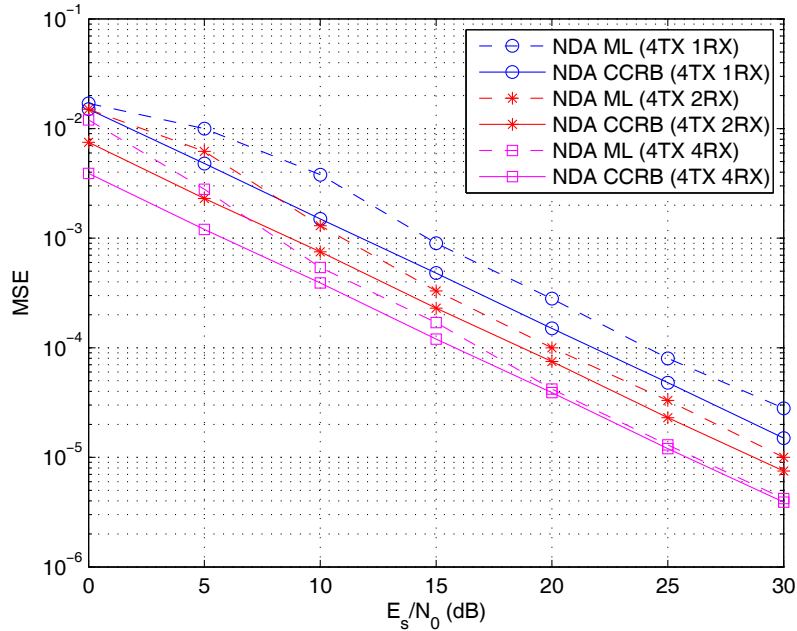
Fig. 20. The MSEs of the non-data-aided ML estimator and the CCRBs with different
number of receive antennas.

D.   Conclusions

This chapter investigated the effects of diversity on the synchronization for MIMO-
OFDM systems. It has been shown that MIMO-OFDM receivers are sensitive to the
residual synchronization errors. However, with multiple transmit and receive anten-
nas, MIMO-OFDM systems can take advantage of the spatial diversity to combat
these synchronization imperfections. Diversity can favorably improve the synchro-
nization performance. The conventional preamble-based synchronization method is
extended to the MIMO scenario. Data-aided and non-data-aided maximum likelihood
symbol timing estimators for MIMO-OFDM systems are introduced and their perfor-
mance analyzed in terms of the number of transmit and receive antennas. Computer
simulations show that by exploiting the spatial diversity, synchronization performance
of MIMO-OFDM systems in terms of detection probability and MSE performance

becomes significantly more reliable when compared to conventional SISO OFDM systems, and thus it can improve the overall signal reception. Therefore, spatial diversity appears as a useful technique to be exploited in the deployment of MIMO-OFDM communication systems.

CHAPTER IV

GENERALIZED LIKELIHOOD RATIO TEST FOR DATA-AIDED TIMING
SYNCHRONIZATION IN MIMO SYSTEMS

In this chapter, the data-aided timing synchronization problem for MIMO and MIMO-OFDM systems in fading channels is considered. By formulating the timing synchronization problem as a hypothesis testing problem, the generalized likelihood ratio test (GLRT) is adopted for a setup that assumes nuisance parameters. Using statistical methods, the asymptotic performance of the test is derived. An upper bound for the detection probability is provided and shown to behave well as a benchmark for sufficiently large number of observations. In addition, the selection of several system design parameters is investigated through simulation results.

A. Introduction

In order to reliably recover the transmitted information in a digital communication link, the receiver must be able to detect the existence of the transmitted signal and to sample the output of the demodulator periodically at the symbol rate or a multiple of the symbol rate. Since the propagation delay from the transmitter to the receiver is generally unknown at the receiver, timing synchronization must be derived from the received signal. In this paper, it is assumed that frequency synchronization is not required, or that the frequency errors are small enough that frequency synchronization can be achieved after temporal synchronization.

Synchronization can be the weakest component of a communication link. This potential weakness is exacerbated when an attempt is made to establish a link in the presence of strong noise and interference, which can effectively break down many synchronizers. Multiple Input Multiple Output (MIMO) communication provides a

number of potential performance benefits compared to traditional single-antenna links [4,5]. It has been widely used in current broadband wireless communication systems such as IEEE 802.11n wireless LAN and 3GPP High Speed Packet Access (HSPA). Reference [6] introduces and compares various timing synchronization techniques for the MIMO channel.

The Orthogonal Frequency Division Multiplexing (OFDM) is one of the multiple carrier modulation techniques that has been used as an efficient transmission technique over frequency selective channels and exhibits important advantages over conventional single carrier techniques. It can be used with multiple antennas to form a MIMO-OFDM system which can further improve the bandwidth efficiency. Since OFDM systems are more sensitive to synchronization errors [17,43], the synchronization problem has been well investigated during the last two decades. For OFDM systems with preambles, the reference correlation approach was proposed in [27,39]. Reference [30] proposes a maximum-likelihood estimator of timing and frequency offset which exploits the delay correlation property of the cyclic prefix present in the OFDM symbol.

This chapter addresses the data-aided timing synchronization in MIMO and MIMO-OFDM systems, i.e., pre-defined synchronization (pilot) sequences are transmitted to aid the synchronization task at the receiver end. In essence, timing synchronization is a continuous parameter estimation problem. However, in practical implementations, most digital communication receivers sample the output of the demodulator periodically at the symbol rate or a multiple of the symbol rate, thus require timing synchronization no better than a fraction of a sample period. Therefore, the potential timing offsets are in a discrete set. Given this discrete set, in principle, timing synchronization is a multiple statistical hypothesis test [6,41]. This type of multiple hypothesis test can be treated as a sequence of binary statistical hy-

pothesis tests. At each potential timing offset, the null hypothesis is that the signal is misaligned or does not exist. And the alternative hypothesis is that the signal of interest is properly aligned in time. At each testing point in time, a test statistic is evaluated given the observed data. Synchronization is declared if the test statistic threshold is exceeded. The performance of a synchronization test statistic is characterized by the probability that synchronization is detected, given the correct timing offset within the allowed receiver window, versus the probability of a false alarm that occurs if synchronization is declared in error. By varying the threshold, a receiver operating characteristic (ROC) curve in the space of the probability of missing a detection versus the probability of a false alarm can be constructed to summarize the detection performance.

Considering the data-aided timing synchronization as a detection problem, test statistics for MIMO communications in flat-fading channels and for MIMO-OFDM systems in frequency selective environments are developed. In composite hypotheses tests where the conditional probability densities contain unknown nuisance parameters, the optimal test statistic is not clear. However, it is believed that the generalized likelihood ratio test (GLRT) is asymptotically optimal in the situation where no uniformly most powerful (UMP) test exists [7]. Following this approach, the performance of the detector is analyzed in an asymptotic sense.

B. Data-aided Synchronization for MIMO Flat Fading Channels

In this section, the GLRT statistic for single carrier MIMO systems is proposed and its asymptotic performance is analyzed. An upper bound for detection probability in the presence of a large number of observations is also derived.

It is assumed that the MIMO channel is frequency flat. For any practical system,

if the bandwidth of the transmitted signal is considerably less than the coherence bandwidth of the channel, and the multipath propagation delays are not to be resolved at the receiver side, then the received signal can be modeled as a MIMO frequency flat fading channel. Assuming N transmit antennas, M receive antennas and n_s complex baseband samples, the MIMO relationship can be represented as follows:

$$\mathbf{Z} = \mathbf{HS} + \mathbf{N} \, , \tag{4.1}$$

where $\mathbf{Z} \in \mathbb{C}^{M \times n_s}$ is the sampled received signal matrix, with each row containing the n_s samples received from one of the M receive antennas. $\mathbf{H} \in \mathbb{C}^{M \times N}$ is the flat fading channel transfer matrix, $\mathbf{S} \in \mathbb{C}^{N \times n_s}$ is the transmitted signal matrix, and $\mathbf{N} \in \mathbb{C}^{M \times n_s}$ is the noise sample matrix and assumes a Gaussian distribution. The noise at each receive antenna can be characterized as being a zero mean Gaussian random variable with variance σ_n^2. It is assumed that the channel is temporally quasi-static, i.e., it can be regarded constant during n_s sampling periods. The transmitted and received complex baseband signal samples at some delay τ are defined by

$$\begin{aligned} \mathbf{S} &= [\mathbf{s}(T_s) \, \mathbf{s}(2T_s) \, \cdots \, \mathbf{s}(n_s T_s)], \\ \mathbf{Z}_\tau &= [\mathbf{z}(T_s - \tau) \, \mathbf{z}(2T_s - \tau) \, \cdots \, \mathbf{z}(n_s T_s - \tau)], \end{aligned}$$

where T_s is the sampling period, and $\mathbf{s}(t)$ and $\mathbf{z}(t)$ are the continuous transmitted and received vectors as a function of time t. In the case of a flat fading channel, the sampling period is much greater than the multipath delay spread, and a single channel filter tap is sufficient to represent the channel. Therefore, the MIMO channel matrix at a relative delay τ, $\mathbf{H}_\tau$, is given by

$$\mathbf{H}_\tau = \begin{cases} \mathbf{H}, & \tau = \tau_0 \\ \mathbf{0}, & \text{otherwise} \end{cases}$$

where the correct delay in terms of receiver's clock is τ_0, and $\mathbf{0}$ denotes a matrix of zeros.

The matrix Gaussian distribution is one of the most important matrix valued distributions in statistics [67]. The probability density function (pdf) of the complex matrix $\mathbf{N}$ can be represented by [68]

$$p(\mathbf{N}|\mathbf{\Omega}, \mathbf{\Sigma}) = \frac{\exp\left\{-\text{tr}\{\mathbf{\Omega}^{-1}(\mathbf{N} - \mathbf{M})^{\dagger}\mathbf{\Sigma}^{-1}(\mathbf{N} - \mathbf{M})\}\right\}}{\pi^{Mn_s}|\mathbf{\Omega}|^{M}|\mathbf{\Sigma}|^{n_s}}, \tag{4.2}$$

where $\mathbf{\Omega} = \mathbf{E}\{\mathbf{N}^{\dagger}\mathbf{N}\}/M \in \mathbb{C}^{n_s \times n_s}$, $\mathbf{\Sigma} = \mathbf{E}\{\mathbf{N}\mathbf{N}^{\dagger}\}/n_s \in \mathbb{C}^{M \times M}$ and $\mathbf{M} \in \mathbb{C}^{M \times n_s}$ is the mean matrix. An equivalent definition involving the Kronecker product $\otimes$ and the vectorization operator $\text{vec}(\cdot)$ shall also be introduced. It specifies that

$$\mathbf{N} \sim \mathcal{CN}_{M,n_s}(\mathbf{M}, \mathbf{\Omega}, \mathbf{\Sigma}) \text{ if } \text{vec}(\mathbf{N}) \sim \mathcal{CN}_{Mn_s}(\text{vec}(\mathbf{M}), \mathbf{\Omega} \otimes \mathbf{\Sigma}).$$

Assuming the noise samples are zero mean and statistically independent at different sampling time instants, i.e., the column vectors in matrix $\mathbf{N}$ are independent, one obtains $\mathbf{\Omega} = \mathbf{I}_{n_s}$. Therefore, the pdf simplifies to a more familiar form

$$p(\mathbf{N}|\mathbf{\Sigma}) = \frac{\exp\left\{-\text{tr}\{\mathbf{N}^{\dagger}\mathbf{\Sigma}^{-1}\mathbf{N}\}\right\}}{\pi^{Mn_s}|\mathbf{\Sigma}|^{n_s}}, \tag{4.3}$$

and equivalently $\text{vec}(\mathbf{N}) \sim \mathcal{CN}_{Mn_s}(\mathbf{0}, \mathbf{I}_{n_s} \otimes \mathbf{\Sigma})$.

The generalized likelihood ratio test (GLRT) is a likelihood ratio test for composite hypotheses in which the parameters of the probability density function are unknown a priori. The principle is straightforward [7]: it consists of finding the maximum-likelihood estimate of the unknown parameters under each hypothesis, and then plugging the estimate in the probability distribution of the corresponding hypothesis and treating the detection problem as if the estimated values were correct. This common sense test gives good results in general.

In our timing synchronization problem, the null hypothesis is that the synchro-

nization (or pilot) signal is absent or misaligned, and the alternative is that the synchronization (or pilot) signal is present and aligned correctly in time. Hence, the parameter test in a formal statistics convention is

$$\mathcal{H}_0: \quad \mathbf{H}_{M \times N} = \mathbf{0}, \mathbf{\Sigma}$$
$$\mathcal{H}_1: \quad \mathbf{H}_{M \times N} \neq \mathbf{0}, \mathbf{\Sigma}.$$

The parameter matrix $\mathbf{\Sigma}$ is the received signal spatial covariance matrix and is a set of nuisance parameters, which are unknown but the same under either hypothesis. As one can find, the above hypothesis test is two-sided. It has been proved that there is no uniformly most powerful (UMP) test exists in a two-sided test [42]. However, it can be shown that the GLRT is UMP among all tests that are invariant [69]. The GLRT for this problem is to decide $\mathcal{H}_1$ if

$$L_G(\tau) = \frac{p(\mathbf{Z}_\tau | \mathbf{S}; \hat{\mathbf{H}}_1, \hat{\mathbf{\Sigma}}_1)}{p(\mathbf{Z}_\tau | \mathbf{H}_0 = \mathbf{0}, \hat{\mathbf{\Sigma}}_0)} > \gamma, \qquad (4.4)$$

where $\hat{\mathbf{H}}_1, \hat{\mathbf{\Sigma}}_1$ are the unrestricted maximum-likelihood estimates of $\mathbf{H}$ and $\mathbf{\Sigma}$, respectively, under $\mathcal{H}_1$, and $\hat{\mathbf{\Sigma}}_0$ is the restricted maximum-likelihood estimate under $\mathcal{H}_1$ when $\mathbf{H} = \mathbf{0}$.

Given the knowledge of the synchronization signal, the pdf of received signal when the transmit signal is present and properly aligned in time is given by

$$p(\mathbf{Z}_\tau | \mathbf{S}; \mathbf{H}, \mathbf{\Sigma}) = \frac{\exp\left\{-\text{tr}\{(\mathbf{Z}_\tau - \mathbf{HS})^\dagger \mathbf{\Sigma}^{-1} (\mathbf{Z}_\tau - \mathbf{HS})\}\right\}}{\pi^{Mn_s} |\mathbf{\Sigma}|^{n_s}}. \qquad (4.5)$$

To maximize the likelihood at some given delay τ, the probability must be maximized with respect to the two matrix parameters: $\mathbf{H}$ and $\mathbf{\Sigma}$. To obtain the maximum-likelihood estimator of the MIMO channel matrix, one needs to take the complex

conjugate gradient of the log-pdf with respect to $\mathbf{H}$ and set it to zero.

$$
\begin{aligned}
\frac{\partial \ln p(\mathbf{Z}_\tau|\mathbf{S};\mathbf{H},\boldsymbol{\Sigma})}{\partial \mathbf{H}^*} &= -\frac{\partial}{\partial \mathbf{H}^*}\mathrm{tr}\{(\mathbf{Z}_\tau - \mathbf{HS})^\dagger \boldsymbol{\Sigma}^{-1}(\mathbf{Z}_\tau - \mathbf{HS})\} \\
&= \frac{\partial}{\partial \mathbf{H}^*}\mathrm{tr}\{\mathbf{H}^\dagger \boldsymbol{\Sigma}^{-1}(\mathbf{Z}_\tau - \mathbf{HS})\mathbf{S}^\dagger\} \\
&= \boldsymbol{\Sigma}^{-1}(\mathbf{Z}_\tau - \mathbf{HS})\mathbf{S}^\dagger = \mathbf{0}
\end{aligned}
$$

Hence, one can easily obtain

$$
\hat{\mathbf{H}} = \mathbf{Z}_\tau\mathbf{S}^\dagger(\mathbf{SS}^\dagger)^{-1}. \tag{4.6}
$$

Substituting this channel estimate into Eq. (4.5) yields

$$
p(\mathbf{Z}_\tau|\mathbf{S};\hat{\mathbf{H}},\boldsymbol{\Sigma}) = \frac{\exp\left\{-\mathrm{tr}\{(\mathbf{Z}_\tau\mathbf{P}_\mathbf{S}^\perp)^\dagger\boldsymbol{\Sigma}^{-1}(\mathbf{Z}_\tau\mathbf{P}_\mathbf{S}^\perp)\}\right\}}{\pi^{Mn_s}|\boldsymbol{\Sigma}|^{n_s}}, \tag{4.7}
$$

where the orthogonal projection matrix $\mathbf{P}_\mathbf{S}^\perp$ is defined as $\mathbf{P}_\mathbf{S}^\perp = \mathbf{I}_{n_s} - \mathbf{S}^\dagger(\mathbf{SS}^\dagger)^{-1}\mathbf{S}$. It projects onto a space orthogonal to the row space spanned by $\mathbf{S}$. Also, one can define the projection matrix $\mathbf{P}_\mathbf{S} = \mathbf{S}^\dagger(\mathbf{SS}^\dagger)^{-1}\mathbf{S} = \mathbf{I}_{n_s} - \mathbf{P}_\mathbf{S}^\perp$, which projects onto the row space spanned by $\mathbf{S}$. It can be easily verified that $\mathbf{P}_\mathbf{S}\mathbf{P}_\mathbf{S} = \mathbf{P}_\mathbf{S}$ and $\mathbf{P}_\mathbf{S}^\perp\mathbf{P}_\mathbf{S}^\perp = \mathbf{P}_\mathbf{S}^\perp$. To obtain a maximum-likelihood estimator of $\boldsymbol{\Sigma}$, one can take a gradient of $\ln p(\mathbf{Z}_\tau|\mathbf{S};\hat{\mathbf{H}},\boldsymbol{\Sigma})$ and set it to zero as follows

$$
\begin{aligned}
\frac{\partial \ln p(\mathbf{Z}_\tau|\mathbf{S};\hat{\mathbf{H}},\boldsymbol{\Sigma})}{\partial \boldsymbol{\Sigma}} &= -\frac{\partial\mathrm{tr}\{(\mathbf{Z}_\tau\mathbf{P}_\mathbf{S}^\perp)^\dagger\boldsymbol{\Sigma}^{-1}(\mathbf{Z}_\tau\mathbf{P}_\mathbf{S}^\perp)\} + n_s\ln|\boldsymbol{\Sigma}|}{\partial \boldsymbol{\Sigma}} \\
&= \left(\boldsymbol{\Sigma}^{-1}(\mathbf{Z}_\tau\mathbf{P}_\mathbf{S}^\perp)(\mathbf{Z}_\tau\mathbf{P}_\mathbf{S}^\perp)^\dagger\boldsymbol{\Sigma}^{-1}\right)^T - n_s(\boldsymbol{\Sigma}^{-1})^T \\
&= \left(\boldsymbol{\Sigma}^{-1}(\mathbf{Z}_\tau\mathbf{P}_\mathbf{S}^\perp\mathbf{Z}_\tau^\dagger)\boldsymbol{\Sigma}^{-1} - n_s\boldsymbol{\Sigma}^{-1}\right)^T = \mathbf{0}.
\end{aligned}
$$

Therefore,

$$
\hat{\boldsymbol{\Sigma}}_1 = \frac{\mathbf{Z}_\tau\mathbf{P}_\mathbf{S}^\perp\mathbf{Z}_\tau^\dagger}{n_s}. \tag{4.8}
$$

Plugging this estimator into the likelihood Eq. (4.7), the maximum pdf is given by

$$
\begin{aligned}
p(\mathbf{Z}_\tau | \mathbf{S}; \hat{\mathbf{H}}, \hat{\mathbf{\Sigma}}) &= \frac{\exp\left\{-\mathrm{tr}\{(\mathbf{Z}_\tau \mathbf{P}_{\bar{\mathbf{S}}}^\perp)^\dagger (\mathbf{Z}_\tau \mathbf{P}_{\bar{\mathbf{S}}}^\perp \mathbf{Z}_\tau^\dagger)^{-1} (\mathbf{Z}_\tau \mathbf{P}_{\bar{\mathbf{S}}}^\perp)\}\right\}}{\pi^{Mn_s} \left|\frac{\mathbf{Z}_\tau \mathbf{P}_{\bar{\mathbf{S}}}^\perp \mathbf{Z}_\tau^\dagger}{n_s}\right|^{n_s}} \\
&= \frac{n_s^{n_s} e^{-Mn_s}}{\pi^{Mn_s} |\mathbf{Z}_\tau \mathbf{P}_{\bar{\mathbf{S}}}^\perp \mathbf{Z}_\tau^\dagger|^{n_s}}
\end{aligned}
\tag{4.9}
$$

In the absence of the synchronization signal, the pdf of the received signal is given by

$$
p(\mathbf{Z}|\mathbf{\Sigma}) = \frac{\exp\left\{-\mathrm{tr}\{\mathbf{Z}^\dagger \mathbf{\Sigma}^{-1} \mathbf{Z}\}\right\}}{\pi^{Mn_s} |\mathbf{\Sigma}|^{n_s}}.
\tag{4.10}
$$

Note that this pdf can also describe the case when the synchronization signal is misaligned. Since many communication standards operating in the ISM band employ OFDM modulation which can be approximated well by Gaussian distributions due to the Central Limit Theorem (CLT), it is assumed that misaligned reference signals can be modeled reasonably well by sampling from complex Gaussian distributions. In such a case, the covariance matrix of the misaligned synchronization signal can be combined into $\mathbf{\Sigma}$.

Similarly, by maximizing the pdf in the missing or misaligned synchronization signal case, the maximum-likelihood estimator of $\mathbf{\Sigma}$ under hypothesis $\mathcal{H}_0$ is given by

$$
\hat{\mathbf{\Sigma}}_0 = \frac{\mathbf{Z}_\tau \mathbf{Z}_\tau^\dagger}{n_s}.
\tag{4.11}
$$

Plugging this estimator into the likelihood Eq. (4.10), the maximum pdf is given by

$$
p(\mathbf{Z}|\hat{\mathbf{\Sigma}}) = \frac{n_s^{n_s} e^{-Mn_s}}{\pi^{Mn_s} |\mathbf{Z}_\tau \mathbf{Z}_\tau^\dagger|^{n_s}}
\tag{4.12}
$$

Consequently, the GLRT statistic can be represented by

$$
\begin{aligned}
L_G(\tau) &= \frac{|\mathbf{Z}_\tau \mathbf{Z}_\tau^\dagger|^{n_s}}{|\mathbf{Z}_\tau \mathbf{P}_{\mathbf{S}}^\perp \mathbf{Z}_\tau^\dagger|^{n_s}} \\
&= |\mathbf{Z}_\tau (\mathbf{I}_{n_s} - \mathbf{P}_{\mathbf{S}})\mathbf{Z}_\tau^\dagger (\mathbf{Z}_\tau \mathbf{Z}_\tau^\dagger)^{-1}|^{-n_s} \\
&= |\mathbf{I}_M - \mathbf{Z}_\tau \mathbf{P}_{\mathbf{S}} \mathbf{Z}_\tau^\dagger (\mathbf{Z}_\tau \mathbf{Z}_\tau^\dagger)^{-1}|^{-n_s} \\
&= |\mathbf{I}_{n_s} - \mathbf{P}_{\mathbf{S}} \mathbf{P}_{\mathbf{Z}_\tau}|^{-n_s},
\end{aligned}
\tag{4.13}
$$

where $\mathbf{P}_{\mathbf{Z}_\tau}$ is the projection matrix that projects onto the row space spanned by $\mathbf{Z}_\tau$ and is defined as $\mathbf{P}_{\mathbf{Z}} = \mathbf{Z}^\dagger (\mathbf{Z}\mathbf{Z}^\dagger)^{-1}\mathbf{Z}$.

To investigate the performance of the maximum-likelihood estimator of the channel matrix $\mathbf{H}$ and fit it into statistics conventions, one needs to consider the estimator in a vector space. One possible way is to vectorize the channel matrix $\mathbf{H}$ by stacking the columns into a long vector. We will show the equivalence of the estimator between the matrix space and the vector space as follows.

Let $\mathbf{z} = \mathrm{vec}(\mathbf{Z})$, $\mathbf{h} = \mathrm{vec}(\mathbf{H})$, and $\mathbf{n} = \mathrm{vec}(\mathbf{N})$. Noting

$$
\mathrm{vec}(\mathbf{IAB}) = (\mathbf{B}^T \otimes \mathbf{I})\mathrm{vec}(\mathbf{A})
\tag{4.14}
$$

and recalling Eq. (4.1), one can show that

$$
\mathbf{z} = (\mathbf{S}^T \otimes \mathbf{I}_M)\mathbf{h} + \mathbf{n}.
\tag{4.15}
$$

Recall the equivalent vector model of the matrix Gaussian distribution, the pdf when the synchronization signal is present and properly aligned can also be represented by

$$
p(\mathbf{z}|\mathbf{S}; \mathbf{h}, \mathbf{C}) = \frac{\exp\left\{-[\mathbf{z} - (\mathbf{S}^T \otimes \mathbf{I}_M)\mathbf{h}]^\dagger \mathbf{C}^{-1}[\mathbf{z} - (\mathbf{S}^T \otimes \mathbf{I}_M)\mathbf{h}]\right\}}{\pi^{Mn_s}|\mathbf{C}|},
\tag{4.16}
$$

where $\mathbf{C} = \mathbf{I}_{n_s} \otimes \boldsymbol{\Sigma}$. Taking the complex conjugate gradient of the log-pdf with respect

to $\mathbf{h}$, and setting it to zero, one obtains

$$
\begin{aligned}
\frac{\partial \ln p(\mathbf{z}|\mathbf{S};\mathbf{h},\mathbf{C})}{\partial \mathbf{h}^*} &= -\frac{\partial}{\partial \mathbf{h}^*}[\mathbf{z} - (\mathbf{S}^T \otimes \mathbf{I}_M)\mathbf{h}]^\dagger \mathbf{C}^{-1}[\mathbf{z} - (\mathbf{S}^T \otimes \mathbf{I}_M)\mathbf{h}] \\
&= (\mathbf{S}^T \otimes \mathbf{I}_M)^\dagger \mathbf{C}^{-1}[\mathbf{z} - (\mathbf{S}^T \otimes \mathbf{I}_M)\mathbf{h}] \\
&= \mathbf{0}.
\end{aligned}
$$

Hence, the maximum-likelihood estimator of $\mathbf{h}$ is

$$
\hat{\mathbf{h}} = [(\mathbf{S}^T \otimes \mathbf{I}_M)^\dagger \mathbf{C}^{-1}(\mathbf{S}^T \otimes \mathbf{I}_M)]^{-1}(\mathbf{S}^T \otimes \mathbf{I}_M)^\dagger \mathbf{C}^{-1}\mathbf{z}.
$$

Recall that $\mathbf{C} = \mathbf{I}_{n_s} \otimes \boldsymbol{\Sigma}$, and the properties of the Kronecker product: $(\mathbf{A} \otimes \mathbf{B})^\dagger = \mathbf{A}^\dagger \otimes \mathbf{B}^\dagger$, $(\mathbf{A} \otimes \mathbf{B})^{-1} = \mathbf{A}^{-1} \otimes \mathbf{B}^{-1}$, and $(\mathbf{A} \otimes \mathbf{B})(\mathbf{X} \otimes \mathbf{Y}) = (\mathbf{A}\mathbf{X}) \otimes (\mathbf{B}\mathbf{Y})$ where matrices inversions and multiplications are proper,

$$
\begin{aligned}
\hat{\mathbf{h}} &= [(\mathbf{S}^T \otimes \mathbf{I}_M)^\dagger (\mathbf{S}^T \otimes \mathbf{I}_M)]^{-1}(\mathbf{S}^T \otimes \mathbf{I}_M)^\dagger (\mathbf{I}_{n_s} \otimes \boldsymbol{\Sigma})^{-1}\mathbf{z} \\
&= \left([\mathbf{S}^\dagger(\mathbf{S}\mathbf{S}^\dagger)^{-1}]^T \otimes \mathbf{I}_M\right)\mathbf{z}.
\end{aligned}
$$

Recalling Eq. (4.14), one can convert the estimator in vector space to matrix space

$$
\hat{\mathbf{H}} = \mathbf{Z}\mathbf{S}^\dagger(\mathbf{S}\mathbf{S}^\dagger)^{-1},
$$

which is the same as Eq. (4.6). Thus, the equivalence between the vector space model and matrix space model has been set up.

It is straightforward to check the unbiasedness of the channel estimator. The Fisher information matrix provides information about the variance of the unbiased

estimator and can be computed as

$$
\begin{aligned}
\mathbf{I}(\mathbf{h}) &= \mathbf{E}\left\{\frac{\partial \ln p(\mathbf{z}|\mathbf{S};\mathbf{h},\mathbf{C})}{\partial \mathbf{h}^*}\frac{\partial \ln p(\mathbf{z}|\mathbf{S};\mathbf{h},\mathbf{C})^\dagger}{\partial \mathbf{h}^*}\right\} \\
&= \mathbf{E}\left\{(\mathbf{S}^T \otimes \mathbf{I}_M)^\dagger \mathbf{C}^{-1}[\mathbf{z} - (\mathbf{S}^T \otimes \mathbf{I}_M)\mathbf{h}]\left((\mathbf{S}^T \otimes \mathbf{I}_M)^\dagger \mathbf{C}^{-1}[\mathbf{z} - (\mathbf{S}^T \otimes \mathbf{I}_M)\mathbf{h}]\right)^\dagger\right\} \\
&= (\mathbf{S}^T \otimes \mathbf{I}_M)^\dagger \mathbf{C}^{-1}(\mathbf{S}^T \otimes \mathbf{I}_M) \\
&= (\mathbf{S}^T \otimes \mathbf{I}_M)^\dagger (\mathbf{I}_{n_s} \otimes \boldsymbol{\Sigma})^{-1}(\mathbf{S}^T \otimes \mathbf{I}_M) \\
&= (\mathbf{S}\mathbf{S}^\dagger)^T \otimes \boldsymbol{\Sigma}^{-1}.
\end{aligned}
\tag{4.17}
$$

Then, as $n_s \to \infty$, the modified GLRT statistic $2\ln L_G$ for complex parameters has the pdf [41]

$$
2\ln L_G(\tau) \overset{a}{\sim} \begin{cases} \chi^2_{2MN} & \text{under } \mathcal{H}_0 \\[2mm] \chi'^2_{2MN}(\lambda) & \text{under } \mathcal{H}_1 \end{cases}
$$

where "a" denotes an asymptotic pdf, χ^2_r denotes a central chi-squared pdf with r degrees of freedom, and χ'^2_r denotes a noncentral chi-squared pdf with r degrees of freedom and noncentrality parameter λ. The noncentrality parameter is

$$
\lambda = 2(\mathbf{h}_1 - \mathbf{h}_0)^\dagger \mathbf{I}(\mathbf{h}_0, \boldsymbol{\Sigma})(\mathbf{h}_1 - \mathbf{h}_0),
\tag{4.18}
$$

where $\mathbf{h}_1$ and $\boldsymbol{\Sigma}$ are the parameters' true values under $\mathcal{H}_1$. Note that Eq. (4.18) holds for the case without nuisance parameters. When nuisance parameters are present, the noncentrality parameter λ is decreased and the chi-squared pdf is more concentrated to the left for the same degrees of freedom as one can find from Fig. 21. Hence with the same threshold, the detection probability is decreased. Intuitively, this is the price paid for having to estimate extra parameters for use in the detector.

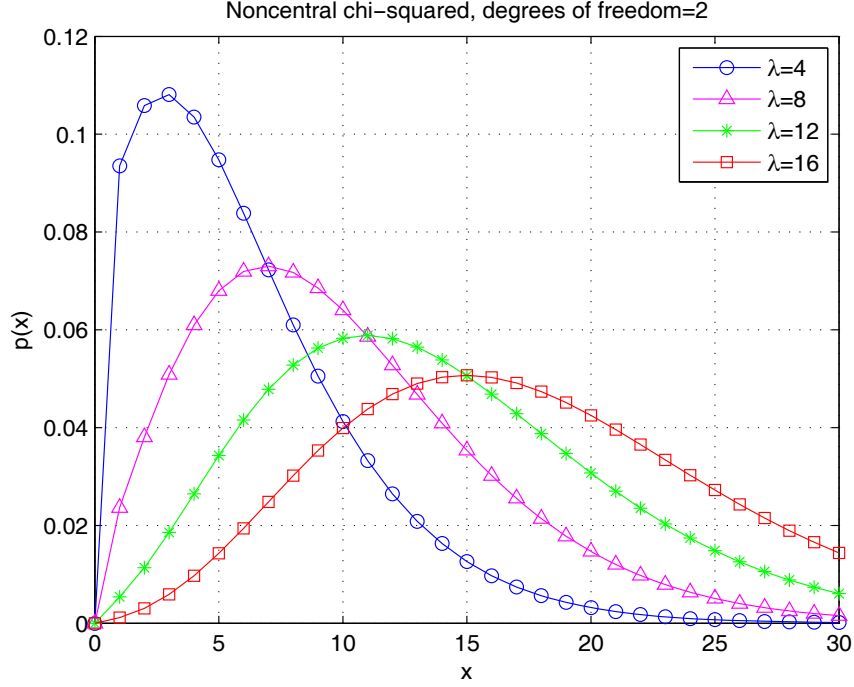Plugging Eq. (4.17) into Eq. (4.18), and assuming $\mathbf{S}\mathbf{S}^\dagger$ and $\boldsymbol{\Sigma}$ admit the following

Fig. 21. Noncentral chi-squared pdfs with different noncentrality parameters.

eigenvalue decompositions, respectively,

$$\mathbf{SS}^{\dagger} = \mathbf{U\Lambda U}^{\dagger} \text{ and } \mathbf{\Sigma} = \mathbf{V\Gamma V}^{\dagger},$$

where $\mathbf{U}$ and $\mathbf{V}$ are unitary matrices, one can obtain

$$
\begin{aligned}
\lambda &= 2\mathbf{h}^{\dagger} \left[(\mathbf{SS}^{\dagger})^{T} \otimes \mathbf{\Sigma}^{-1} \right] \mathbf{h} \\
&= 2\mathbf{h}^{\dagger} \left[(\mathbf{U\Lambda}^{1/2}\mathbf{U}^{\dagger})^{T} \otimes (\mathbf{V\Gamma}^{-1/2}\mathbf{V}^{\dagger}) \right] \left[(\mathbf{U\Lambda}^{1/2}\mathbf{U}^{\dagger})^{T} \otimes (\mathbf{V\Gamma}^{-1/2}\mathbf{V}^{\dagger}) \right] \mathbf{h} \\
&= 2\text{vec}^{\dagger} \left((\mathbf{V\Gamma}^{-1/2}\mathbf{V}^{\dagger})\mathbf{H}(\mathbf{U\Lambda}^{1/2}\mathbf{U}^{\dagger}) \right) \text{vec} \left((\mathbf{V\Gamma}^{-1/2}\mathbf{V}^{\dagger})\mathbf{H}(\mathbf{U\Lambda}^{1/2}\mathbf{U}^{\dagger}) \right) \\
&= 2\text{tr} \left\{ (\mathbf{U\Lambda}^{1/2}\mathbf{U}^{\dagger})\mathbf{H}^{\dagger}(\mathbf{V\Gamma}^{-1/2}\mathbf{V}^{\dagger})(\mathbf{V\Gamma}^{-1/2}\mathbf{V}^{\dagger})\mathbf{H}(\mathbf{U\Lambda}^{1/2}\mathbf{U}^{\dagger}) \right\} \\
&= 2\text{tr} \left\{ \mathbf{\Sigma}^{-1}\mathbf{HSS}^{\dagger}\mathbf{H}^{\dagger} \right\}, \quad\quad\quad (4.19)
\end{aligned}
$$

where the fourth equality follows the vec($\cdot$) operator's property that $\text{vec}^{\dagger}(\mathbf{A})\text{vec}(\mathbf{B}) =$

$\text{tr}\{\mathbf{A}^\dagger\mathbf{B}\}$. Assuming the noise is spatially uncorrelated, i.e., $\mathbf{\Sigma} = \sigma_n^2\mathbf{I}_M$, one obtains

$$\lambda = \frac{2\|\mathbf{HS}\|_F^2}{\sigma_n^2} = 2Mn_s\text{SNR}, \tag{4.20}$$

where the signal-to-noise ratio SNR is defined as

$$\text{SNR} = \|\mathbf{HS}\|_F^2/(\sigma_n^2 Mn_s). \tag{4.21}$$

Assuming the knowledge of the true values for the MIMO channel $\mathbf{H}$ (or equivalently $\mathbf{h}$) and the covariance matrix $\mathbf{\Sigma}$ is available, one can approximate the GLRT statistic with chi-squared random variables under either hypothesis $\mathcal{H}_0$ or $\mathcal{H}_1$. Since the asymptotic pdf under $\mathcal{H}_0$ does not depend on any unknown parameters, the threshold required to maintain a constant false alarm rate (CFAR) can be found, i.e, CFAR detector exists [41]. However, since the nuisance parameter is present in the model, we can provide only an upper bound for the detection probability or equivalently a lower bound for the missing rate. And since the GLRT is considered asymptotically optimal in the situation where no uniformly most powerful (UMP) test exists [7], this asymptotic bound can also serve as a benchmark when comparing various tests developed through different approaches. The bound can be obtained as follows.

I. For any given false alarm rate P_{FA}, one can determine the corresponding threshold T, such that

$$\int_T^\infty p_1(x)dx = P_{FA},$$

where

$$p_1(x) = \begin{cases} \dfrac{x^{\frac{r}{2}-1}\exp(-\frac{x}{2})}{2^{\frac{r}{2}}\Gamma(\frac{r}{2})} & x \geq 0 \\[2ex] 0 & x < 0 \end{cases}$$

is the central chi-squared pdf with $r = 2MN$ degrees of freedom, and $\Gamma(u)$ is the

Gamma function defined as

$$\Gamma(u) = \int_0^\infty t^{u-1} \exp(-t)dt.$$

II. For the given SNR, one can obtain the noncentrality parameter λ through Eq. (4.20) or Eq. (4.19). Then an upper bound of detection probability $P_{D,a}$, which is the detection probability in the asymptotic case, can be computed as

$$P_{D,a} = \int_T^\infty p_2(x)dx,$$

where

$$p_2(x) = \begin{cases} \dfrac{x^{\frac{r}{2}-1}\exp(-\frac{x+\lambda}{2})}{2^{\frac{r}{2}}} \sum_{k=0}^\infty \dfrac{\left(\frac{\lambda x}{4}\right)^k}{k!\Gamma(\frac{r}{2}+k)} & x \geq 0 \\ \\ 0 & x < 0 \end{cases}$$

is the noncentral chi-squared pdf with $r = 2MN$ degrees of freedom and noncentrality parameter λ. Equivalently, a lower bound of the missing rate is given as

$$P_{miss,lb} = 1 - P_{D,a}.$$

In the following, the performances of the GLRT statistic developed for flat fading channels are shown empirically through computer simulations. The performances are illustrated in terms of receiver operating characteristic (ROC) curves in various system configurations. The probabilities on axes are displayed for potential correct or incorrect temporal alignment tests. The probability of false alarm measures the fraction of false alarms given the synchronization sequence is absent or misaligned. The probability of a missing is the rate of omission an event when the synchronization sequence is correctly aligned in time.

For a MIMO wireless communication link with N transmit antennas and M receive antennas, N different synchronization (or pilot) sequences, each of n_s symbols, are transmitted through the N transmit antenna in parallel. These sequences are
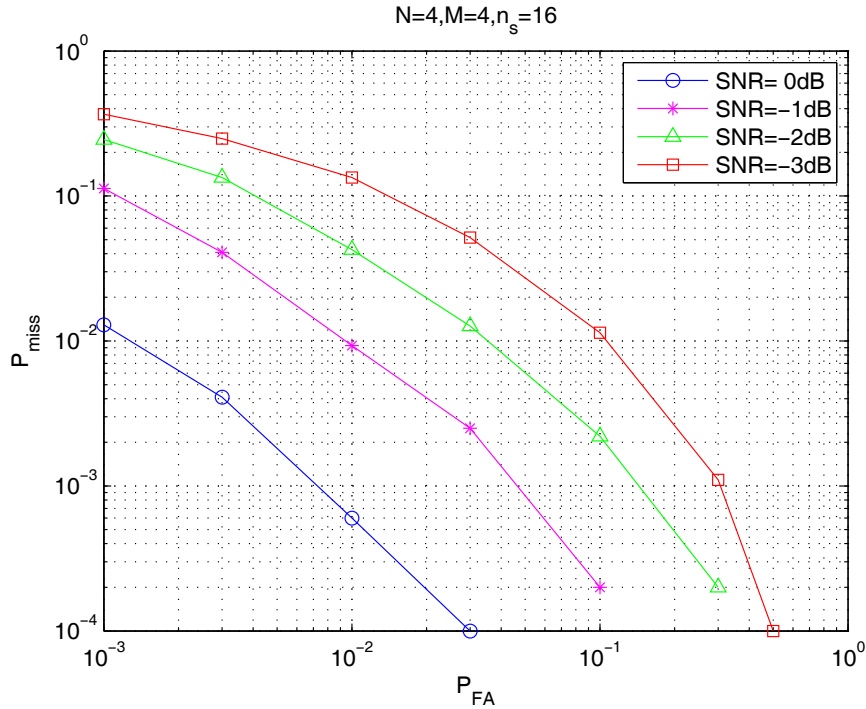
Fig. 22. Comparison of ROCs for a 4×4 MIMO link in Rayleigh flat fading environment with different SNRs.

constructed randomly from a quadrature phase-shift-keying (QPSK) constellation. For each synchronization test, the receiver collects n_s received vector samples from M antennas. The SNR is defined in Eq. (4.21). The channel assumes Rayleigh frequency flat fading. The elements in the MIMO channel matrix $\mathbf{H}$ are sampled from a circular complex Gaussian distribution with zero mean and unit variance.

Fig. 22 shows the ROC curves for a 4-by-4 MIMO link with various SNRs. There are 4 transmit antennas and 4 receive antennas with synchronization sequences of length 16. The SNRs investigated are 0, -1, -2, and -3 dB. Fig. 23 illustrates the ROC curves for a SISO link case, i.e., with a single transmit antenna and a single receive antenna. The proposed GLRT works well in both cases, e.g., with SNR=0dB, for $P_{FA} = 1\%$, the missing rate is 6×10^{-4} in the MIMO case and 10^{-2} in the SISO case. As the SNR decreases, the missing rate increases (the detection probability
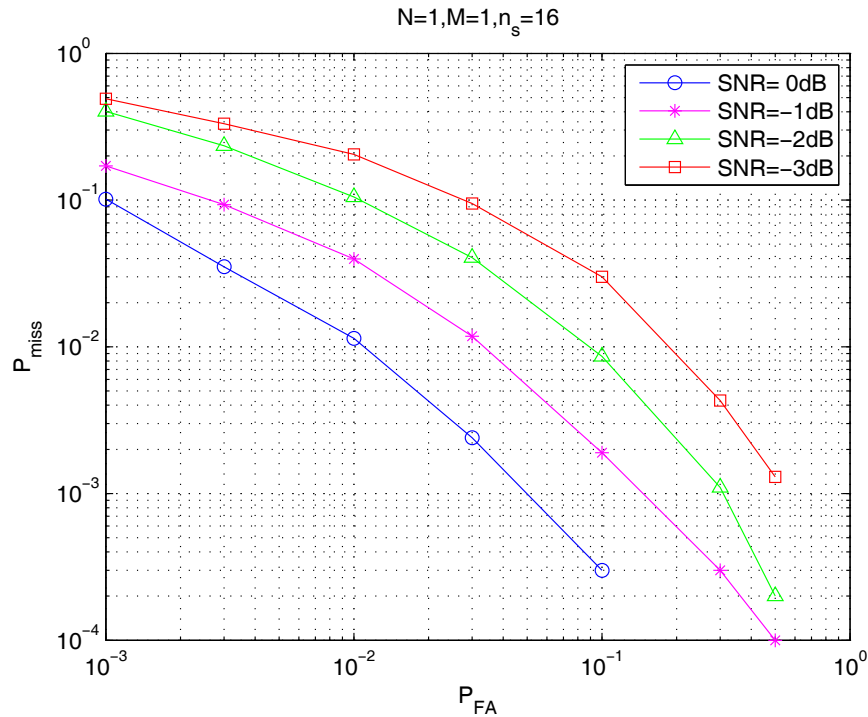
Fig. 23. Comparison of ROCs for SISO link in Rayleigh flat fading environment with different SNRs.

decreases), a fact which corroborates our intuition.

Fig. 24 compares the performances of the GLRT under different MIMO configurations at SNR 0 dB. It is easy to find that MIMO setups outperform the SISO setup. Generally, with the same number of transmit antennas, the more receive antennas are used the more reliable the communication link is. However, with the same number of receive antennas, more transmit antennas actually degrade the performance. One can find that the 1-by-1 case outperforms the 4-by-1 case. This is because the synchronization sequences are not orthogonal to each other. More transmit antennas cause interference at the receiver side. Although one could specify to use orthogonal synchronization sequences in some limited cases, the fading channel still destroys the orthogonality. As for synchronization purpose, stepping up from SISO link to 2-by-2 MIMO provides relatively large benefit, e.g., for $P_{FA} = 1\%$, the missing rate is re-
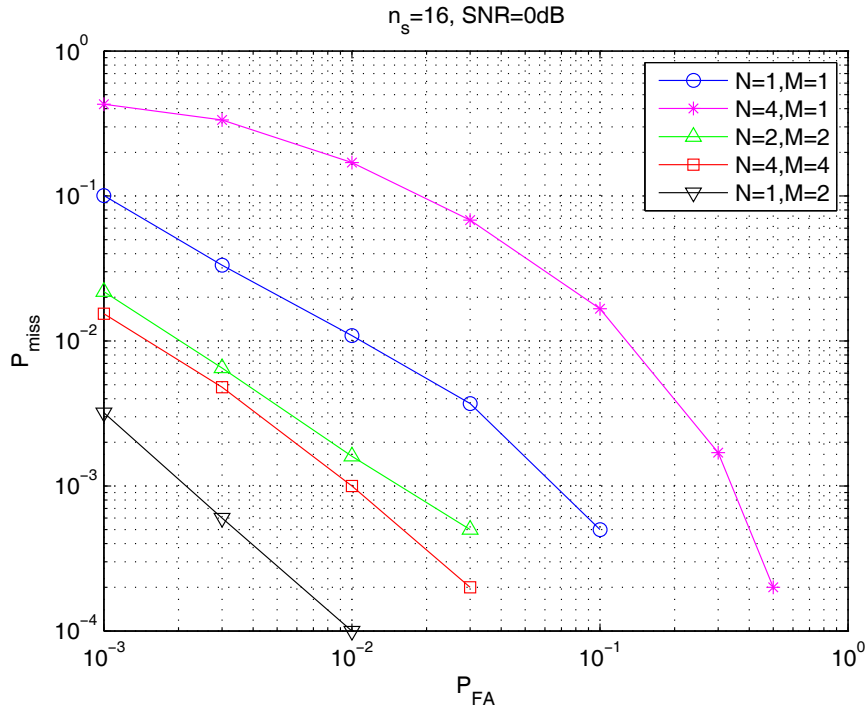
Fig. 24. Comparison of ROCs for different MIMO setups in Rayleigh flat fading environment at SNR 0 dB.

duced from 10^{-2} to 10^{-3}. However, only marginal benefit can be obtained from an upgrade from 2-by-2 to 4-by-4 setup.

Figs. 25 and 26 show the asymptotic behavior for a 4-by-4 MIMO link with the synchronization sequence length equal to 32 and 64, respectively. As the synchronization length increases, the lower bound for missing rate gets tighter. Although the asymptotic bound requires an infinite number of observations, i.e., infinitely large n_s, it still serves as a good lower bound with sufficiently large observation window, such as $n_s = 64$. Fig. 27 confirms our observation with the SISO case.
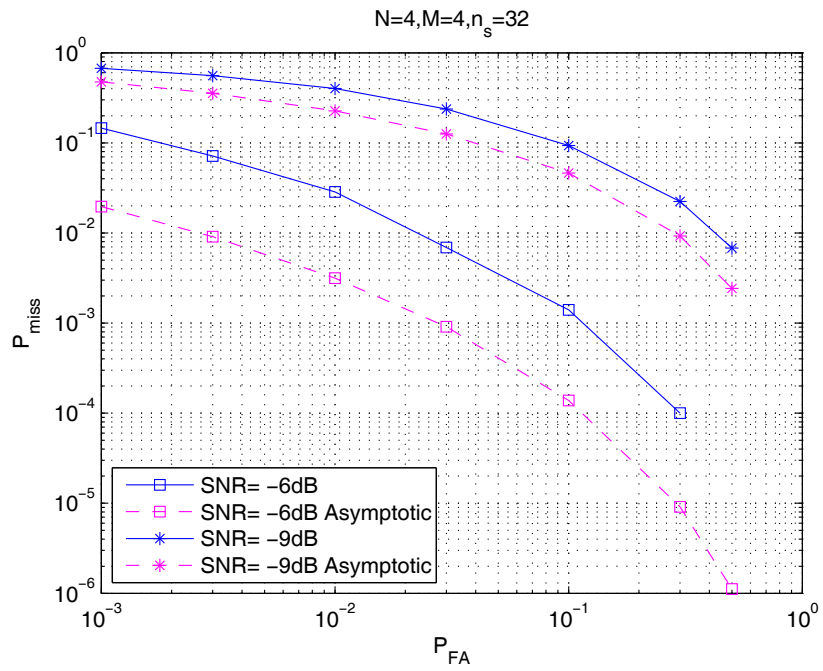
Fig. 25. Performance of the detector for a 4×4 MIMO system in Rayleigh flat fading environment with $n_s = 32$.
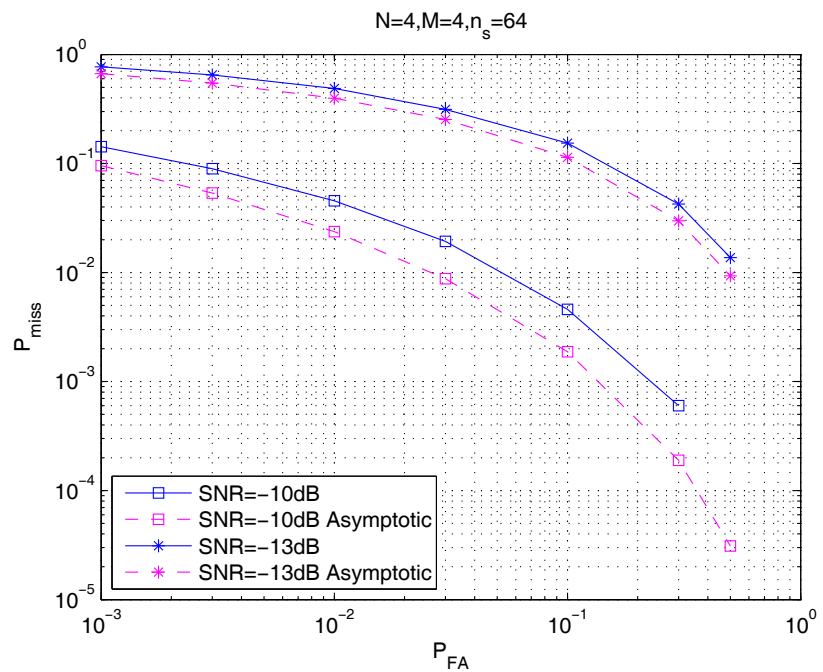

Fig. 26. Performance of the detector for a 4×4 MIMO system in Rayleigh flat fading environment with $n_s = 64$.
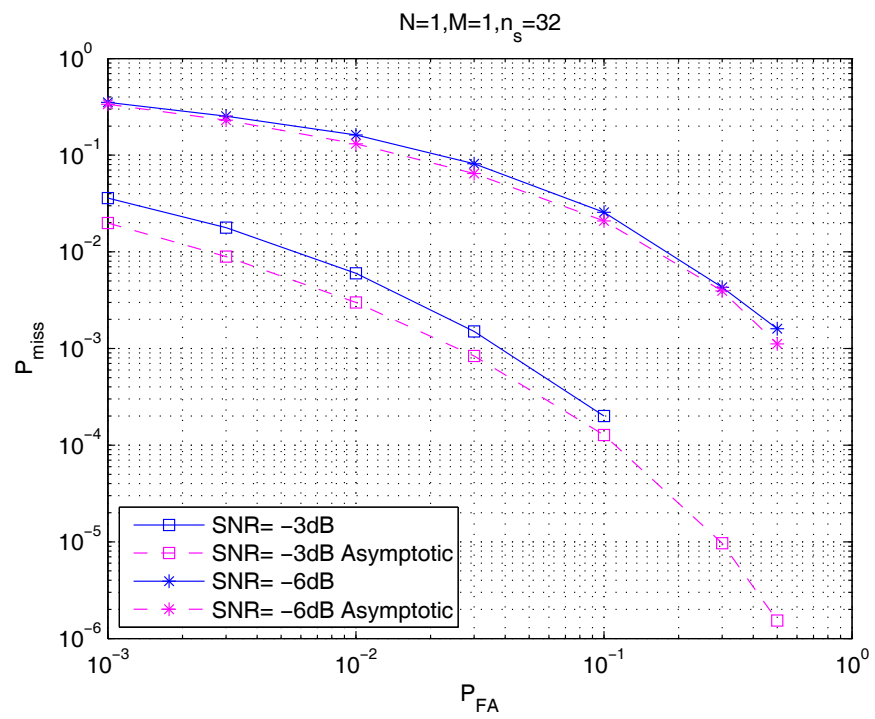
Fig. 27. Performance of the detector for a SISO link in Rayleigh flat fading environment with $n_s = 32$.

C.   Synchronization for MIMO-OFDM Systems Using Pilot Symbols

In this section, the GLRT formulation for timing synchronization in MIMO-OFDM systems with pilot symbols across multiple observations is set up and analyzed. A performance bound for detection probability or missing rate is also derived.

OFDM is a multicarrier approach that exploits the computational efficiency of the fast Fourier transform (FFT). The transmitted signals are constructed by applying an inverse FFT to a block of symbols. Each symbol is assigned to a subcarrier (or tone) and has a duration proportional to the number of symbols in the block. An OFDM symbol is defined to be this entire block of transformed symbols. OFDM converts a broadband frequency selective channel into a parallel collection of frequency flat subchannels [3]. The subcarriers have the minimum frequency separation required to maintain orthogonality of their corresponding time domain waveforms. OFDM uses the available bandwidth very efficiently. Therefore, it is natural to think of combining the OFDM technique with the MIMO configuration to enhance the system performance in frequency selective environments.

It is common in OFDM systems to periodically populate the OFDM symbol with a number of known values in the frequency domain to ease the channel estimation task. These pilot symbols occupy a small fraction of the total number of tones. Without loss of generality, it is assumed that the frequencies of the pilot tones are fixed. In MIMO systems, a sequence of OFDM symbols employed with independent modulation of the pilot symbol sequences are emitted from each transmit antenna. Hence, the pilot sequences can be used for synchronization purpose. Since each pilot tone in frequency domain undergoes a frequency flat fading, one can extend the study in the previous section to address the timing synchronization problem in frequency selective channels by considering a MIMO-OFDM system. Since this approach for

synchronization operates in the frequency domain, it is relatively insensitive to the exact timing offset.

Although a variety of potential test statistics are available that could exploit the OFDM pilot sequence structure, given its superior performance, the GLRT approach is addressed here. The number of pilot tones is denoted as n_p. In the following, the subscript p indicates a pilot index. The baseband angular frequency for the pth pilot subcarrier is denoted ω_p. The number of OFDM symbols used is n_s. Assuming N transmit antennas, and M receive antennas, for the temporal offset τ contained within the length of cyclic prefix, the received signal for the pth pilot frequency can be modeled by the following MIMO relationship:

$$\mathbf{Z}_p = e^{j\omega_p \tau} \mathbf{H}_p \mathbf{S}_p + \mathbf{N}_p, \tag{4.22}$$

where $\mathbf{Z}_p$ is the $M \times n_s$ received signal vector, $\mathbf{H}_p$ is the $M \times N$ flat fading channel matrix, $\mathbf{S}_p$ is the $N \times n_s$ transmitted pilot symbols matrix, and $\mathbf{N}$ is the $M \times n_s$ Gaussian noise matrix.

We state our timing synchronization problem in a hypothesis testing setup:

$$\mathcal{H}_0: \quad \mathbf{H}_p = \mathbf{0}, \boldsymbol{\Sigma}_p, \ p = 1, 2, \cdots, n_p$$
$$\mathcal{H}_1: \quad \mathbf{H}_p \neq \mathbf{0}, \boldsymbol{\Sigma}_p, \ p = 1, 2, \cdots, n_p.$$

Following the same assumption in last section that the noise vectors are temporally uncorrelated, the matrix Gaussian pdf with the pilot sequence present and approximately aligned in time for the pth pilot tone is given by

$$p(\mathbf{Z}_p|\mathbf{S}_p; \mathbf{H}_p, \boldsymbol{\Sigma}_p) = \frac{\exp\left\{-\mathrm{tr}\{(\mathbf{Z}_p - e^{j\omega_p \tau}\mathbf{H}_p\mathbf{S}_p)^\dagger \boldsymbol{\Sigma}_p^{-1}(\mathbf{Z}_p - e^{j\omega_p \tau}\mathbf{H}_p\mathbf{S}_p)\}\right\}}{\pi^{Mn_s}|\boldsymbol{\Sigma}_p|}, \tag{4.23}$$

where $\boldsymbol{\Sigma}_p$ is the spatial covariance matrix of the noise on the pth pilot tone. Therefore,

for the collection of n_p pilot tones, the joint pdf can be represented by

$$p(\mathcal{Z}|\mathcal{S},\mathcal{H},\Sigma) = \prod_p p(\mathbf{Z}_p|\mathbf{S}_p,\mathbf{H}_p,\boldsymbol{\Sigma}_p),$$

where $\mathcal{Z}$, $\mathcal{S}$, $\mathcal{H}$ and Σ indicate the set of $\mathbf{Z}_p$, $\mathbf{S}_p$, $\mathbf{H}_p$ and $\boldsymbol{\Sigma}_p$ for the n_p pilot sequences. Here it is assumed that the channels and the noise covariance matrices are independent between pilot tones.

The maximum-likelihood channel estimator can be obtained by taking the complex conjugate gradient of the log-pdf with respect to $\mathbf{H}_p$ and setting it to zero:

$$\frac{\partial}{\partial \mathbf{H}_p^*} \ln p(\mathcal{Z}|\mathcal{S},\mathcal{H},\Sigma) = \frac{\partial}{\partial \mathbf{H}_p^*} \ln p(\mathbf{Z}_p|\mathbf{S}_p,\mathbf{H}_p,\boldsymbol{\Sigma}_p) = 0$$

Solving for $\mathbf{H}_p$ gives

$$\hat{\mathbf{H}}_p = e^{j\omega_f \tau} \mathbf{Z}_p \mathbf{S}_p^\dagger (\mathbf{S}_p \mathbf{S}_p^\dagger)^{-1}$$

Similarly as in the last previous section, substituting the channel estimator into the log-pdf and taking gradient with respect to $\boldsymbol{\Sigma}_p$, one obtains

$$\hat{\boldsymbol{\Sigma}}_p = \frac{\mathbf{Z}_p \mathbf{P}_{\mathbf{S}_p}^\perp \mathbf{Z}_p^\dagger}{n_s},$$

where $\mathbf{P}_{\mathbf{S}_p}^\perp = \mathbf{I}_{n_s} - \mathbf{S}_p^\dagger (\mathbf{S}_p \mathbf{S}_p^\dagger)^{-1} \mathbf{S}_p = \mathbf{I}_{n_s} - \mathbf{P}_{\mathbf{S}_p}$. Plugging these estimators into Eq. (4.23), the maximum pdf is represented by

$$p(\mathbf{Z}_p|\mathbf{S}_p; \hat{\mathbf{H}}_p, \hat{\boldsymbol{\Sigma}}_p) = \frac{n_s^{n_s} e^{-Mn_s}}{\pi^{Mn_s} |\mathbf{Z}_p \mathbf{P}_{\mathbf{S}_p}^\perp \mathbf{Z}_p^\dagger|^{n_s}} . \tag{4.24}$$

In the absence of pilot sequence or largely misaligned pilot sequence, the joint pdf can be expressed as

$$p(\mathcal{Z}|\Sigma) = \prod_p p(\mathbf{Z}_p|\boldsymbol{\Sigma}_p),$$

where

$$p(\mathbf{Z}_p|\boldsymbol{\Sigma}_p) = \frac{\exp\left\{-\mathrm{tr}\{\mathbf{Z}_p^\dagger \boldsymbol{\Sigma}_p^{-1} \mathbf{Z}_p\}\right\}}{\pi^{Mn_s} |\boldsymbol{\Sigma}_p|^{n_s}} \tag{4.25}$$

is the pdf for the pth pilot tone. Similarly, the maximum pdf can be represented by

$$p(\mathbf{Z}_p|\hat{\boldsymbol{\Sigma}}_p) = \frac{n_s^{n_s} e^{-Mn_s}}{\pi^{Mn_s}|\mathbf{Z}_p\mathbf{Z}_p^{\dagger}|^{n_s}}. \tag{4.26}$$

Therefore, one can form the GLRT statistic as

$$L_G = \frac{p(\mathcal{Z}|\hat{\Sigma})}{p(\mathcal{Z}|\mathcal{S};\hat{\mathcal{H}},\hat{\Sigma})} = \prod_p |\mathbf{I}_{n_s} - \mathbf{P}_{\mathbf{S}_p}\mathbf{P}_{\mathbf{Z}_p}|^{-n_s}, \tag{4.27}$$

where $\mathbf{P}_{\mathbf{Z}_p} = \mathbf{Z}_p^{\dagger}(\mathbf{Z}_p\mathbf{Z}_p^{\dagger})^{-1}\mathbf{Z}_p$.

In OFDM systems, the pilot tones are usually scattered uniformly across the whole bandwidth to ease the channel estimation. Therefore, in frequency selective environments, it is valid to assume that the channel coefficients at different pilot frequencies are independent, i.e., $\mathbf{H}_p$'s are independent with each other for different p's. With this assumption, one can follow the same derivation in vector space as in the last section to show that the Fisher information matrix for the channel estimators is

$$\mathbf{I}(\mathbf{h}) = \begin{bmatrix} \mathbf{I}(\mathbf{h}_1) & & & \\ & \mathbf{I}(\mathbf{h}_2) & & \\ & & \ddots & \\ & & & \mathbf{I}(\mathbf{h}_{n_p}) \end{bmatrix},$$

where $\mathbf{I}(\mathbf{h}_p) = \left(\mathbf{S}_p\mathbf{S}_p^{\dagger}\right)^T \otimes \boldsymbol{\Sigma}_p^{-1}$, $\mathbf{h}_p = \text{vec}(\mathbf{H}_p)$, $\mathbf{h} = \begin{bmatrix} \mathbf{h}_1^T & \mathbf{h}_2^T & \cdots & \mathbf{h}_{n_p}^T \end{bmatrix}^T$, and n_p is the number of pilot tones. Therefore, the modified GLRT statistic can be modeled asymptotically as [41]

$$2\ln L_G \overset{a}{\sim} \begin{cases} \chi^2_{2MNn_p} & \text{under } \mathcal{H}_0 \\ \chi'^2_{2MNn_p}(\lambda) & \text{under } \mathcal{H}_1 \end{cases}$$

with the noncentrality parameter

$$\lambda = \sum_p 2\mathrm{tr}\left\{\mathbf{\Sigma}_p^{-1}\mathbf{H}_p\mathbf{S}_p\mathbf{S}_p^{\dagger}\mathbf{H}_p^{\dagger}\right\}. \tag{4.28}$$

If the noise is further assumed to be spatially uncorrelated and with identical variance σ_n^2, one obtains

$$\lambda = \frac{\sum_p 2\|\mathbf{H}_p\mathbf{S}_p\|_F^2}{\sigma_n^2} = 2\eta M n_s \mathrm{SNR}, \tag{4.29}$$

where the SNR in MIMO-OFDM systems is defined as the ratio of the received OFDM symbol power per receive antenna to the noise sample variance, and η is the power fraction of the pilot tones in one OFDM symbol. It is bounded from 0 to 1. If the pilot tone is transmitted with the same power as other data tones, $\eta = n_p/L$, where L is the total number of subcarriers in an OFDM symbol.

Since the asymptotic pdf under hypothesis $\mathcal{H}_0$ is not related to any unknown parameters, the CFAR detector exists. With the same argument made in the previous section, although the noncentrality parameter is overestimated, an upper bound for the detection probability can be obtained from the asymptotic distribution through the following steps.

I. For any given false alarm rate P_{FA}, one can determine the corresponding threshold T, such that

$$\int_T^\infty p_1(x)dx = P_{FA},$$

where

$$p_1(x) = \begin{cases} \dfrac{x^{\frac{r}{2}-1}\exp(-\frac{x}{2})}{2^{\frac{r}{2}}\Gamma(\frac{r}{2})} & x \geq 0 \\ 0 & x < 0 \end{cases}$$

is the central chi-squared pdf with $r = 2MNn_p$ degrees of freedom.

II. For the given SNR, one can obtain the noncentrality parameter λ through Eq. (4.29) or Eq. (4.28). Then an upper bound of detection probability $P_{D,a}$ can be

computed as

$$P_{D,a} = \int_T^\infty p_2(x)dx,$$

where

$$p_2(x) = \begin{cases} \frac{x^{\frac{r}{2}-1}\exp(-\frac{x+\lambda}{2})}{2^{\frac{r}{2}}} \sum_{k=0}^\infty \frac{\left(\frac{\lambda x}{4}\right)^k}{k!\Gamma(\frac{r}{2}+k)} & x \geq 0 \\ \\ 0 & x < 0 \end{cases}$$

is the noncentral chi-squared pdf with $r = 2MNn_p$ degrees of freedom and noncentrality parameter λ. And equivalently, a lower bound of the missing rate is given as $P_{miss,lb} = 1 - P_{D,a}$.

In the following, the performances of the GLRT in frequency selective fading channels are evaluated via computer simulations. The performance are shown in ROC curves in various system setups. In a MIMO-OFDM system configured with N transmit antennas and M receive antennas, each transmit antenna sends an OFDM symbol with $L = 128$ subcarriers at a time. Within the OFDM symbol, there are n_p pilot tones, each of which bears a pilot symbol drawn randomly from the QPSK constellation. The pilot tones are transmitted with the same power as other data tones. The receiver collects n_s such OFDM symbols from the M receive antennas. The overall broadband channel assumes frequency selective fading.

Fig. 28 shows the ROC curves for a 4-by-4 MIMO-OFDM system with various SNRs. There are 4 transmit antennas and 4 receive antennas with the observation window of 16 OFDM symbols. The number of pilot tones is 16, which reflects $\eta = 0.125$. This means an overhead of 12.5% in transmission power dedicated for data-aided synchronization and channel estimation purposes. The SNRs investigated are 12, 11, and 10 dB. Fig. 29 illustrates the ROC curves for a regular SISO OFDM system with 16 pilot tones. At SNR=12dB, for $P_{FA} = 1\%$, the missing rate is around 1% in both cases.
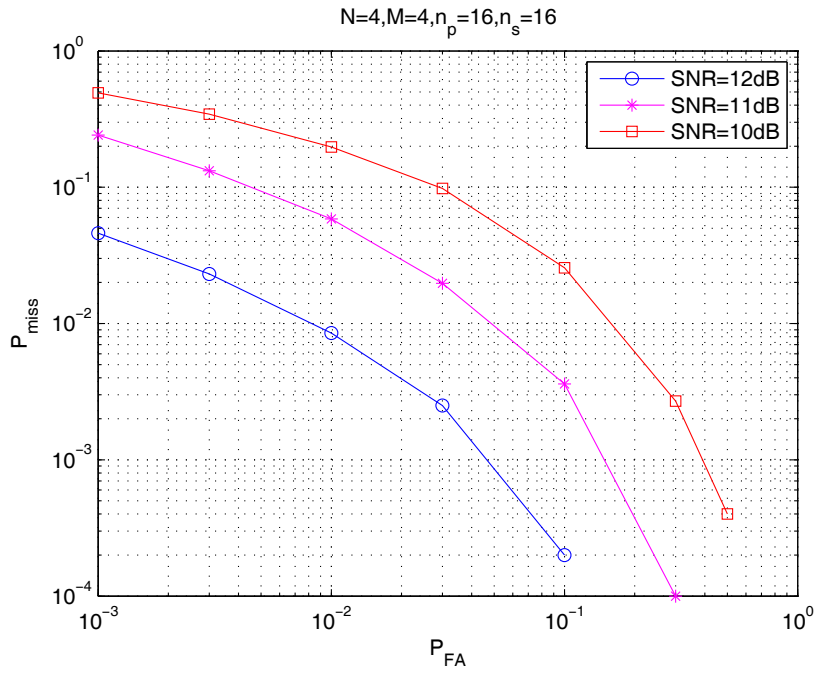
Fig. 28. Comparison of ROCs for a 4×4 MIMO-OFDM system in a frequency selective environment with different SNRs.
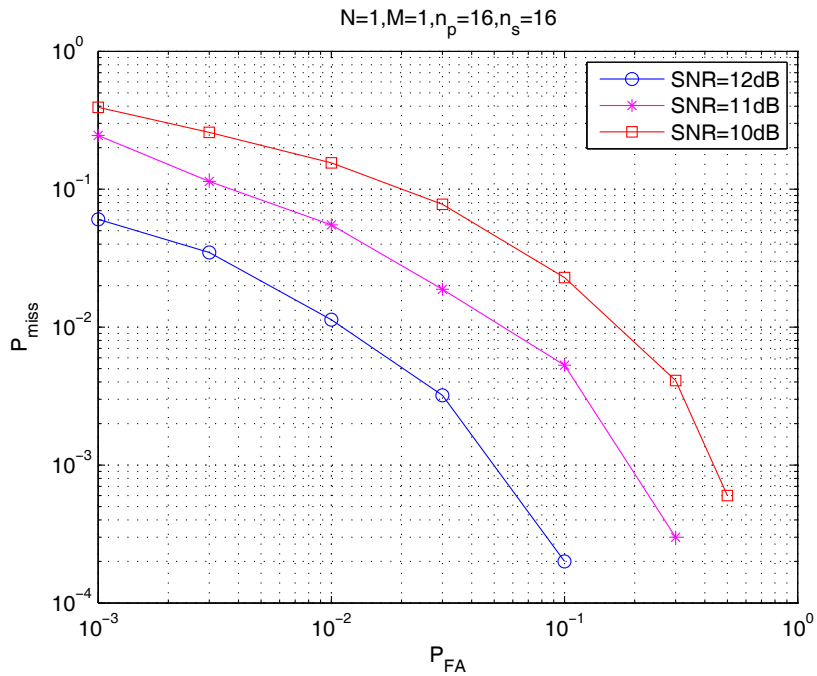

Fig. 29. Comparison of ROCs for a SISO-OFDM system in a frequency selective environment with different SNRs.
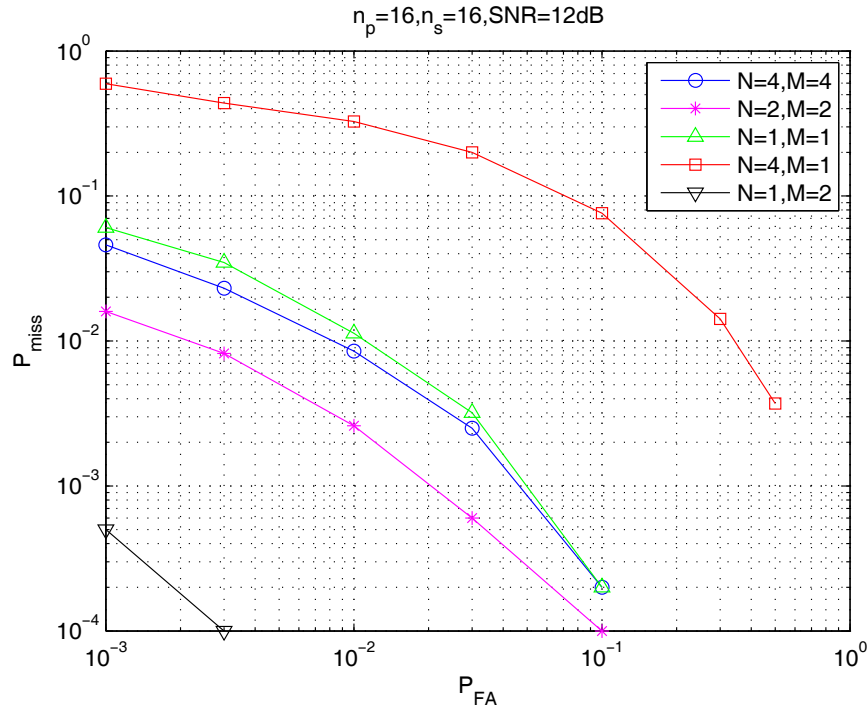
Fig. 30. Comparison of ROCs for different MIMO configurations in frequency selective environment with SNR 12 dB.

Fig. 30 compares the performances of the GLRT under different MIMO configurations at SNR 12 dB. 16 pilot tones are used. It can be found that with the same number of transmit antennas, the more receive antennas are used the better the synchronization performance is in terms of detection probability. Furthermore, with the same number of receive antennas, more transmit antennas lead to worse performance due to the additional interference caused at the receiver side. These phenomena can also be found in the previous section. However, contrary to the MIMO system studied in the previous section, in MIMO-OFDM systems, increasing the number of antennas does not always improve the synchronization performance. In the configuration with $N = M$, the 4-by-4 setup performs almost identical to the SISO case, while the 2-by-2 setup outperforms both.

Fig. 31 illustrates the ROC curves for a 4-by-4 MIMO-OFDM system configured
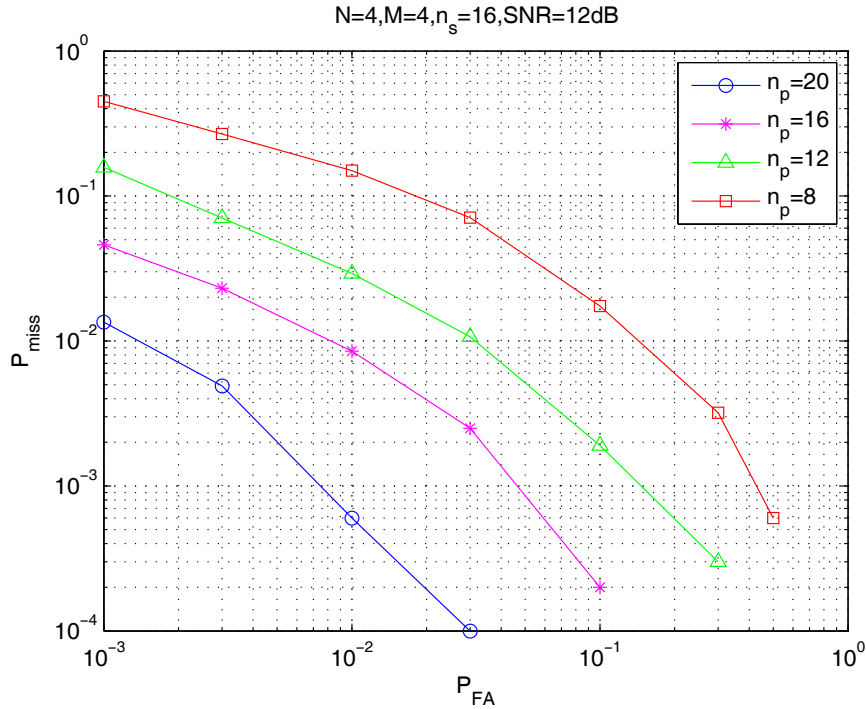
Fig. 31. Comparison of ROCs for a 4×4 MIMO-OFDM system with different number of pilot tones in a frequency selective fading environment, $n_s = 16$.

with various number of pilot tones. The observation window is set to be 16 OFDM symbols and the SNR is 12 dB. The numbers of pilot tones investigated are 20, 16, 12, and 8, which reflects different levels of overhead from 15.63% to 6.25%. Coinciding with intuition, more pilot tones provide better performance. However, choosing the number of pilot tones is never an easy task. Besides the impact on the synchronization performance, more pilot tones cause more overhead and thus reduce the rate for information transmission. Meanwhile, too few pilot tones make the channel estimation difficult in frequency selective channels. In order to get a good channel estimation in frequency domain, the system needs at least two pilot tones within the coherence bandwidth.

Figs. 32 and 33 show the asymptotic behavior for a 4-by-4 MIMO-OFDM system with observation window of 32 and 64 OFDM symbols, respectively. 16 pilot tones are
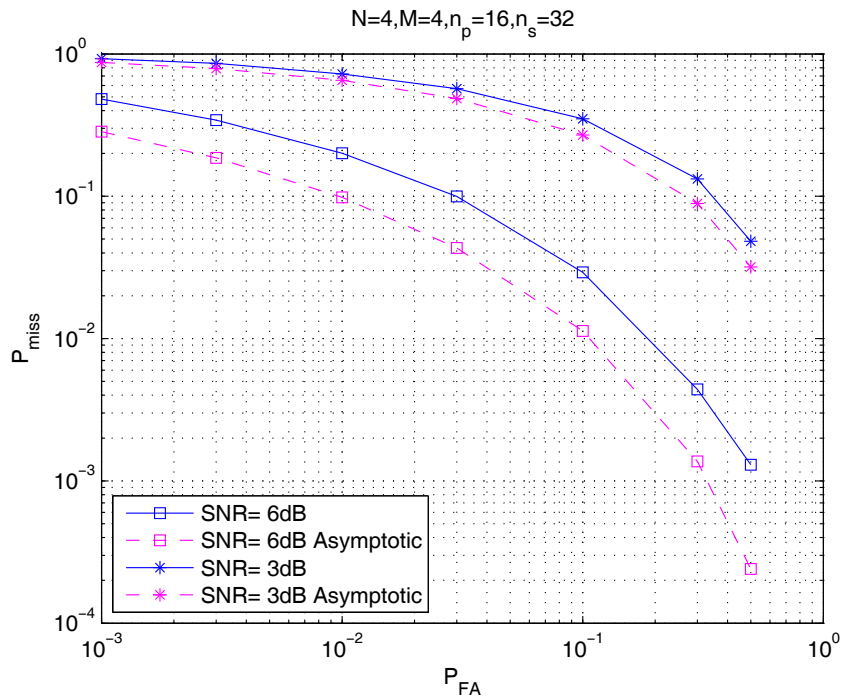
Fig. 32. Performance of the detector for a 4×4 MIMO-OFDM system in a frequency selective fading environment with $n_s = 32$.

used in both cases. As the observation length increases, the lower bound for missing rate gets tighter. Although the bound holds asymptotically, it can still be used as a benchmark with sufficiently large n_s.

D.   Conclusion

In this chapter, timing synchronization was treated as a multiple hypotheses testing problem. GLRT statistics have been developed for MIMO and MIMO-OFDM systems in frequency flat and frequency selective fading environments respectively for their superiority in the presence of nuisance parameters. The performance of the test has been analyzed in both cases. The asymptotic bound serves a good benchmark for the case of more than 64 observations. The choices of a few design parameters in MIMO and MIMO-OFDM systems have also been discussed.
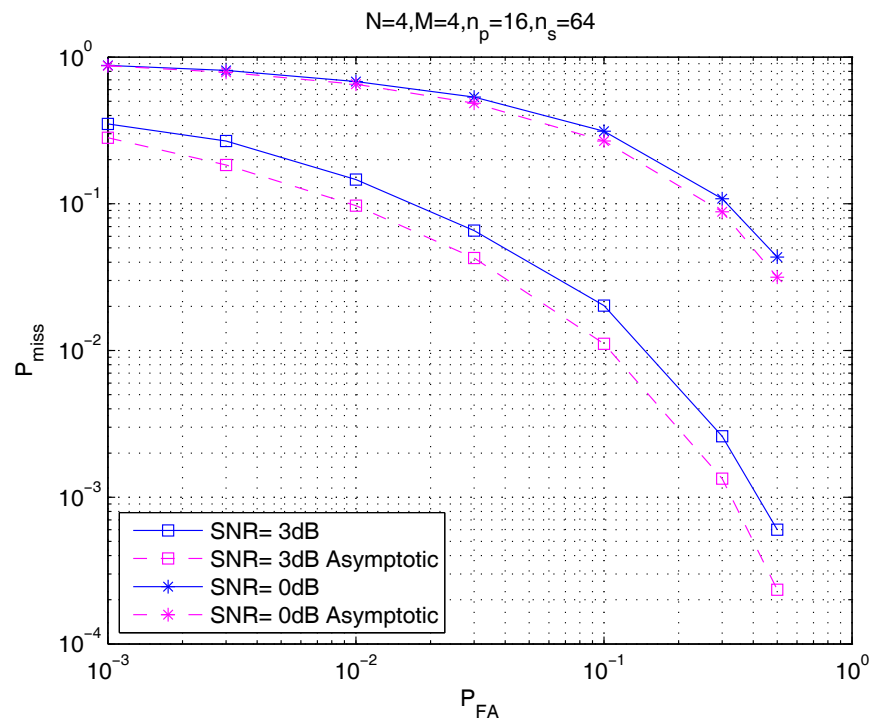
Fig. 33. Performance of the detector for a 4×4 MIMO-OFDM system in a frequency selective fading environment with $n_s = 64$.

CHAPTER V

CONCLUSIONS AND FUTURE WORK

A.   Concluding Remarks

In this dissertation, the sensitivity analysis of both SISO and MIMO OFDM systems to the residual synchronization errors and spatial diversity has been investigated.

For SISO-OFDM systems, in wide-sense stationary uncorrelated scattering frequency selective fading channels, the sampling clock timing offset results in a rotation of the subcarrier constellation, while carrier frequency offsets and phase jitter cause inter-carrier interference. A tight upper bound of the inter-carrier interference distortion has been obtained. And a closed-form expression for the SINR degradation due to imperfect synchronization is reported. Simulation results have shown that the multi-band ZP-OFDM system is very sensitive to carrier frequency offsets. With large carrier frequency offset, the system's symbol error rate is limited by the inter-carrier interference. In MIMO-OFDM systems, similar conclusions are drawn.

As a compensatory measure, multiple antennas can be employed to improve the synchronization performance by exploiting the available spatial diversity. A preamble-based synchronization scheme has been extended to multi-antenna situations. The performance of the synchronization method in terms of detection probability of acquisition, standard deviations of boundary of frame and carrier frequency offset has been assessed via theoretical analysis and computer simulations. It has been found that diversity can favorably improve the synchronization performance while employing more receive antennas is more efficient in this regard. Data-aided and non-data-aided maximum likelihood symbol timing estimators for MIMO-OFDM systems have also been presented. Computer simulations show that by exploiting the spatial diversity,

synchronization performance of MIMO-OFDM systems in terms of detection probability and MSE performance becomes significantly more reliable when compared to conventional SISO OFDM systems, and thus it can improve the overall signal reception. Therefore, spatial diversity appears as a compensatory measure that can be employed in the deployment of MIMO-OFDM communication systems.

In MIMO-OFDM systems with pilot symbols, timing synchronization can be treated as a multiple hypotheses testing problem. The generalized likelihood ration test (GLRT) statistic has been proposed for frequency flat and frequency selective fading channels. Given the superiority of the GLRT in presence of nuisance parameters, the proposed timing synchronization method can be regarded as another form of compensatory method. Furthermore, the asymptotic performance of the test without nuisance parameters has been analyzed. It can serves as an upper bound for detection probability. From computer simulations, the asymptotic bound is tight for the case when more than 64 observations are available. Therefore, it serves as a good benchmark for comparing performances of different timing synchronizers. The choices of a few design parameters such as number of antennas and pilot tones in MIMO-OFDM systems have also been discussed.

B. Suggestions for Future Work

By no means this dissertation can cover all the aspects of the synchronization problem of OFDM systems and compensatory measures. Based upon the work in this dissertation, there are at least two directions can be pursued for future research. One is to further extend the research on compensatory measures by taking into account the space-time codes. The study and analysis done in this dissertation is based solely on uncoded symbols while in real MIMO-OFDM communication systems, space-time

coding will be employed on the signal before transmission. Therefore, a synchronization algorithm and corresponding performance analysis considering space-time codes is more useful for practical systems.

Second, the synchronization problem considered here is for point-to-point systems. A natural extension is to study similar problems in OFDMA multiple access communication schemes with more than one user. And this may need to incorporate the higher layers procedures of the communication network.

REFERENCES

[1] R. Van Nee and R. Prasad, *OFDM for Wireless Multimedia Communications*. Norwood, MA: Artech House, December 2000.

[2] A. Bahai, B. Saltzberg, and M. Ergen, *Multi-Carrier Digital Communications: Theory and Applications of OFDM*, 2nd ed. Springer Verlag, September 2004.

[3] G. Stuber, J. Barry, S. McLaughlin, Y. Li, M. Ingram, and T. Pratt, "Broadband MIMO-OFDM wireless communications," *Proceedings of the IEEE*, vol. 92, no. 2, pp. 271–294, Feb. 2004.

[4] G. J. Foschini, "Layered space-time architecture for wireless communication in a fading environment when using multi-element antennas," *Bell Labs Technical Journal*, vol. 1, no. 2, pp. 41–59, 1996.

[5] I. E. Telatar, "Capacity of multi-antenna Gaussian channels," *European Transaction on Telecommunications*, vol. 10, no. 6, pp. 585–595, Nov./Dec. 1999.

[6] D. Bliss and P. Parker, "Temporal synchronization of MIMO wireless communication in the presence of interference," *IEEE Transactions on Signal Processing*, vol. 58, no. 3, pp. 1794–1806, Mar. 2010.

[7] B. C. Levy, *Principles of Signal Detection and Parameter Estimation*. New York: Springer, 2008.

[8] S. Weinstein and P. Ebert, "Data transmission by frequency-division multiplexing using the discrete fourier transform," *IEEE Transactions on Communication Technology*, vol. 19, no. 5, pp. 628–634, Oct. 1971.

[9] J. Bingham, "Multicarrier modulation for data transmission: an idea whose time has come," *IEEE Communications Magazine*, vol. 28, no. 5, pp. 5–14, May. 1990.

[10] L. Cimini, Jr., "Analysis and simulation of a digital mobile channel using orthogonal frequency division multiplexing," *IEEE Transactions on Communications*, vol. 33, no. 7, pp. 665–675, Jul. 1985.

[11] T. Keller and L. Hanzo, "Adaptive multicarrier modulation: a convenient framework for time-frequency processing in wireless communications," *Proceedings of the IEEE*, vol. 88, no. 5, pp. 611–640, May. 2000.

[12] *Radio Broadcasting Systems; Digital Audio Broadcasting (DAB) to Mobile, Portable and Fixed Receivers*, ETS 300 401, ETSI Std., 1995.

[13] *Digital Video Broadcasting (DVB-T); Frame Structure, Channel Coding, Modulation for Digital Terrestrial Television*, ETS 300 744, ETSI Std., 1997.

[14] *ISO/IEC Standard for Information Technology - Telecommunications and Information Exchange Between Systems - Local and Metropolitan Area Networks - Specific Requirements Part 11: Wireless LAN Medium Access Control (MAC) and Physical Layer (PHY) Specifications (Includes IEEE Std 802.11, 1999 Edition; IEEE Std 802.11A.-1999; IEEE Std 802.11B.-1999; IEEE Std 802.11B.-1999/Cor 1-2001; and IEEE Std 802.11D.-2001)*, ISO/IEC Std., 2005.

[15] T. Pollet, M. Van Bladel, and M. Moeneclaey, "BER sensitivity of OFDM systems to carrier frequency offset and wiener phase noise," *IEEE Transactions on Communications*, vol. 43, no. 234, pp. 191–193, Feb. 1995.

[16] M. Morelli, C.-C. Kuo, and M.-O. Pun, "Synchronization techniques for orthogonal frequency division multiple access (OFDMA): A tutorial review," *Proceedings*

of the IEEE, vol. 95, no. 7, pp. 1394–1427, Jul. 2007.

[17] C. R. Athaudage, "BER sensitivity of OFDM systems to time synchronization error," in *the 8th International Conference on Communication Systems*, vol. 1, Nov. 2002, pp. 42–46.

[18] Y. Mostofi and D. C. Cox, "Analysis of the effect of timing synchronization errors on pilot-aided OFDM systems," in *the 37th Asilomar Conference on Signals, Systems and Computers*, vol. 1, Nov. 2003, pp. 638–642.

[19] Y. Zhao and S. G. Haggman, "Sensitivity to doppler shift and carrier frequency errors in OFDM systems-the consequences and solutions," in *IEEE 46th Vehicular Technology Conference*, vol. 3, April, 1996, pp. 1564–1568.

[20] X. Wang, T. T. Tjhung, Y. Wu, and B. Caron, "SER performance evaluation and optimization of OFDM system with residual frequency and timing offsets from imperfect synchronization," *IEEE Transaction on Broadcasting*, vol. 49, no. 2, pp. 170–177, June 2003.

[21] B. Muquet, Z. Wang, and G. B. Giannakis, "Cyclic prefixing or zero padding for wireless multicarrier transmissions?" *IEEE Transaction on Communications*, vol. 50, pp. 2136–2148, Dec. 2002.

[22] A. Batra, J. Balakrishnan, and G. Aiello, "Design of a multiband OFDM system for realistic UWB channel environments," *IEEE Transaction on Microwave Theory and Technique*, vol. 52, pp. 2123–2138, Sept. 2004.

[23] A. Batra, J. Balakrishnan, and A. Dabak, "Multi-band OFDM physical layer proposal for IEEE 802.15 task group 3a," IEEE P802.15-04/0493r1, Tech. Rep., Sept. 2004.

[24] P. Wolniansky, G. Foschini, G. Golden, and R. Valenzuela, "V-BLAST: an architecture for realizing very high data rates over the rich-scattering wireless channel," in *Proceedings of 1998 URSI International Symposium on Signals, Systems, and Electronics*, Sept. 1998, pp. 295–300.

[25] V. Tarokh, N. Seshadri, and A. Calderbank, "Space-time codes for high data rate wireless communication: performance criterion and code construction," *IEEE Transactions on Information Theory*, vol. 44, no. 2, pp. 744–765, Mar. 1998.

[26] V. Tarokh, H. Jafarkhani, and A. Calderbank, "Space-time block codes from orthogonal designs," *IEEE Transactions on Information Theory*, vol. 45, no. 5, pp. 1456–1467, Jul. 1999.

[27] T. Schmidl and D. Cox, "Robust frequency and timing synchronization for OFDM," *IEEE Transactions on Communications*, vol. 45, no. 12, pp. 1613–1621, Dec. 1997.

[28] P. H. Moose, "A technique for orthogonal frequency division multiplexing frequency offset correction," *IEEE Transactions on Communications*, vol. 42, no. 10, pp. 2908–2914, Oct. 1994.

[29] M. Luise and R. Reggiannini, "Carrier frequency acquisition and tracking for OFDM systems," *IEEE Transactions on Communications*, vol. 44, no. 11, pp. 1590–1598, Nov. 1996.

[30] J. van de Beek, M. Sandell, and P. Borjesson, "Ml estimation of time and frequency offset in OFDM systems," *IEEE Transactions on Signal Processing*, vol. 45, no. 7, pp. 1800–1805, Jul. 1997.

[31] H. Liu and U. Tureli, "A high-efficiency carrier estimator for OFDM communications," *IEEE Communications Letters*, vol. 2, no. 4, pp. 104–106, Apr 1998.

[32] A. Mody and G. Stuber, "Synchronization for MIMO OFDM systems," in *Proceedings of GLOBECOM '01*, vol. 1, 2001, pp. 509–513.

[33] A. Goldsmith, *Wireless Communications*. Cambridge University Press, 2005.

[34] A. Czylwik, "Synchronization for systems with antenna diversity," in *Proceedings of VTC '99-Fall*, vol. 2, 1999, pp. 728–732.

[35] U. Tureli, R. Ambati, D. Kivanc, and H. Liu, "Performance analysis of OFDM carrier synchronization with diversity," in *Proceedings of VTC '02-Fall*, vol. 1, 2002, pp. 33–37.

[36] U. Tureli, P. Honan, and H. Liu, "Low-complexity nonlinear least squares carrier offset estimator for OFDM: identifiability, diversity and performance," *IEEE Transactions on Signal Processing*, vol. 52, no. 9, pp. 2441–2452, Sept. 2004.

[37] B. Sklar, *Digital Communications: Fundamentals and Applications*, 2nd ed. Prentice Hall, 2001.

[38] D. Wang and J. Zhang, "Timing synchronization for MIMO-OFDM WLAN systems," in *Proceedings of WCNC '07*, Mar. 2007, pp. 1177–1182.

[39] F. Tufvesson, O. Edfors, and M. Faulkner, "Time and frequency synchronization for OFDM using PN-sequence preambles," in *IEEE 50th Vehicular Technology Conference*, vol. 4, 1999, pp. 2203–2207.

[40] E. Zhou, X. Zhang, H. Zhao, and W. Wang, "Synchronization algorithms for MIMO OFDM systems," in *the 2005 IEEE Wireless Communications and Networking Conference*, vol. 1, Mar. 2005, pp. 18–22.

[41] S. M. Kay, *Fundamentals of Statistical Signal Processing, Volume II: Detection Theory*. New Jersey: Prentice Hall, 1998.

[42] S. M. Kendall and A. Stuart, *The Advanced Theory of Statistics*. New York: Macmillan, 1979, vol. 2.

[43] Y. Zhou, A. I. Karsilayan, and E. Serpedin, "Sensitivity of multiband ZP-OFDM ultra-wide-band and receivers to synchronization errors," *IEEE Transactions on Signal Processing*, vol. 55, no. 2, pp. 729–734, Jan. 2007.

[44] Y. Zhou, Y.-C. Wu, E. Serpedin, and K. Qaraqe, *OFDM and OFDMA with Linear Diversity for Future Wireless Communications*. Bentham Science Publishers, 2010, ch. The Effects of Spatial Diversity on the Synchronization of MIMO-OFDM Systems.

[45] K. Shi, Y. Zhou, B. Kelleci, T. Fischer, E. Serpedin, and A. Karsilayan, "Impact of narrowband interference on multi-band OFDM ultra wideband communication systems," in *12th Digital Signal Processing Workshop, 4th Signal Processing Education Workshop*, Sep. 2006, pp. 50–54.

[46] ——, "Impacts of narrowband interference on OFDM-UWB receivers: Analysis and mitigation," *IEEE Transactions on Signal Processing*, vol. 55, no. 3, pp. 1118–1128, Mar. 2007.

[47] B. Kelleci, T. Fischer, K. Shi, Y. Zhou, A. Karsilayan, and E. Serpedin, "Narrowband interference suppression in multi-band OFDM ultra wideband communication systems: A mixed-mode approach," in *the 12th Digital Signal Processing Workshop, 4th Signal Processing Education Workshop*, Sep. 2006, pp. 55–59.

[48] Y. Zhou and E. Serpedin, "Generalized likelihood ratio test for data-aided timing

synchronization in MIMO systems," *submitted to IEEE Transaction on Communications*, 2010.

[49] FCC, "First report and order, revision of part 15 of the commission's rules regarding ultra-wideband transmission systems," FCC, Tech. Rep. ET Docket 98-153, Feb. 2002.

[50] A. Saleh and R. Valenzuela, "A statistical model for indoor multipath propagation," *IEEE Journal on Selected Areas in Communications*, vol. SAC-5, pp. 128–137, Feb. 1987.

[51] J. Foerster, "Channel modeling sub-committee report final," IEEE P802.15-02/368r5-SG3a, Tech. Rep., Dec. 2002.

[52] M. Speth, S. Fechtel, G. Fock, and H. Meyr, "Optimum receiver design for wireless broad-band systems using OFDM: Part I," *IEEE Transactions on Communications*, vol. 47, no. 11, pp. 1668–1677, Nov 1999.

[53] M. Speth and H. Meyr, "Synchronization requirements for COFDM systems with transmit diversity," in *Proceedings of GLOBECOM '03*, vol. 3, Dec. 2003, pp. 1252–1256.

[54] S. Alamouti, "A simple transmit diversity technique for wireless communications," *IEEE Journal on Selected Areas in Communications*, vol. 16, no. 8, pp. 1451–1458, Oct. 1998.

[55] J. Ha, A. N. Mody, J. H. Sung, J. R. Barry, S. W. Mclaughlin, and G. L. Stüber, "LDPC coded OFDM with Alamouti/SVD diversity technique," *Wireless Personal Communications*, vol. 23, no. 1, pp. 183–194, 2002.

[56] H. Minn, V. Bhargava, and K. Letaief, "A robust timing and frequency synchronization for OFDM systems," *IEEE Transactions on Wireless Communications*, vol. 2, no. 4, pp. 822–839, July 2003.

[57] H. Minn, M. Zeng, and V. Bhargava, "On timing offset estimation for OFDM systems," *IEEE Communications Letters*, vol. 4, no. 7, pp. 242–244, Jul 2000.

[58] P. Dharmawansa, N. Rajatheva, and H. Minn, "An exact error probability analysis of OFDM systems with frequency offset," *IEEE Transactions on Communications*, vol. 57, no. 1, pp. 26–31, January 2009.

[59] M. Ghogho and A. Swami, *Signal Processing for Wireless Communication Handbook*. CRC, 2004, ch. Carrier frequency synchronization for OFDM systems.

[60] ——, "Blind channel identification for OFDM systems with receive antenna diversity," in *Proceedings of 4th IEEE Workshop on Signal Processing Advances in Wireless Communications*, June 2003, pp. 378–382.

[61] M. Schellmann, V. Jungnickel, and C. von Helmolt, "On the value of spatial diversity for the synchronisation in MIMO-OFDM systems," in *Proceedings of IEEE 16th International Symposium on Personal, Indoor and Mobile Radio Communications*, vol. 1, Sept. 2005, pp. 201–205.

[62] J. Lei and T.-S. Ng, "A consistent OFDM carrier frequency offset estimator based on distinctively spaced pilot tones," *IEEE Transactions on Wireless Communications*, vol. 3, no. 2, pp. 588–599, March 2004.

[63] M. Ghogho and A. Swami, "Frame and frequency acquisition for OFDM," *IEEE Signal Processing Letters*, vol. 15, pp. 605–608, 2008.

[64] Y.-C. Wu and E. Serpedin, "Symbol timing estimation in MIMO correlated flat-fading channels," *Wireless Communications and Mobile Computing*, vol. 4, no. 7, pp. 773–790, 2004.

[65] J. Riba, J. Sala, and G. Vazquez, "Conditional maximum likelihood timing recovery: estimators and bounds," *IEEE Transactions on Signal Processing*, vol. 49, no. 4, pp. 835–850, Apr 2001.

[66] P. Stoica and R. Moses, *Spectral Analysis of Signals*. Pearson Prentice Hall, 2005.

[67] S. F. Arnold, *The Theory of Linear Models and Multivariate Analysis*. New York: Wiley, 1981.

[68] P. Dutilleul, "The MLE algorithm for the matrix normal distribution," *Journal of Statistical Computation and Simulation*, vol. 64, no. 2, pp. 105–123, 1999.

[69] E. L. Lehmann and J. P. Romano, *Testing Statistical Hypotheses*, 3rd ed. New York: Springer, 2005.

APPENDIX A

APPENDIX FOR CHAPTER II

To simplify the exposition, in what follows a matrix form representation is adopted. It turns out that $\mathbf{z} = [Z_0, \cdots, Z_{N-1}]^T$ can be expressed as:

$$\mathbf{z} = e^{-j\frac{2\pi q \Delta l}{N}} \mathbf{F} \mathbf{R}_{ZP} \mathbf{D}_P \mathbf{H} \mathbf{T}_{ZP} \mathbf{F}^\dagger \mathbf{s} , \tag{A.1}$$

where $\mathbf{s} = [s_0, \cdots s_{N-1}]^T$ is the vector of transmitted information bits, $\mathbf{F}$ stands for the FFT matrix. The matrices

$$\mathbf{R}_{ZP} = \begin{bmatrix} & \mathbf{I}_V \\ \mathbf{I}_N & \\ & 0 \end{bmatrix}_{N \times P} , \tag{A.2}$$

$$\mathbf{T}_{ZP} = \begin{bmatrix} \mathbf{I}_N \\ 0 \end{bmatrix}_{P \times N} , \tag{A.3}$$

perform zero-padding and overlap-and-add operations, respectively. The matrix $\mathbf{H}$ is a lower triangular Toeplitz matrix defined [1] as

$$\mathbf{H} = \text{toeplitz}([h_0, h_1, \cdots, h_{L-1}]; [h_0, 0, \cdots, 0]), \tag{A.4}$$

and $\mathbf{D}_P$ is a diagonal matrix representing the residual carrier frequency error and is defined in terms of its diagonal elements as: $\mathbf{D}_P = \text{diag}(1, \alpha, \cdots, \alpha^{P-1})$, with $\alpha = \exp\left(j2\pi\Delta q/N\right)$, and $\Delta q = \Delta f T_s$ is the normalized carrier frequency offset (NCFO) with T_s the symbol duration of ZP-OFDM. It can be shown that

$$\mathbf{D}_P \mathbf{H} = \mathbf{H}' \mathbf{D}_P , \tag{A.5}$$

---

[1]Notation $A = \text{toeplitz}(b; c)$ denotes a Toeplitz matrix A with its first column and row vectors given by the vectors b and c, respectively.

where $\mathbf{H}' = toeplitz([h_0', h_1', \cdots, h_{L-1}']; [h_0', 0, \cdots, 0])$, and $h_0' = h_0$, $h_1' = h_1\alpha$, $\cdots$, $h_{L-1}' = h_{L-1}\alpha^{L-1}$.

Furthermore, one can check that $\mathbf{D}_P\mathbf{T}_{ZP} = \mathbf{T}_{ZP}\mathbf{D}_N$. Therefore,

$$\mathbf{z} = e^{-j\frac{2\pi q\Delta l}{N}}\mathbf{F}\mathbf{R}_{ZP}\mathbf{H}'\mathbf{T}_{ZP}\mathbf{D}_N\mathbf{F}^{\dagger}\mathbf{s} . \tag{A.6}$$

Note that left multiplying $\mathbf{R}_{ZP}$ and right multiplying $\mathbf{T}_{ZP}$ changes $\mathbf{H}'$ into a circulant matrix $\mathbf{H}_{circ}$ with $\left[h_0', \cdots, h_{L-1}', 0, \cdots, 0\right]^T$ as its first column. Matrix $\mathbf{H}_{circ}$ can be further decomposed as $\mathbf{H}_{circ} = \mathbf{F}^{\dagger}\mathbf{\Lambda}'\mathbf{F}$, where $\mathbf{\Lambda}'$ is a diagonal matrix whose diagonal entries are the FFT of the N-point sequence $\left\{h_0', \cdots, h_{L-1}', 0, \cdots, 0\right\}$. Therefore,

$$\mathbf{z} = e^{-j\frac{2\pi q\Delta l}{N}}\mathbf{\Lambda}'\mathbf{F}\mathbf{D}_N\mathbf{F}^{\dagger}\mathbf{s} . \tag{A.7}$$

Let $\Phi = \mathbf{F}\mathbf{D}_N\mathbf{F}^{\dagger}$. It is not difficult to observe that the (m, n) element of matrix Φ can be expressed as

$$\Phi_{m,n} = \frac{\sin(\pi(n - m + \Delta q))}{N\sin(\pi(n - m + \Delta q)/N)}e^{j\pi\frac{N-1}{N}(n-m+\Delta q)} . \tag{A.8}$$

The ICI at subcarrier m caused by the other subcarriers is given by:

$$ICI_m = \mathbf{E}\left\{\left|\sum_{n,n\neq m}\mathbf{\Lambda}'(m)\Phi_{m,n}\mathbf{s}(n)\right|^2\right\} , \tag{A.9}$$

where $\mathbf{\Lambda}'(m)$ is the m-th diagonal element of $\mathbf{\Lambda}'$ and $\mathbf{s}(n)$ denotes the n-th element of vector $\mathbf{s}$. Furthermore, a tight upper bound on ICI can be derived as follows

$$ICI_m \leq \mathbf{E}\left\{\sum_{n,n\neq m}|\mathbf{\Lambda}'(m)\Phi_{m,n}\mathbf{s}(n)|^2\right\} = \mathbf{E}\{|\mathbf{\Lambda}'(m)|^2\}\sum_{n,n\neq m}|\Phi_{m,n}|^2\mathbf{E}\{|\mathbf{s}(n)|^2\} . \tag{A.10}$$

Since $\{h_0, \cdots, h_{L-1}\}$ are independent circularly symmetric complex Gaussian random variables, $[h_0', \cdots, h_{L-1}', 0, \cdots, 0]^T$ forms a complex Gaussian random vector with diagonal covariance matrix $\mathbf{C}_h$. Thus, $FFT\left\{h_0', \cdots, h_{L-1}', 0, \cdots, 0\right\}$ has covariance

matrix $\mathbf{C}_H = \mathbf{F}\mathbf{C}_h\mathbf{F}^\dagger$. One can verify that $(\mathbf{C}_H)_{n,n} = \sum_{j=1}^{N}(\mathbf{C}_h)_{j,j}$ for $n = 1, \cdots, N$.

Therefore, $\mathbf{E}\left\{|\mathbf{\Lambda}'(m)|^2\right\} = \sum_{p=0}^{L-1}\left\{|h_p|^2\right\} = 1$. Thus,

$$
\begin{aligned}
ICI(\Delta q) &= \frac{1}{N}\sum_{m=0}^{N-1}ICI_m \leq \frac{1}{N}\sum_{m=0}^{N-1}\sum_{n,n\neq m}|\Phi_{m,n}|^2 \\
&= \frac{1}{N}\sum_{m=0}^{N-1}\sum_{\substack{n=0 \\ n\neq m}}^{N-1}\left|\frac{\sin(\pi(n-m+\Delta q))}{N\sin(\pi(n-m+\Delta q)/N)}\right|^2.
\end{aligned}
\tag{A.11}
$$

The power of $J_{1q} + J_{2q}$ can be obtained through direct calculations.

$$
\begin{aligned}
\mathbf{E}\left\{|J_{1q}|^2\right\} &= \mathbf{E}_{s,h,\phi}\left\{\frac{1}{N^2}\sum_{l_1=0}^{N-1}\sum_{k_1=0}^{N-1}\sum_{n_1=0}^{N-1}s_{n_1}e^{j\frac{2\pi k_1 n_1}{N}}h_{l_1-k_1}\phi_{l_1}e^{-j\frac{2\pi l_1(q+\Delta q)}{N}}\right. \\
&\quad \left. \times\sum_{l_2=0}^{N-1}\sum_{k_2=0}^{N-1}\sum_{n_2=0}^{N-1}s_{n_2}^*e^{-j\frac{2\pi k_2 n_2}{N}}h_{l_2-k_2}\phi_{l_2}e^{j\frac{2\pi l_2(q+\Delta q)}{N}}\right\} \\
&= \frac{\sigma_\phi^2}{N}\sum_{k=0}^{N-1}\sum_{l=k}^{min(k+V-1,N-1)}\sigma_{h,l-k}^2.
\end{aligned}
\tag{A.12}
$$

Similarly,

$$
\mathbf{E}\left\{|J_{2q}|^2\right\} = \frac{\sigma_\phi^2}{N}\sum_{k=0}^{N-1}\sum_{l=0}^{k-N+V-1}\sigma_{h,l+N-k}^2.
\tag{A.13}
$$

Due to the independence assumption on different paths, it is straightforward to check also that

$$
\mathbf{E}\left\{J_{1q}J_{2q}^*\right\} = \mathbf{E}\left\{J_{1q}^*J_{2q}\right\} = 0.
\tag{A.14}
$$

VITA

Yi Zhou received the B.S. and M.S. degrees both in Electrical Engineering from Southeast University, Nanjing, China, in 2001 and 2004, respectively. He started his Ph.D. degree in Fall 2004 at Texas A&M University, College Station, TX and graduated in December 2010. His research interests are in general area of signal processing for communications, in particular, receiver algorithm design, synchronization techniques, and space-time processing.

He can be reached at the email address zhouyi79@hotmail.com or at the following permanent address:

Department of Electrical & Computer Engineering

Texas A&M University

College Station, TX 77843-3128

USA

The typist for this thesis was Yi Zhou.